$Bi_4Ge_3O_{12}$ phase coexisting in the bulk glass ceramic as confirmed by XRD results may play a more important role in controlling the ε_r values of the glass ceramics. On the other hand, the larger dielectric loss (tanδ) was observed at higher annealing temperature and found to increase gradually up to the annealing time ~~equal~~ 12 hours, above which it decreases with increasing annealing time. This can be related to the density which found to decrease, indicating higher amount of $Bi_4Ge_3O_{12}$ existing in the bulk glass ceramics, when the annealing dwell-time was higher.

Figure 5 shows the temperature dependence of the dielectric constant (ε_r) of annealed Bi_2GeO_5 glass ceramic with fixed frequencies at 1 KHz. The overall dielectric constant of all annealed samples ~~is~~ found to increase with increasing ~~of~~ measurement temperature. For the room temperature up to 250°C, the dielectric constant values ~~were~~ slightly increased while ~~it~~ rapidly ~~increases~~ at higher temperature ~~from 250°C onward~~. However, the phase transition temperature of all annealed Bi_2GeO_5 glass ceramics were not found due to the Bi_2GeO_5 single phase has a higher phase transition temperature of more than 527°C [7], ~~which~~ the measurement was limited by the limitation of the equipment.

In order to study the ferroelectric properties of all annealed Bi_2GeO_5 glass ceramics, the measurements of polarization hysteresis were performed at room temperature using a Sawyer-Tower circuit. The plots of the polarization versus electric field (P-E) loops at room temperature of all annealed samples in Fig. 6 display the slim loop with low remnant polarization (P_r). Moreover, it can be clearly indicated that annealing parameters in both temperature and dwell-time have improved the ferroelectric properties of Bi_2GeO_5 glass ceramics as can be seen in Fig. 7. The results represent the increases of remnant polarization (P_r) and coercive field (E_c) in P-E loop with increasing annealing temperature and dwell-time. However, the ~~appearance~~ P-E loop of all annealed Bi_2GeO_5 glass ceramics are not the feature of truly ferroelectric, it may be represent a lossy capacitor behavior which caused by the effect of low dielectric constant of residual glass matrix.

Conclusions

To study the effect of thermal annealing parameters on the properties of Bi_2GeO_5 glass ceramic, the samples have been prepared by conventional quenching, heat treatment method at 475°C for 18 h and then subsequently annealed at various temperatures and dwell-times. It was found that the thermal annealing promotes the phase formation of the Bi_2GeO_5 phase, leading to the alteration in their density and electrical properties. The dielectric constant of these glass ceramics were greatly improved while dielectric loss degraded with increasing thermal annealing parameters. The best dielectric properties at room temperature were found at 375°C/12 h, exhibiting the maximum values of the dielectric constant (ε_r) of 246 and low dielectric loss (tanδ) of 0.024. Finally, the P-E loops of annealed Bi_2GeO_5 glass ceramic were obtained. The P_r values were found to improve with increasing annealing temperature and dwell-time, but the P-E loop may not represent the truly hysteresis loop as it is more to be a lossy capacitor.

Acknowledgments

The authors would like to thank the Thailand Research Fund (TRF), National Metal and Materials Technology Center (MTEC), Office of the Higher Education Commission (OHEC) Thailand, the Royal Golden Jubilee Ph. D. Program, Graduate School and Faculty of Science, Chiang Mai University, Thailand for financial support.

References

1. X. Wang, X. Yao, and H. Ishiwara, *J. Mater. Sci. Engi. B.* **137**, 278 (2007).
2. R. Nitsche, *J. Appl. Phys.* **36**, 2358 (1965).
3. A. A. Ballman, *J. Cryst. Growth.* **1**, 37 (1967).
4. S. C. Abrahams, P. B. Jamieson, and J. L. Bernstein, *J. Chem. Phys.* **47**, 4034 (1967).
5. A. V. Firsov, N. E. Skorokhodov, A. V. Astaf'ev, S. Yu. Stefanovich, and Yu. N. Venevtsev, *Kristallografiya.* **29**, 509 (1984).
6. B. Auriviltius, C. I. Lindblom, and P. Stenson, *Acta. Chem. Scand.* **18**, 1554 (1964).
7. K. Pengpat and D. Holland, *J. Eur. Ceram. Soc.* **23**, 1599 (2003).
8. K. Pengpat and D. Holland, *Phys. Chem. Glass.—Eur. J. Glass. Sci. Tech. B.* **45**, 79 (2004).
9. P. Kantha, S. Sirisoonthorn, and K. Pengpat, *J. Adv. Mater. Res.* **55–57**, 437 (2008).
10. P. Kantha, K. Pengpat, G. Rujijanagul, T. Tunkasiri, S. Eitssayeam, U. Intatha, and S. Sirisoonthorn, *Adv. Mater. Nano.: AIP Conf. Proc.* **1151**, 166 (2009).
11. N. Vittayakorn, G. Rujijanagul, and D. P. Cann, *J. Curr. Appl. Phys.* **7**, 582 (2007).
12. B. D. Cullity, Elements of X-ray Diffraction, second ed., Addison-Wesley Publishing Co., London, UK, 1977.
13. L. Baia, T. Iliescu, S. Simon, and W. Kiefer, *J. Molec. Struc.* **599**, 9 (2001).
14. R. S. Chaliha, K. Annapurna, A. Tarafder, V. S. Tiwari, P. K. Gupta, and B. Karmakar, *J. Opti. Mater.* **32**, 1202 (2010).

GFER #577392, VOL 415, ISS 1

The Structural and Electrical Properties of (1-x)$BaTiO_3$ – x$BaFe_{0.5}Nb_{0.5}O_3$ Ceramics

Uraiwan Intatha, Sukum Eitssayeam, Kamonpan Pengpat, Gobwute Rujijanagul, and Tawee Tunkasiri

QUERY SHEET

This page lists questions we have about your paper. The numbers displayed at left can be found in the text of the paper for reference. In addition, please review your paper as a whole for correctness.

There are no Editor Queries for this paper.

TABLE OF CONTENTS LISTING

The table of contents for the journal will list your paper exactly as it appears below:

The Structural and Electrical Properties of (1-x)$BaTiO_3$ – x$BaFe_{0.5}Nb_{0.5}O_3$ Ceramics
Uraiwan Intatha, Sukum Eitssayeam, Kamonpan Pengpat, Gobwute Rujijanagul, and Tawee Tunkasiri

Ferroelectrics, 415:1–6, 2011

ISSN: 0015-0193 print / 1563-5112 online
DOI: 10.1080/00150193.2011.577392

Taylor & Francis
Taylor & Francis Group

The Structural and Electrical Properties of (1-x)$BaTiO_3$ – x$BaFe_{0.5}Nb_{0.5}O_3$ Ceramics

URAIWAN INTATHA,[1,*] SUKUM EITSSAYEAM,[2] KAMONPAN PENGPAT,[2] GOBWUTE RUJIJANAGUL,[2] AND TAWEE TUNKASIRI[1,2]

[1]School of Science, Mae Fah Luang University, Chiang Rai 57100, Thailand
[2]Department of Physics & Materials Science, Faculty of Science, Chiang Mai University, Chiang Mai 50200, Thailand

The structural and electrical properties of (1 − x) $BaTiO_3$ – x$BaFe_{0.5}Nb_{0.5}O_3$ ceramics system were investigated as a function of the $BaFe_{0.5}Nb_{0.5}O_3$ content by X-ray diffraction (XRD), dielectric and ferroelectric measurement techniques. Studies were performed on the samples prepared by solid state reaction for x = *0, 0.2, 0.4 and 0.6. The XRD analysis demonstrated that with increasing BFN content in (1−*x*)BT–*x*BFN, the structural change occurred from the tetragonal to the cubic phase at room temperature. Changes in the dielectric, ferroelectric and piezoelectric behavior were then related to these structures depending on the BFN content.*

Keyword: lead free piezoelectric; dielectric properties; piezoelectric properties

Introduction

Barium iron niobate ($BaFe_{0.5}Nb_{0.5}O_3$: BFN) has been much scientific attention because of its giant dielectric constant over wide range of temperature and frequency, which makes it potentially useful for important applications in microelectronics and memory devices, as the dielectric constant of a material ultimately decides the degree of miniaturization [1]. BFN was first synthesized via solid state reaction technique by Saha and Sinha in 2002 [2]. After that, several researchers including Yokosuka [3], Tezuka *et al*. [4], Raevski *et al*. [5], Saha and Sinha [2, 6], Intatha *et al*. [7, 8] have reported that the BFN-based electroceramics exhibit a relaxor behavior by showing very attractive dielectric and electrical properties over a wide range of temperatures. However, its high dielectric loss still exists considerable problems of these materials.

$BaTiO_3$ (BT) is known as a very useful ferroelectric material, especially in capacitor applications. $BaTiO_3$ undergoes a series of structural phase transitions as a function of temperature, from an ideal paraelectric cubic perovskite structure to the ferroelectrics tetragonal (120°C) and rhombohedral (−90°C) structures [9]. The high dielectric constant (on the order of 10^3) in $BaTiO_3$ stems from the presence of permanent electrical dipoles inherent to the crystal structure. However, the dielectric constant of barium titanate rises sharply with temperature, exhibiting a peak at the Curie point ($T_C = 130$°C), beyond which

Received June 20, 2010; in final form July 10, 2010.
*Corresponding author. E-mail: i_uraiwan@yahoo.com

it falls hyperbolically, following the Curie-Weiss law [8]. Since ferroelectric devices are to be used over a wide temperature range, pure barium titanate cannot be utilized for practical applications [10]. It must be modified with various additives, giving rise to solid solutions of varying temperature characteristics, tailored to the application [10–12].

Therefore, the modified solid solution method of $(1 - x)BaTiO_3$ (BT) – $xBaFe_{0.5}Nb_{0.5}O_3$ (BFN) system when x have been varied between 0.0 to 0.6 mole were studied in order to develop the properties of both BFN and BT based ceramics.

Experimental Procedure

The (1−x)BT– xBFN ceramics used in this study are prepared as powders by a conventional mixed – oxide method. The $(1-x)BaTiO_3$–$xBaFe_{0.5}Nb_{0.5}O_3$ ((1−x)BT – xBFN) powders were prepared by mixing the starting powder materials $BaCO_3$ (>99%), TiO_2 (>99%), Fe_2O_3 (99.9%) and Nb_2O_5 (99.9%) in the desired mole ratios, ($x = 0$, 0.2, 0.4 and 0.6). These powders were ball-milled for 24 hrs in polyethylene container with zirconia balls. Ethanol was used as a milling medium. After drying at 120°C, the mixed powders were then calcined at 1200°C for 4 h with heating and cooling rate of 5°C/min. Subsequently, the calcined samples were pressed into disc shape and sintered at 1350°C for 2 hrs with constant heating and cooling rates of 5°C/min. Phase formations of the calcined powders and sintered specimens was studied by an X-ray diffractometer using CuK_α radiation (Philips model X-pert) at 40 kV and 30 mA in the 2θ range from 20 to 60 degrees with 0.01° steps. For electrical property characterizations, the sintered samples were ground to obtain parallel faces, and the faces were then coated with silver paste to form electrodes. The samples were heat-treated at 750°C for 12 min to ensure the contact between the electrodes and the ceramic surfaces. The dielectric properties and the electromechanical coupling factor of the sintered ceramics were measured with an automated dielectric measurement system. The system consists of an impedance/gain—phase analyzer (Solartron model SI1260) and a tube furnace; both furnace temperature and dielectric properties were controlled and recorded by a computer. The capacitance was determined over the temperature range 30°C to 200°C at the frequency 1 kHz. To measure relevant electric properties, the prepared ceramic samples were polarized in silicone oil bath at 50°C under 3.0 kV/mm for 15 min. Samples were left at room temperature for 24 hrs after poling, and the piezoelectric measurements were measured using a piezoelectric-d_{33}-meter. The electric hysteresis loop was measured using a Sawyer-Tower circuit.

Results and Discussion

The XRD patterns of the sintered $(1-x)$BT–xBFN ceramics are shown in Fig. 1. It is seen that the $(1-x)$BT–xBFN system formed a series of continuous solid solutions of perovskite structure without any trace of pyrochlore phases. For $x = 0$ (pure BT) the X-ray diffraction pattern shows (002)/(200) peak splitting confirming its tetragonal symmetry. By increasing the BFN content, the intensity ratios of the (002)/(200) peaks tend to increase. The X-ray diffraction patterns of ceramics with high BFN content showed the co-existence of both tetragonal and cubic phases. The lattice parameters of the two co-existing phases in the ceramics were calculated by a refinement method. The cell parameters and tetragonality (c/a) obtained for the $(1-x)$BT–xBFN compositions are given in Fig. 2. The result of the cell refinement showed that the cell parameters of $(1-x)$BT – xBFN system depend on the BFN content. The value of the c/a parameter decreased from 1.09 to 1.00 when the

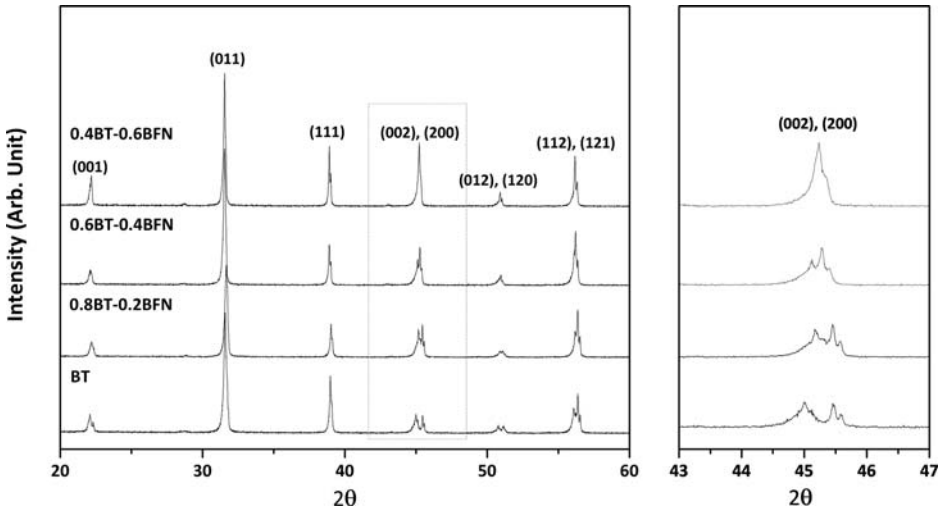

Figure 1. XRD patterns of the (1−*x*)BT–*x*BFN ceramics.

BFN content increased from $x = 0$ to 0.6. At higher x values the parameter (a) of the cubic BT-BFN phase slightly decreased from 3.990–4.020 Å. These values are comparable to that in the Inorganic Crystal Structure database ICSD No. 43622 ($a = 4.045$). However, high resolution XRD analysis is necessary to detect the possible superposition of phases and to restrict the range of compositions for better characterization of the BT-BFN system in range of structure change.

The relationships between dielectric properties and temperatures are shown in Fig. 3. It was clearly shown that the relative dielectric constant depends on temperature measured at 1 kHz on the ceramic sample of (1−x)BT – xBFN system. The broadness of the dielectric constant peak increased with increasing BFN content. Since the Curie temperature for all of investigated compositions decreased as expected from 135°C to below 35°C. Not

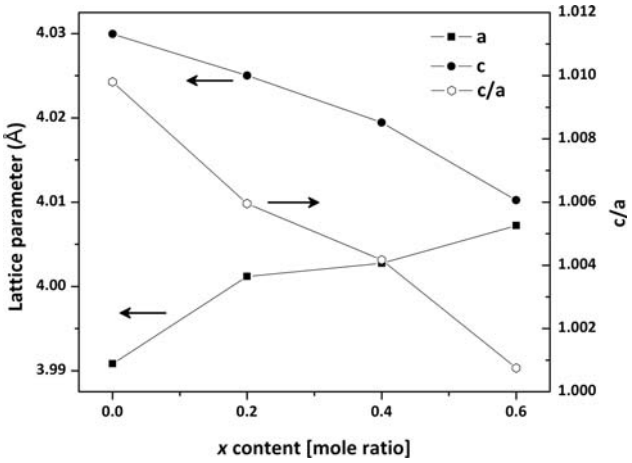

Figure 2. Lattices parameter of the (1−*x*)BT–*x*BFN ceramics.

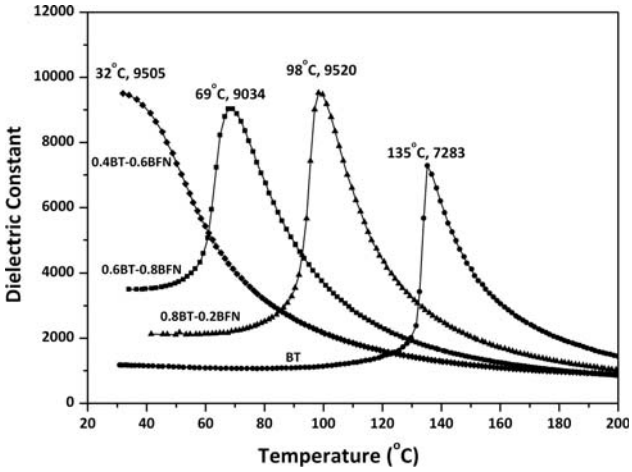

Figure 3. Temperature dependence of dielectric constant of the (1−*x*)BT–*x*BFN ceramics.

only the Curie temperature decreased, but also the maximum dielectric constant increases from ∼7,200 to ∼9500 for BT and 0.4BT–0.6BFN respectively. Furthermore, it was seen that the role of BFN affected the dielectric properties of samples. To further understand the dielectric behavior of the (1−x)BT – xBFN system, the permittivity of a first-order normal ferroelectric can be described by the Curie–Weiss law and a second-order relaxor ferroelectric can be described by a simple quadratic law. This arises from the fact that the total number of relaxor contributing to the permittivity response in the vicinity of the permittivity peak is temperature dependent. The relative permittivity can be calculated via the following equation:

$$\frac{\varepsilon_m}{\varepsilon(f,T)} = 1 + \frac{(T - T_m(f))^y}{2\delta^2} \tag{1}$$

where ε_{m} is the maximum value of the permittivity at $T = T_m(f)$. The value of γ is the expression of the degree of dielectric relaxation, while δ is used to measure the degree of diffuseness of the phase transition. In a material with a "pure" diffuse phase transition, γ is expected to be 2 [13]. For (1−x)BT – xBFN compositions, the diffusibility (γ) and diffuseness parameter (δ) can be estimated from the slope and intercept of the dielectric data shown in Fig. 4, and tabulated in Table 1.The 0.4BT–0.6BFN ceramic has a large γ value (1.82), confirming that it is a relaxsor behavior. The values of γ and δ increase

Table 1
The dielectric and piezoelectric properties of (1−*x*)BT–*x*BFN ceramics.

	T_c (°C)	$\varepsilon_{\max}$	δ	γ	d_{33} (pC/N)	k_p (%)
BT	135	7,383	−12.26	1.14	154	26
0.8BT – 0.2BFN	98	9,520	−13.41	1.40	108	22
0.6BT – 0.4BFN	69	9,034	−13.60	1.41	105	21.5
0.4BT – 0.6BFN	32	9,505	−15.63	1.82	—	—

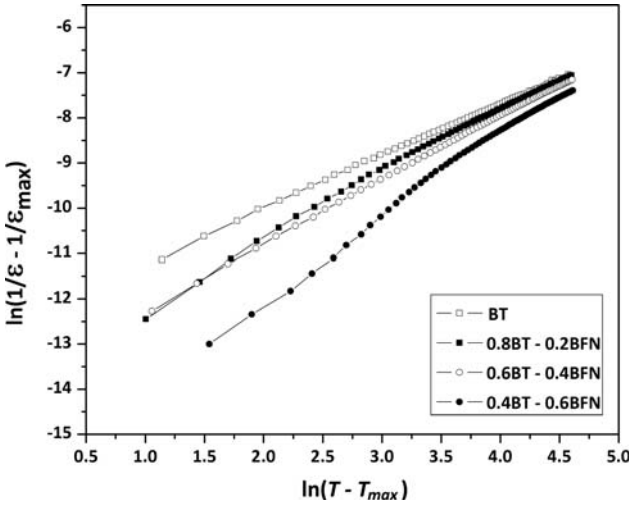

Figure 4. Plots of $\ln(\frac{1}{\varepsilon} - \frac{1}{\varepsilon_m})$ vs. $\ln(T - T_m)$ for the (1−*x*)BT–*x*BFN ceramics.

with increasing BFN content, confirming the diffuse phase transitions in BT–BFN solid solutions. The piezoelectric constant d_{33} and the elctromechanical coupling factor k_p are shown in Table 1. The d_{33} and k_p decrease with increasing BFN fraction up to x = 0.6, which show the maximum values of 154 pC/N and 26% at pure BT. It should be noted that BFN addition in BT showed the improvement only dielectric properties. The hysteresis loop measurement of the (1−*x*)BT–*x*BFN is shown in Fig. 5. The shape of hysteresis loop is similar to one of pure BT. The hysteresis loop with *x* up to 0.4 are not typical, because the external electric field is not sufficient to saturate the polarization and with the composition beyond this indicating lossy linear capacitor behavior. This is consistent with the XRD,

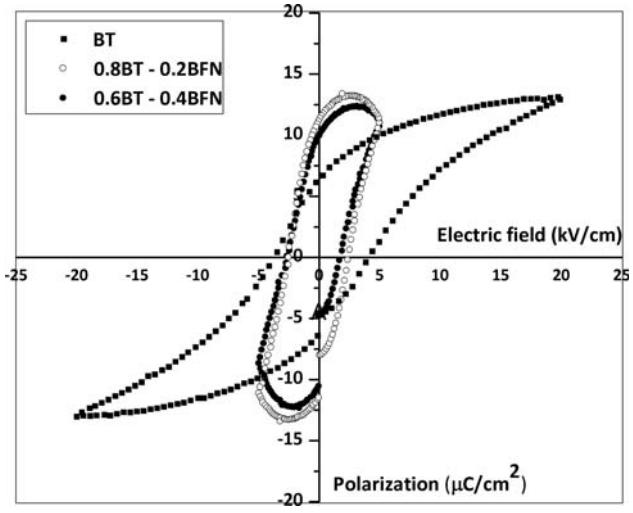

Figure 5. *P–E* hysteresis loops for the (1−*x*)BT–*x*BFN ceramics.

dielectric and piezoelectric results. The optimum mole ratio of $(1-x)$BT–xBFN ceramics was found at a composition x = 0.4. However, in order to confirm the morphotopic phase boundary of $(1-x)$BT–xBFN ceramics may require farther study in more details.

Conclusion

The effect of BFN on the structure, dielectric and piezoelectric properties of $(1-x)$BT–xBFN system was investigated for various chemical compositions. The $(1-x)$BT–xBFN ceramics were prepared by the mixed oxide method. Lattice parameters of the tetragonal phase and cubic phase were found to vary with chemical composition. They were identified as a single BT phase material with a perovskite structure having the symmetry from tetragonal to cubic when the ratio of BFN increased. The broadness of dielectric constant peak increased and Curie temperatures showed a tendency to decrease with increasing BFN content. However, a piezoelectric coefficient d_{33} and k_p decreased with increasing BFN content. The optimum mole ratio of $(1-x)$BT–xBFN ceramics was found at a composition x = 0.4 where at higher value of x the minimum c/a and lossy linear capacitor hysteresis loop behavior were obtained.

Acknowledgments

This work was supported by The Thailand Research Fund (TRF), Office of the Higher Education Commission (OHEC) and faculty of Science, Chiang Mai University, Thailand. Finally. The authors would like to express their thanks to Scientific and Technological Instrument Center, Mae Fah Luang University for providing important facilities using in this project.

Reference

1. L. Ni and X. M. Chen, *Solid State Commun.* **149**, 379 (2009).
2. S. Saha and T. P. Sinha, *J. Phys.: Condens. Matter.* **14**, 249 (2002).
3. M. Yokosuka, *Jpn. J. Appl. Phys.* **34**, 5338 (1995).
4. K. Tezuka, K. Henmi, Y. Hinatsu, and N. M. Masaki, *J. Solid State Chem.* **154**, 591 (2000).
5. I. P. Raevski, S. A. Prosandeev, A. S. Bogatin, M. A. Malitskaya, and L. Jastrabik, *J. Appl. Phys.* **93**, 4130 (2003).
6. S. Saha and T. P. Sinha, *Phys. Rev. B* **65**, 134103 (2002).
7. U. Intatha, S. Eitssayeam, K. Pengpat, K. J. D. MacKenzie, and T. Tunkasiri, *Matter. Lett.* **67**, 196 (2007).
8. U. Intatha, S. Eitssayeam, J. Wang, and T. Tunkasiri, *Curr. Appl. Phys.* **10**, 21 (2010).
9. M. E. Lines and A. M. Glass, *Principles and Applications of Ferroelectrics and Related Materials* (Clarendon press, Oxford, 1977).
10. A. Chelkowski, Dielectric Physics (Elsevier, New York, 1980).
11. Y. Xu, Ferroelectric Materials and Their Applications (Elsevier, New York, 1991).
12. S. L. Swartz, *IEEE Trans. Elec. Ins.* **25**, 935 (1990).
13. L. E. Cross, *Mater. Chem. Phys.* **43**, 108 (1996).

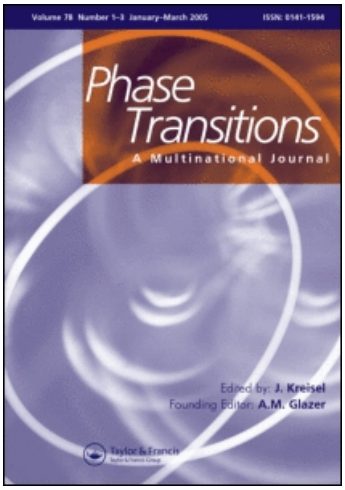

Phase Transitions
Publication details, including instructions for authors and subscription information:
http://www.informaworld.com/smpp/title~content=t713647403

Dielectric properties of lead-free solid solution of $Bi_{0.487}Na_{0.487}La_{0.017}TiO_3$ and $BaTiO_3$

Nuttapon Pisitpipathsin[a]; Kamonpan Pengpat[a]; Puripat Kantha[a]; Wilaiwan Leenakul[a]; Sukum Eitsayeam[a]; Gobwute Rujijanakul[a]; Tawee Tunkasiri[a]
[a] Department of Physics and Materials Science, Faculty of Science, Chiang Mai University, Chiang Mai, Thailand

Online publication date: 20 November 2010

To cite this Article Pisitpipathsin, Nuttapon , Pengpat, Kamonpan , Kantha, Puripat , Leenakul, Wilaiwan , Eitsayeam, Sukum , Rujijanakul, Gobwute and Tunkasiri, Tawee(2010) 'Dielectric properties of lead-free solid solution of $Bi_{0.487}Na_{0.487}La_{0.017}TiO_3$ and $BaTiO_3$', Phase Transitions, 83: 10, 875 — 883
To link to this Article: DOI: 10.1080/01411594.2010.509165
URL: http://dx.doi.org/10.1080/01411594.2010.509165

Phase Transitions
Vol. 83, Nos. 10–11, October–November 2010, 875–883

Dielectric properties of lead-free solid solution of $Bi_{0.487}Na_{0.487}La_{0.017}TiO_3$ and $BaTiO_3$

Nuttapon Pisitpipathsin, Kamonpan Pengpat*, Puripat Kantha, Wilaiwan Leenakul, Sukum Eitsayeam, Gobwute Rujijanakul and Tawee Tunkasiri

Department of Physics and Materials Science, Faculty of Science, Chiang Mai University, Chiang Mai, Thailand

(*Received 24 May 2010; final version received 22 June 2010*)

Bismuth sodium titanate ($Bi_{0.5}Na_{0.5}TiO_3$; BNT) is one of the most preferred materials for the preparation of lead-free ceramics; however its dielectric property is lower than that of lead-based materials. Thus, the substitution of A and B-site cations is considered to be one of the best solutions in order to improve both the dielectric and piezoelectric properties. In this study, lead-free ceramics from bismuth sodium lanthanum titanate ($Bi_{0.487}Na_{0.487}La_{0.017}TiO_3$; BNLT) and barium titanate ($BaTiO_3$; BT) systems were prepared by a modified two-step mixed oxide method. BT powder was added to BNLT powder with the desired compositions of $(1-x)$BNLT–xBT, where $x = 0.00$, 0.02, 0.04, 0.06, 0.08, and 0.10. It was found that the addition of BT in the BNLT improved the electrical properties of ceramics. Phase transition of rhombohedral to tetragonal structure was significantly dependent on the amount of BT added. It was also found that the change in crystal structure affected the ferroelectric property of the ceramics where the transition from ferroelectric to antiferroelectric started from the samples with $x \geq 0.06$ mol% and higher. This may be useful in terms of using these materials in the desired applications.

Keywords: phase transition; dielectric properties; lead free; ferroelectric properties; BNT

1. Introduction

Due to their excellent piezoelectric properties, lead-based piezoelectric ceramics, such as $PbTiO_3$–$PbZrO_3$ [lead zirconium titanate (PZT)], have dominated the field of piezoelectric ceramics for more than half a century. However, the volatilization of PbO during the processing and the wastes of products containing Pb cause a series of vital environmental problems. In this respect, numerous investigators have been developing a number of lead-free piezoelectric ceramics to replace the lead-based ceramics.

Bismuth sodium titanate ($Bi_{0.5}Na_{0.5}TiO_3$; BNT) is one of the excellent candidates for lead-free piezoelectric ceramics with a high Curie temperature (T_C 320°C) [1,2]. It shows strong ferroelectric properties with large remanent polarization (P_r) at room temperature. However, it also has a high coercive field (E_c) [3], making the poling of ceramics difficult.

*Corresponding author. Email: kpengpat@gmail.com

ISSN 0141–1594 print/ISSN 1029–0338 online

DOI: 10.1080/01411594.2010.509165
http://www.informaworld.com

Thus, the BNT ceramic usually exhibits a weak piezoelectric property. Recently, the ceramics based on barium titanate ($BaTiO_3$; BT) are also candidates for lead-free relaxors, because $BaTiO_3$ has a high Curie temperature, a low dielectric loss at high temperature, weak E_c, and spontaneous polarization of $25\,\mu C\,cm^{-2}$ at room temperature [4]. Many scientists have attempted to improve the ferroelectric and piezoelectric properties of BNT-based ceramics. Recently, some investigations have been concentrated on the search for the new morphotropic phase boundaries in the BNT-based binary and ternary systems, such as BNT–$BaTiO_3$ [5], BNT–$KNbO_3$ [6], and BNT–Ba(Ti, Zr)O_3 [7] solid-solution ceramic systems. The ferroelectric and piezoelectric properties of these ceramics were significantly improved.

Another interesting study was reported by Herabut and Safari [8]. They studied the La-doped BNT ceramics with the chemical formula of $(Bi_{0.5}Na_{0.5})(1-1.5x)La_xTiO_3$ and found improvement in the piezoelectric and dielectric properties when compared with those of the pure BNT ceramic. The optimum composition of this bismuth sodium lanthanum titanate (BNLT) system was obtained from the ceramics with 1.7 mol% La^{3+}. This brought out the original idea of our previous study [9] in the fabrication of the ceramics from $(1-x)$BNLT–xBT system, where the range of x values was chosen near the morphothopic phase boundary (MPB) of BNT–BT system (about 4–6 mol% BT). The physical, dielectric, and piezoelectric properties of the BNLT–BT ceramics were investigated. However, there was no report on the ferroelectric properties in the previous work. In this study, the $(1-x)(Bi_{0.487}Na_{0.487}La_{0.017})TiO_3$–$xBaTiO_3$ ($(1-x)$BNLT–xBT) lead-free ceramics were fabricated by an ordinary sintering method, and their phase transition and electrical properties were studied systematically. The relationships between the phase transition and ferroelectricity of the specimens were also described.

2. Experimental

Two-step mixed oxide method was employed for producing $(1-x)(Bi_{0.487}Na_{0.487}La_{0.017}TiO_3)$–$x(BaTiO_3)$ ceramics, where $x = 0.0$, 0.02, 0.04, 0.06, 0.08, and 1.0 using high purity (purity > 99.0%) powders of bismuth oxide (Bi_2O_3), sodium carbonate (Na_2CO_3), lanthanum oxide (La_2O_3), titanium oxide (TiO_2), and barium carbonate ($BaCO_3$) as starting materials. BNLT and BT batch compositions were calcined separately at 900°C and 1200°C, respectively, which are the optimum calcination temperatures for producing highly pure powders of both phases. Both powders were then mixed corresponding to the above formula by ball milling for 24 h with acetone as the dispersion media. After drying and sieving the mixtures, the obtained powder was made into pellets of 10 mm in diameter by uniaxial pressing in a stainless steel die. The pellets were sintered between 1050°C and 1150°C in an electric furnace in an air atmosphere under controlled heating and cooling rates of $5^\circ C\,min^{-1}$ with 2 h dwell time.

Phase identification and density of the sintered ceramic samples were investigated using X-ray diffraction (XRD; Siemens D-500) and Archimedes' method, respectively. The two parallel surfaces of the sintered ceramics were polished and coated with silver paste as electrodes for electrical contact. The real dielectric constant (ε') of all ceramic samples was measured at various frequencies of 10, 100, and 500 kHz and their temperature *versus* ε' curves were also observed using an LCZ meter (Model 4276 A, Hewlett Packard). The ferroelectric properties at different temperatures were examined using a ferroelectric tester (Radiant Technologies Inc.) at $60\,kV\,cm^{-1}$.

3. Results and discussion

The XRD patterns of the $(1-x)$BNLT–xBT ceramics with $0 \leq x \leq 0.10$ are illustrated in Figure 1. All the ceramics exhibit a pure perovskite structure and no second phases are observed, implying that Ba^{2+} ions mainly diffused into BNLT lattices during sintering and formed a solid solution. Similar to pure BNLT, it can be seen that at $x < 0.04$, the ceramic has a rhombohedral perovskite structure and at higher BT content ($x \geq 0.04$), the structure of the ceramic started to change into a tetragonal one. This is because the pure BNLT (i.e., $x = 0$) possesses rhombohedral symmetry, while BT has a tetragonal structure. Moreover, a tetragonal phase appears and increases continuously with increasing BT content. It is also noticed that the ceramic samples with x between 0.04 and 0.06 possess a mixture of rhombohedral and tetragonal phase, with splitting (001)/(100) peak at 2θ between 21° and 25° (Figure 1).

Figure 2 shows the temperature dependence of real dielectric constant (ε') and imaginary dielectric constant (ε'') of $(1-x)$BNLT–xBT ceramics at 10, 100, and 500 kHz. The structure of $(1-x)$BNLT–xBT ceramic specimen changes coincided with the abrupt jump in ε'–T curve. The ε' decreases with increasing frequency. All ceramics exhibit two dielectric anomalies at T_2 and T_m where T_2 is the depolarization temperature which corresponds to the transition from a ferroelectric state to the so-called "antiferroelectric" state, while T_m is the maximum temperature at which ϵ_r reaches a maximum value and corresponds to a transition from an "antiferroelectric state" to a paraelectric state. This transition is not the simple paraelectric–ferroelectric phase transition as a result of random ordering of Bi^{3+}, Na^{+}, and La^{3+} in the A-site of perovskite unit cell. The detailed discussion of the phase transition study in the pure $Na_{1/2}Bi_{1/2}TiO_3$ can be found in [10]. For the ceramics situated at or near the rhombohedral site of the MPB (e.g., pure BNT and 0.94BNLT–0.06BT), their dielectric curves below T_2 exhibit strong frequency

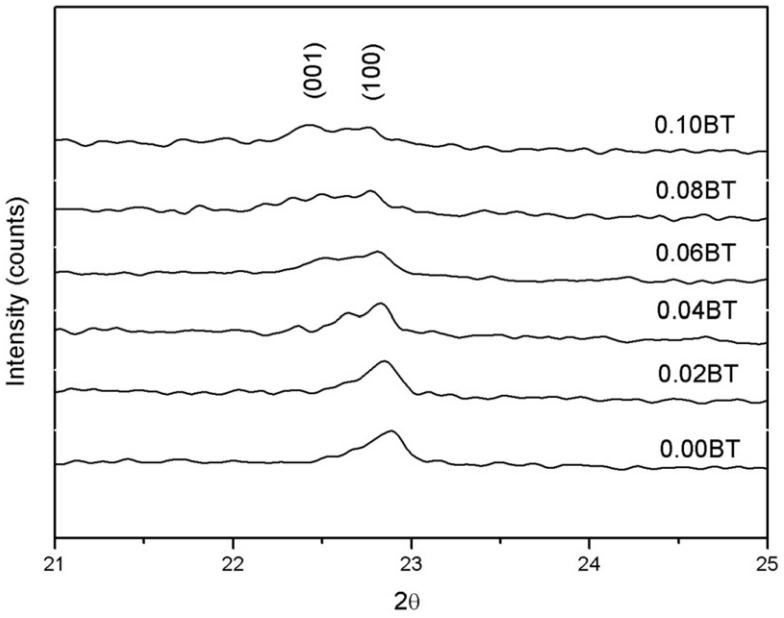

Figure 1. XRD patterns of $(1-x)$BNLT–xBT ceramics at 2θ between 21° and 25°.

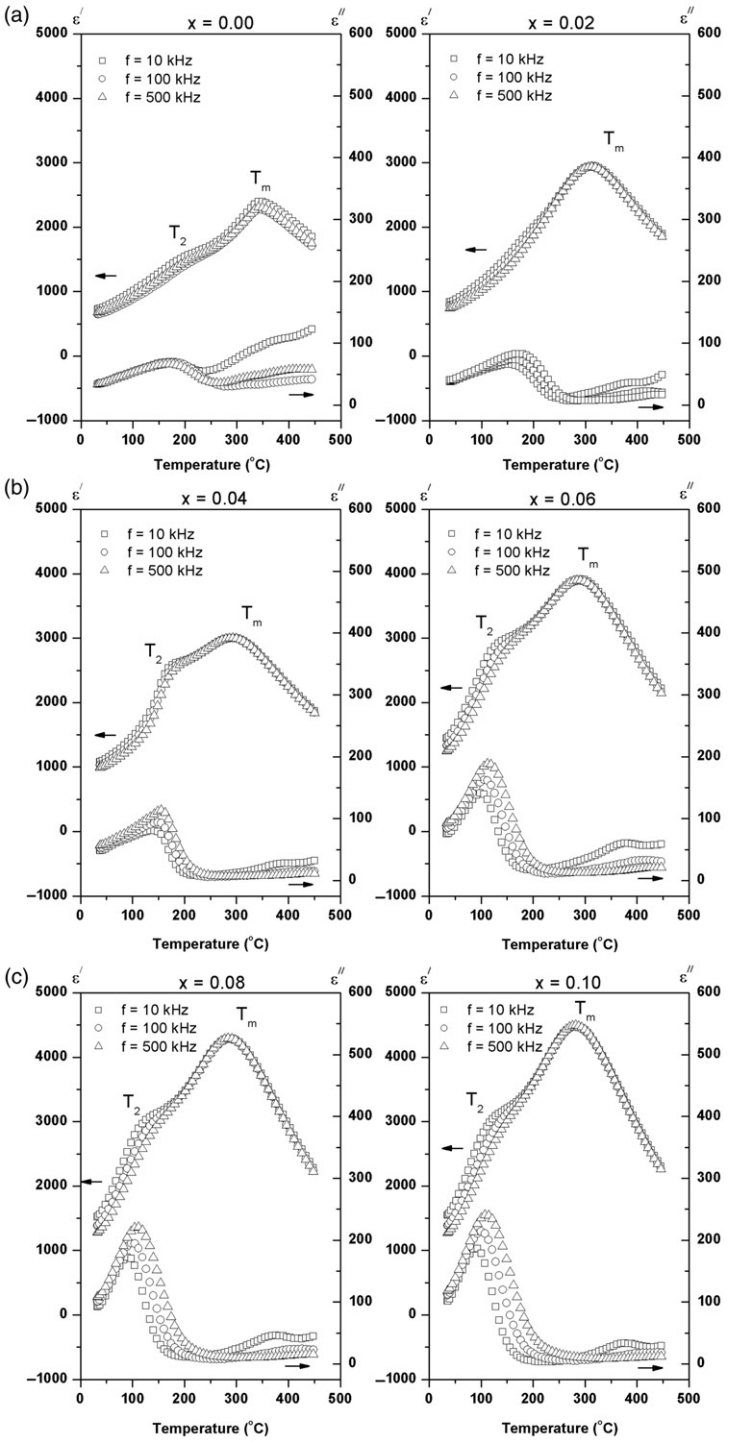

Figure 2. Dependences of ε' and ε'' for the $(1-x)$BNLT–xBT ceramics at 10, 100, and 500 kHz; (a) $x = 0.0$–0.02; (b) $x = 0.04$–0.06; and (c) $x = 0.08$–0.10.

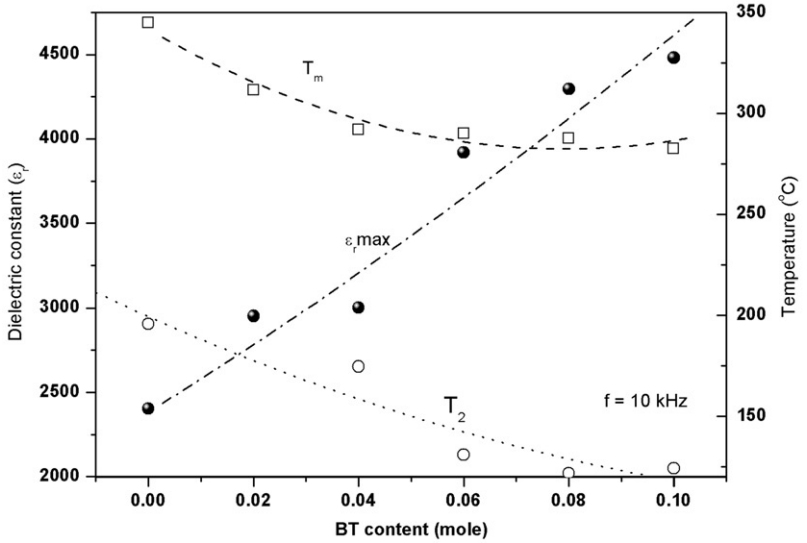

Figure 3. Variations of T_2 and T_m with various values of x for the $(1-x)$BNLT–xBT ceramics at 10 kHz.

dependences, implying that these ceramics undergo a relaxor phase transition at T_2. The dielectric curves around T_m for all ceramics are relatively broad, suggesting that the phase transition at T_m is a diffuse phase type. The most broadened dielectric peak at T_m is attributed to Na^+, Bi^{3+}, La^{3+}, and Ba^{2+} which are randomly distributed in the 12-fold coordination sites; so the observed diffuse phase transition behavior at T_m is reasonably attributed to the disordering of A-site cations.

Figure 3 shows the variation of dielectric constant at T_m of the BNLT–BT ceramics at different BT contents. It can be found that the increase of the BT content induced the reduction of T_m and the increase of the maximum dielectric constant. This is consistent with the study done by Oh and Kim [5].

Figure 4 shows the plots of hysteresis loops at room temperature for six compositions of $(1-x)$BNLT–xBT ceramics with $x = 0.00$, 0.02, 0.04, 0.06, 0.08, and 0.10. The results display the most prominent features and explains the polarization *versus* electric field (P–E) curves for BNLT–BT ceramics with increasing BT content. The P–E loops of $(1-x)$BNLT–xBT ceramics with $x \leq 0.04$ exhibit ferroelectric hysteresis behavior as shown in Figure 4(a). For $x \geq 0.06$, we observe double hysteresis loops, indicative of an antiferroelectric behavior related to diffuse phase transition of Figure 4(b). Furthermore, the ferroelectric characteristics can be assessed with the hysteresis loop squareness (R_{sq}) [11], which can be calculated from the empirical expression $R_{sq} = (P_r/P_s) + (P_{1.1Ec}/P_s)$, where P_s is the saturated polarization obtained at some finite field strength below the dielectric breakdown and $P_{1:1Ec}$ the polarization at the field equal to 1.1 Ec. For the ideal square loop, $R_{sq} = 2.00$ [12]. As listed in Table 1, the loop squareness parameter R_{sq} decreases when BT was added in BNLT–BT solid solution.

Figure 5 shows the coercive electric field and remanent polarization with increasing the BT content at room temperature. The well ferroelectric properties are generally shown in the sample with high value of the remanent polarization (P_r) and low value of the coercive electric field (E_c). From Figure 5, the BT addition in the BNLT ceramic with $x = 0.04$ caused the reduction of E_c value while high P_r was maintained. Therefore, it may be

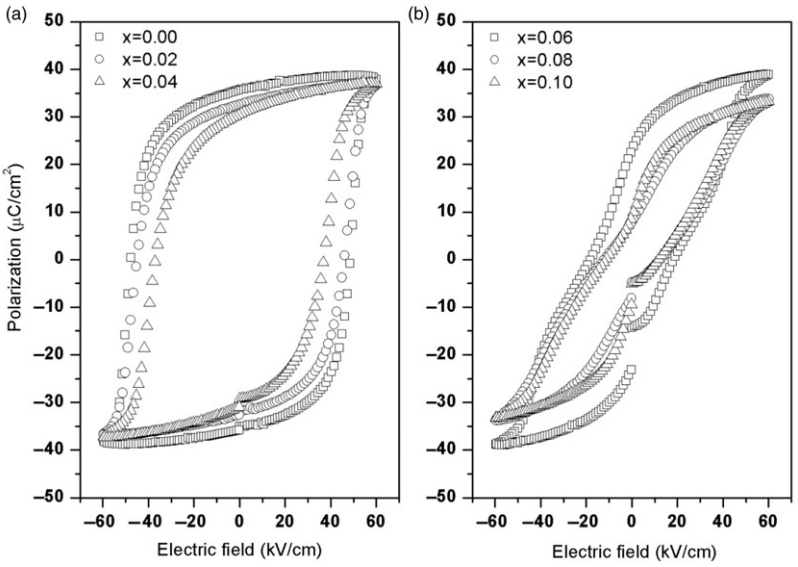

Figure 4. P–E loops for the $(1-x)$BNLT–xBT ceramics at room temperature and frequency 1 kHz; (a) $x = 0.00$–0.04 and (b) $x = 0.06$–0.10.

Table 1. Electrical properties of $(1-x)$BNLT–xBT ceramics.

X (mol%)	0.00	0.02	0.04	0.06	0.08	0.10
ε_r (T_{mL})	2404	2952	3003	3920	4295	4481
$\tan\delta$ (%)	3.95	0.69	0.38	0.82	0.49	0.21
T_m	344.9	311.7	291.8	289.9	287.5	282.6
T_2	195.8	–	174.7	130.9	121.8	124.2
P_r ($\mu C\,cm^{-2}$)	35.7	32.6	30.9	23.1	8.1	9.4
P_{sat} ($\mu C\,cm^{-2}$)	38.3	37.5	37.2	36.3	30.9	30.4
P_{max} ($\mu C\,cm^{-2}$)	37.7	36.6	37.0	38.9	33.8	33.4
E_c ($kV\,cm^{-1}$)	48.7	46.1	36.9	18.2	12.3	11.9
R_{sq}	1.7	1.5	1.2	0.7	0.3	0.3

assumed that 0.06BNLT–0.04BT system has good ferroelectric properties with the high value of remanent polarization of $30.9\,\mu C\,cm^{-2}$ and the coercive electric field of $36.9\,kV\,cm^{-1}$.

Figure 6 shows the P–E loops of the $(1-x)$BNLT–xBT ceramics with $x = 0$, 0.06, and 0.10 measured under an electric field of $60\,kV\,cm^{-1}$ at different temperatures. At room temperature, all the ceramics exhibit a typical ferroelectric P–E loop. However, because of the high coercive field ($48.7\,kV\,cm^{-1}$, Figure 4a), the P–E loop of the pure BNLT ceramic is flattened. As temperature increases to 150°C, the loop becomes well saturated because of the significant decrease in E_c. The loop becomes slightly slimmer together with an increase in P_r with temperature increasing up to 180°C. At temperatures above 180°C, the loop was deformed and was slightly different from the typical ferroelectric characteristics. The P_r was found to slightly decrease. Similar to pure BNLT ceramics, the $(1-x)$BNLT–xBT

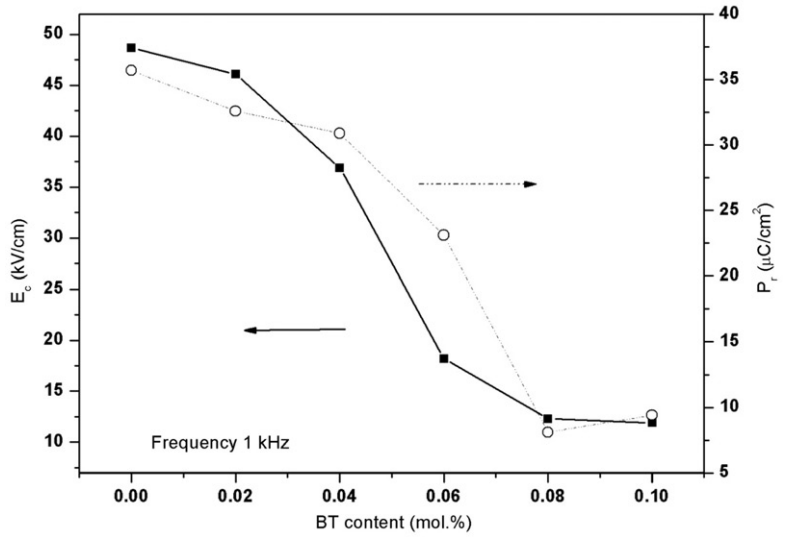

Figure 5. Coercive electric field and remanent polarization with increasing BT content of $(1-x)$BNLT–xBT ceramics at room temperature.

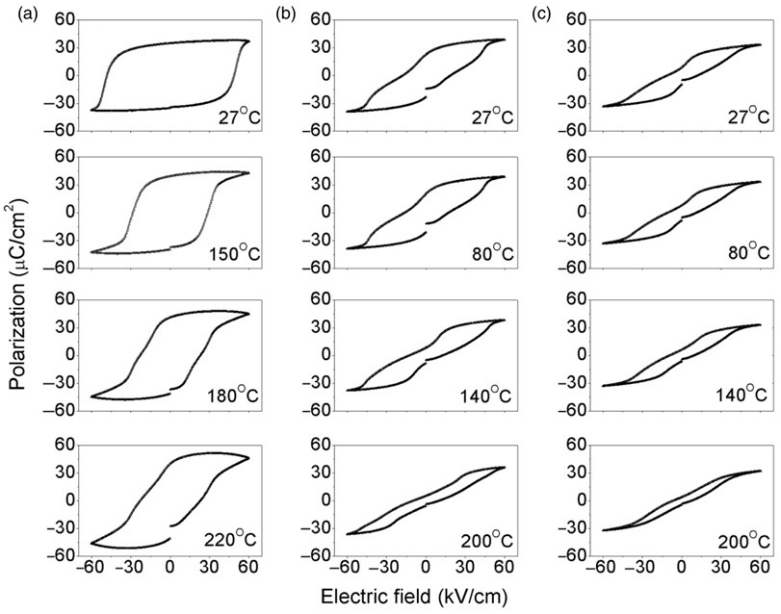

Figure 6. P–E loops for the $(1-x)$BNLT–xBT ceramics at different temperatures: (a) $x=0.00$; (b) $x=0.06$ and (c) $x=0.10$.

ceramics with $x=0.06$ and 0.10 exhibit similar temperature dependences of the ferroelectric properties (Figure 6b and c), and deform to antiferroelectric-like shape with increasing temperature. The detailed properties of $(1-x)$BNLT–xBT ceramics are given in Tables 1 and 2. These results are closely similar to the previous study [13,14] as it was found that

Table 2. Ferroelectric properties of $(1-x)$BNLT–xBT ceramics.

	P_r ($\mu C\,cm^{-2}$)				E_c ($kV\,cm^{-1}$)			
X (mol%)	27°C	150°C	180°C	220°C	27°C	150°C	180°C	220°C
0.00	35.7 27°C	39.4 80°C	41.1 140°C	40.3 200°C	48.7 27°C	28.7 80°C	22.9 140°C	22.7 200°C
0.06	23.1	20.8	8.5	5.4	18.2	17.1	12.8	9.5
0.10	9.4	8.2	6.3	4.1	11.9	10.9	9.2	6.9

double P–E loops are observed in BNLT-based ceramics, and they were suggested as the results of the transition to an antiferroelectric phase at T_2 [15], while deformed P–E loops are also observed in BNT-based ceramics at higher temperatures. Moreover, it was suggested that the anomalies in P–E loops resulted from the electro–mechanical interaction between the polar and non-polar regions which co-existed in the ceramics at high temperatures [13,14].

4. Conclusion

The $(1-x)$ $Bi_{0.487}Na_{0.487}La_{0.017}TiO_3$–$x$$BaTiO_3$ lead-free ceramics have been prepared by a modified two-step mixed oxide method. The increase in ε'' was directly related to the phenomenon of diffuse phase transition. Relaxor behavior is observed in the $(1-x)$BNLT–xBT ceramics. It is suggested that this should result from the cation disordering in the 12-fold coordination sites. The substitution of Ba^{2+} induced the coercive field (E_c) and remanent polarization (P_r) decreased. The P–E loops of ceramics show an antiferroelectric behavior with the addition of BT content in the $(1-x)$BNLT–xBT ceramics with x about 0.06–0.10 mol%. Deformed or slim P–E loops are observed at high temperatures, implying that polar and non-polar regions may co-exist in the ceramics at temperatures above T_2.

Acknowledgements

The authors thank the Thailand Research Fund (TRF), National Metal and Materials Technology Center (MTEC), Office of the Higher Education Commission (OHEC), the Royal Golden Jubilee PhD Program, and Faculty of Science, Chiang Mai University, Thailand for providing financial support. N. Pisitpipathsin thanks the Graduate School, Chiang Mai University for providing financial support.

References

[1] S. Danwittayakul, N. Vaneesorn, S. Jinawath, and A. Thanaboonsombut, *Influence of isovalent and aliovalent substitutions at Ti site on bismuth sodium titanate-based compositions on piezoelectric properties*, Ceram. Int. 34 (2008), pp. 765–768.

[2] L. Gao, Y. Huang, Y. Hu, and H. Du, *Dielectric and ferroelectric properties of* $(1-x)BaTiO_{3-x}$ $Bi_{0.5}Na_{0.5}TiO_3$ *ceramics*, Ceram. Int. 33 (2007), pp. 1041–1046.

[3] C. Xu, D. Lin, and K.W. Kwok, *Structure, electrical properties and depolarization temperature of* $(1-x)Bi_{0.5}Na_{0.5}TiO_{3-x}$ $BaTiO_3$ *lead-free piezoelectric ceramics*, Solid State Sci. 10 (2008), pp. 934–940.
[4] S.H. Wemple, M. Didomenico Jr, and I. Camlibel, *Dielectric and optical properties of melt-grown* $BaTiO_3$, J. Phys. Chem. Solids 29 (1968), pp. 1797–1803.
[5] T. Oh and M.-H. Kim, *Phase relation and dielectric properties in* $(1-x)Bi_{1/2}Na_{1/2}TiO_{3-x}$ $BaTiO_3$ *lead-free ceramics*, Mater. Sci. Eng., B 132 (2006), pp. 239–246.
[6] N. Pisitpipathsin, W. Koontasing, S. Eitssayeam, U. Intatha, G. Rujijinagul, K. Pengpat, and T. Tunkasiri, *Morphotropic phase boundary of lead-free piezoelectric ceramics from BNT-KN system*, Adv. Mater. Res. 55–57 (2008), pp. 225–228.
[7] C. Peng, J.-F. Li, and W. Gong, *Preparation and properties of* $(Bi_{1/2}Na_{1/2}TiO_3)$-$Ba(Ti,Zr)O_3$ *lead-free piezoelectric ceramics*, Mater. Lett. 59 (2005), pp. 1576–1580.
[8] A. Herabut and A. Safari, *Processing and electromechanical properties of* $(Bi_{0.5}Na_{0.5})_{(1-1.5x)}La_xTiO_3$ *ceramics*, J. Am. Ceram. Soc. 80 (1997), pp. 2954–2958.
[9] P. Jarupoom, K. Pengpat, N. Pisitpipathsin, S. Eitssayeam, U. Intatha, G. Rujijinagul, and T. Tunkasiri, *Development of electrical properties in lead-free bismuth sodium lanthanum titanate-barium titanate ceramic near morphotropic phase boundary*, Curr. Appl. Phys. 8 (2008), pp. 253–257.
[10] J. Petzelt, S. Kamba, J. Fabra, D. Noujni, V. Porokhonskyy, A. Pashkin, I. Franke, K. Roleder, J. Suchanicz, and R. Klein, *Infrared, Raman and high-frequency dielectric spectroscopy and the phase transitions in* $Na_{1/2}Bi_{1/2}TiO_3$, J. Phys. Condens. Matter 16 (2004), pp. 2719–2731.
[11] A. Prasatkhetragarn, N. Vittayakorn, S. Ananta, R. Yimnirun, and D.P. Cann, *Synthesis and dielectric and ferroelectric properties of ceramics in* $(1-x)$ $Pb(Zr_{1/2}Ti_{1/2})O_{3-(x)}$ $Pb(Co_{1/3}Nb_{2/3})O_3$ *system*, Jpn. J. Appl. Phys. 47 (2008), pp. 998–1002.
[12] A. Prasatkhetragarn, M. Unruan, A. Ngamjarurojana, Y. Laosiritaworn, S. Ananta, R. Yimnirun, and D.P. Cann, *Effects of Zr/Ti ratio on dielectric and ferroelectric properties of* $0.8Pb(Zr_xTi_{1-x})O_{3-0.2}$ $Pb(Co_{1/3}Nb_{2/3})O_3$ *ceramics*, Curr. Appl. Phys. 9 (2009), pp. 802–806.
[13] J. Suchanicz, J. Kusz, H. Böhm, H. Duda, and J.P. Mercurio, *Structural and dielectric properties of* $(Na_{0.5}Bi_{0.5})_{0.70}Ba_{0.30}TiO_3$ *ceramics*, J. Eur. Ceram. Soc. 22 (2003), p. 1559.
[14] J. Suchanicz, *Behaviour of* $Na_{0.5}Bi_{0.5}TiO_3$ *ceramics in the A.C. electric field*, Ferroelectrics 209 (1998), pp. 561–568.
[15] T. Takennaka, K. Maruyama, and K. Sakata, $(Bi_{1/2}Na_{1/2})TiO_{3-x}BaTiO_3$ *system for lead-free piezoelectric ceramics*, Jpn. J. Appl. Phys., Part 1 30 (1991), pp. 2236–2239.

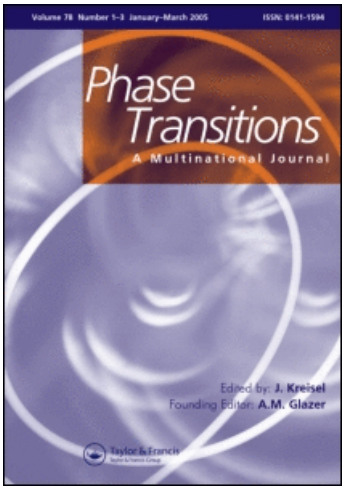

Phase Transitions
Publication details, including instructions for authors and subscription information:
http://www.informaworld.com/smpp/title~content=t713647403

Phase transition behavior in (1 - *x*)PZT-*x*BiAlO$_3$ ceramics

N. Tawichai[a]; T. Tunkasiri[ab]; S. Eitssayeam[a]; K. Pengpat[a]; G. Rujijanagul[ac]
[a] Department of Physics and Materials Science, Faculty of Science, Chiang Mai University, Chiang Mai 50200, Thailand [b] School of Science, Mae Fah Luang University, Chiang Rai 57100, Thailand [c] Science and Technology Research Institute, Chiang Mai University, Chiang Mai 50200, Thailand

Online publication date: 20 November 2010

To cite this Article Tawichai, N. , Tunkasiri, T. , Eitssayeam, S. , Pengpat, K. and Rujijanagul, G.(2010) 'Phase transition behavior in (1 - *x*)PZT-*x*BiAlO$_3$ ceramics', Phase Transitions, 83: 10, 994 — 1000
To link to this Article: DOI: 10.1080/01411594.2010.509612
URL: http://dx.doi.org/10.1080/01411594.2010.509612

Phase Transitions
Vol. 83, Nos. 10–11, October–November 2010, 994–1000

Phase transition behavior in $(1 - x)$PZT–xBiAlO$_3$ ceramics

N. Tawichai[a], T. Tunkasiri[ab], S. Eitssayeam[a], K. Pengpat[a] and G. Rujijanagul[ac]*

[a]*Department of Physics and Materials Science, Faculty of Science, Chiang Mai University, Chiang Mai 50200, Thailand;* [b]*School of Science, Mae Fah Luang University, Chiang Rai 57100, Thailand;* [c]*Science and Technology Research Institute, Chiang Mai University, Chiang Mai 50200, Thailand*

(*Received 24 May 2010; final version received 29 June 2010*)

In this study, a new ceramic with the composition $(1-x)$Pb$(Zr_{0.52}Ti_{0.48})O_3$–xBiAlO$_3$ was fabricated using the solid state method. Phase transition characteristic and dielectric response were investigated. With increase in the content of BiAlO$_3$, a transformation from the tetragonal to the rhombohedral phase was observed. The addition also enhanced the degree of phase transition diffuseness and produced a decrease in the ferroelectric-to-paraelectric phase transition temperature. The results suggested that BiAlO$_3$ has a strong effect on the transition behavior of the solid solution. It is proposed that lattice distortion and compositional fluctuation are responsible for these effects.

Keywords: phase transition; dielectric properties; ceramics; BiAlO$_3$

1. Introduction

For many years, ferroelectric materials have attracted considerable attention for many electronic applications. One of the most interesting ferroelectric materials, lead zirconate titanate (Pb$(Zr_{1-x}Ti_x)O_3$) or PZT, has been extensively investigated in the literature because of its high dielectric, piezoelectric, and ferroelectric properties. For the most part, PZT ceramics with favorable electrical properties have been found with compositions near the morphotropic phase boundary (MPB), i.e., at $PbZrO_3$:$PbTiO_3 \sim 0.52$:0.48 [1]. The electrical properties of PZT can, therefore, be improved by doping with ions such as La^{3+}, Sr^{2+}, or Ba^{2+} [2,3] and many commercial PZT ceramics have been synthesized in the vicinity of the MPB with altered doping elements. Further, PZT and relaxor ferroelectric materials were used to form binary or ternary ferroelectric material systems, which also have better electrical performances [4,5].

The modified PZT or PZT-based materials have been widely used in electronic applications such as actuators, transducers, and motors [2].

Recently, Baettig et al. [6] predicted a large piezoelectricity and ferroelectric polarization in bismuth aluminate (BiAlO$_3$; BAO). Due to the high levels of properties predicted by theory, it was proposed that this may be a new material with properties close to the well-known PZT. Therefore, many studies examining BAO have been carried out [7–9].

*Corresponding author. Email: rujijanagul@yahoo.com

ISSN 0141–1594 print/ISSN 1029–0338 online

DOI: 10.1080/01411594.2010.509612
http://www.informaworld.com

For example, Yu and Ye synthesized a new binary solid solution between $BaTiO_3$ (BT) and BAO [7]. The electrical properties of the new system were investigated. It was found that BAO has a significant effect on the dielectric properties and phase transition of the BT–BAO system. Further, the addition of BAO the enhanced piezoelectric and ferroelectric properties of $(K_{0.5}Na_{0.5})$ NbO_3–BAO system [10]. However, BT and $(K_{0.5}Na_{0.5})$ NbO_3 exhibits lower electrical properties compared to PZT. It is, therefore, interesting to develop a new solid solution between PZT and BAO. It is expected that higher electrical properties could be obtained from this binary system. In this study, a range of new solid solutions $(1-x)$PZT–xBAO were synthesized. Phase formation, dielectric response, and phase transition behaviors of the new system were also investigated.

2. Experimental

Ceramics of $(1-x)$PZT–xBAO were synthesized using a conventional solid-state mixed oxide method. The $(1-x)$PZT–xBAO powders, where x ranged from 0 to 0.1, were first prepared by mixing the starting materials of PbO (>99%), ZrO_2 (>99%), TiO_2 (>99%), Bi_2O_3 (99%), and Al_2O_3 (99.9%) powders. These powders were ball-milled for 24 h in a polyethylene container with yttria-stabilized zirconia balls. After drying at 120°C, the mixed powders were calcined at temperatures ranging from 800 to 950°C for 2 h with a heating and cooling rate of $10^{\circ}C\,min^{-1}$. After grinding and sieving, the calcined powder was mixed with a 3 wt% poly(vinyl alcohol) binder. Subsequently, the calcined powders were pressed into disk shapes and sintered at temperatures ranging from 1100°C to 1200°C for 2 h with constant heating and cooling rates of $10^{\circ}C\,min^{-1}$. The phase formation of the samples was investigated using the X-ray diffraction technique (XRD) with a Cu-Kα radiation X-ray diffractometer. The density of the sintered samples was measured by Archimedes' method using distilled water as a fluid medium. In each composition, the ceramic with the lowest impurity and highest density was selected for electrical characterization. For dielectric measurements, the sintered samples were ground and polished to obtain parallel faces, and silver paste was painted on both sides of the samples. The samples with silver paste were then fired at 650°C for 15 min. The dielectric constant (ε_r) and tangent loss ($\tan\delta$) of the sintered ceramics were measured as a function of temperature with an automated dielectric measurement system. The system consists of a LCR meter and furnace; both temperature and dielectric properties were controlled and recorded by a computer.

3. Results and discussion

3.1. *Phase formation and crystal structure*

Figure 1 shows XRD patterns of the $(1-x)$PZT–xBAO ceramics, where $x = 0.00$–0.10. The XRD analysis revealed that the main phase of all samples is perovskite. However, a pure perovskite phase was observed only for samples where $x \leq 0.02$. Extra impurity peaks were observed for samples where $x \geq 0.02$ at $2\theta \sim 28.1^{\circ}$. This second phase was identified as BAO according to JCPDS file no. 04–0579. The appearance of the BAO phase indicates that the solubility limit of BAO into PZT is very small. Further, the formation of segregated BAO can produce a compositional fluctuation in the solid solution.

Evolution of the (2 0 0) peak as a function of BAO concentration is illustrated in the inset of Figure 2. The XRD pattern for the sample where $x = 0.00$ shows a strong splitting of the (2 0 0) peak. For compositions $0.01 \leq x \leq 0.05$, an ambiguous splitting of the (2 0 0)

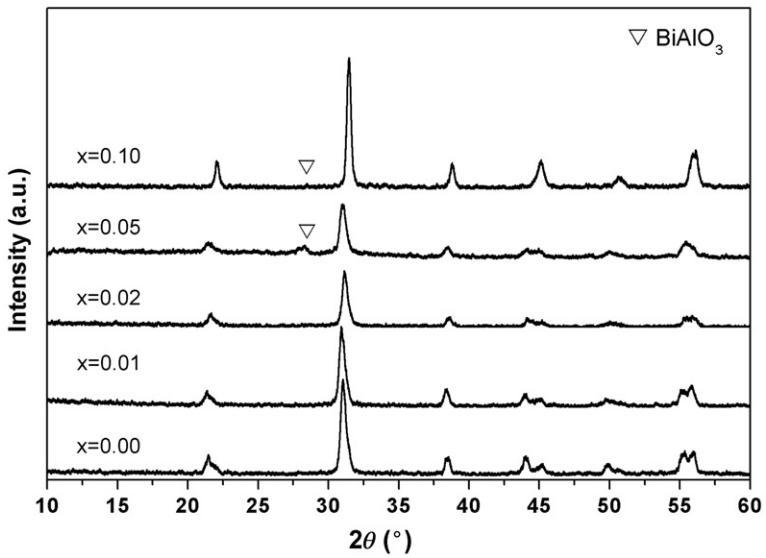

Figure 1. XRD patterns at room temperature of $(1-x)$PZT–xBAO ceramics as a function of BAO content.

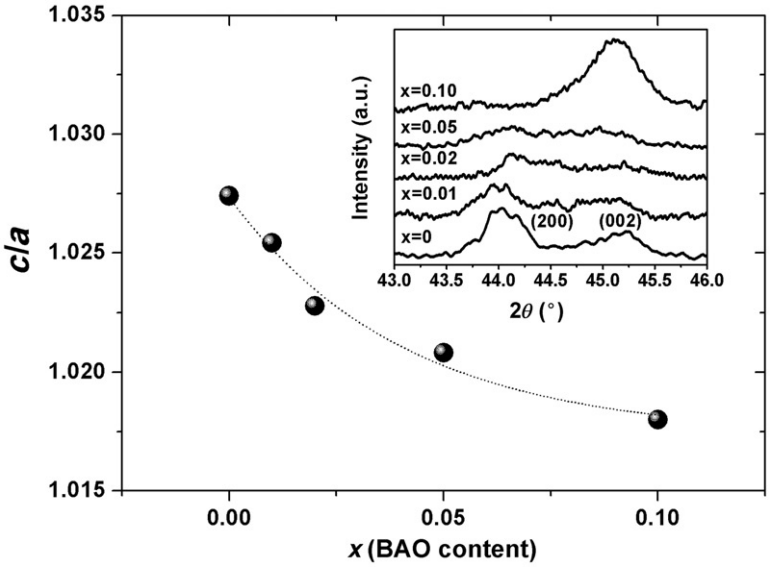

Figure 2. Tetragonality (c/a) as a function of BAO. Inset shows the evolution of (2 0 0) peak splitting.

peak was observed, indicating that there was a superposition of multiple peaks. For $x = 0.10$, the (2 0 0) splitting peaks merged into single peaks. Generally, the single peak of (2 0 0) reflection results for the rhombohedral phase, whereas it splits into two peaks in the tetragonal phase [5]. Therefore, the present result implies that there was a transformation from the tetragonal-rich phase to a prevailing rhombohedral phase in these samples.

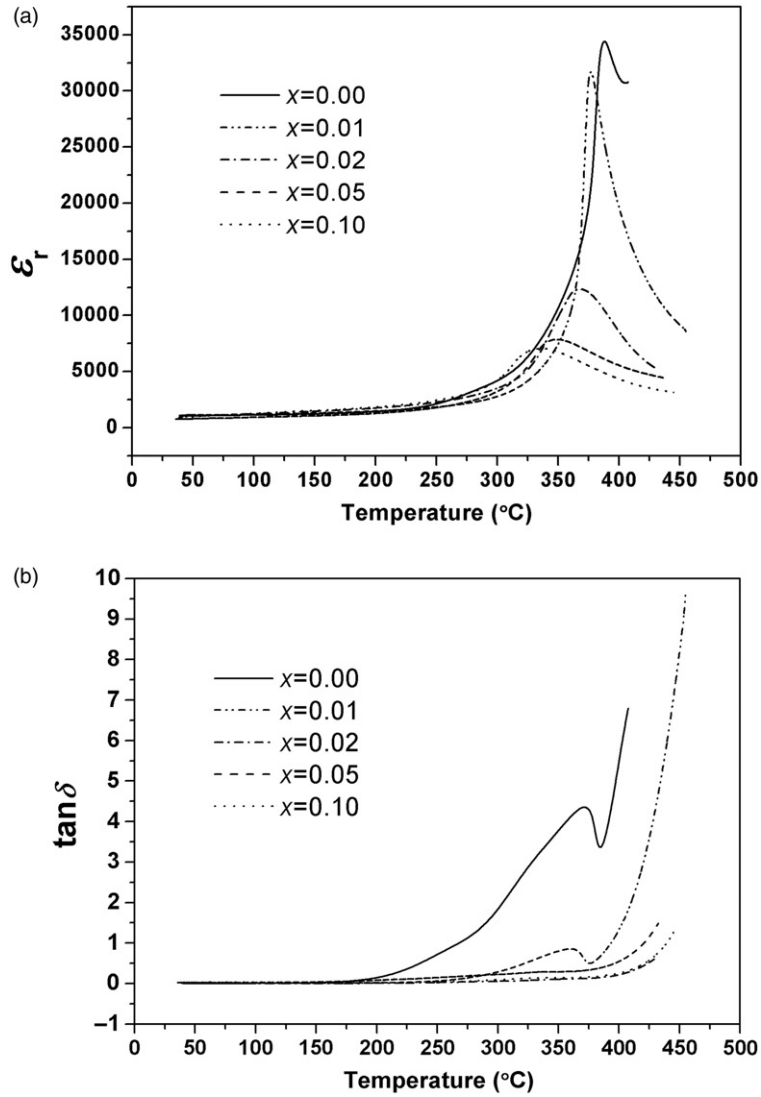

Figure 3. (a) Dielectric *vs.* temperature and (b) tangent loss ($\tan\delta$) of $(1-x)$PZT–xBAO ceramics.

To determine the degree of lattice distortion, tetragonality (c/a) of the samples was calculated. A plot of c/a as a function of BAO is displayed in Figure 2. The exponentially decreasing value of c/a with increase in the amount of BAO indicates a significant distortion of the lattice.

3.2. *Phase transition and dielectric properties*

The characteristic temperatures of the dielectric constant (ε_r) at 1 kHz for $(1-x)$PZT–xBAO, $x = 0.0$–0.10, are shown in Figure 3(a). The ferroelectric-to-paraelectric phase transition temperature (T_m) was obtained from the temperature at the dielectric peak. The value of T_m as a function of BAO content is shown in Figure 4. T_m decreased from 387°C for

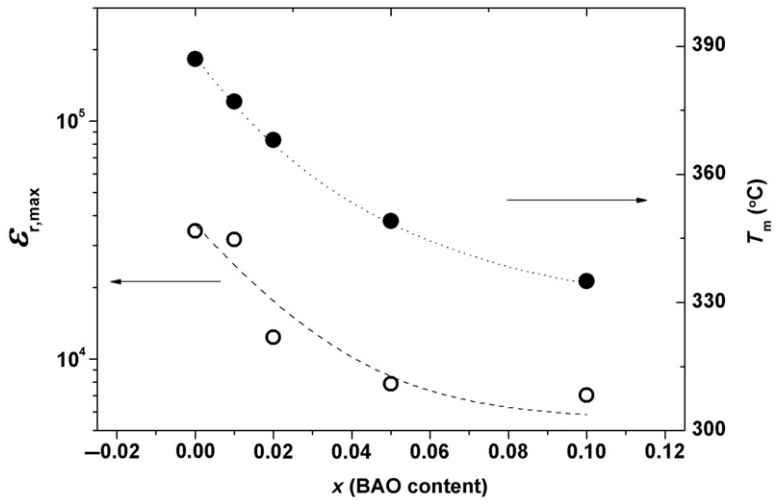

Figure 4. Maximum dielectric constant ($\varepsilon_{r,max}$) and transition temperature (T_m) of the ceramics as a function of BAO content.

the sample where $x = 0.00$ to 335°C for the sample where $x = 0.10$. This trend has been observed for other BAO solid solutions [7,10], suggesting that BAO has a strong effect on the transition temperature. Lattice distortion may be a reason for the decrease in T_m. Generally for the ferroelectric materials, a smaller value of c/a corresponds to a lower transition temperature. This fact is also valid for other ferroelectric materials [11].

The maximum dielectric constant ($\varepsilon_{r,max}$) at T_m as a function of BAO concentration is shown in Figure 4. High $\varepsilon_{r,max}$ values of more than 31,000 were found for the compositions where $x = 0.0$ and 0.01. This value is slightly lower than that found in the work done by Lal et al. [12] who prepared pure $Pb(Zr_{0.52}Ti_{0.48})O_3$ powder by a spray dried method. The different methods of preparation may be the reason for the difference in the dielectric constant. However, the value of $\varepsilon_{r,max}$ at T_m decreased from 34,400 for the sample where $x = 0.0$ to 7040 for the sample where $x = 0.10$. Further, there was a strong change in $\varepsilon_{r,max}$ for the compositions where x is between 0.01 and 0.02. The plot of the dielectric constant *versus* temperature exhibited a broader curve with increase in BAO. The broadness in the curve is a characteristic of structural disorder. This feature has been observed for the BT–BAO system [7]. Generally, compositional fluctuation can result in broadness or diffusiveness of the dielectric peak in the curve of the dielectric constant *versus* temperature. This can produce a microscopic heterogeneity and different local Curie points, resulting in a decrease in the average transition temperature or a shift down in the observed T_m [7]. Also, this heterogeneity may reduce the dielectric constant peak. This factor may produce a significant drop in the dielectric constant for the samples where $x = 0.02$–0.10. The values of tangent loss ($\tan\delta$) as a function of temperature and BAO concentration for the BT–BAO ceramics are shown in Figure 3(b). For pure PZT ceramic, values of $\tan\delta$ were higher than 1, especially at higher temperatures. This is probably due to the higher conductivity of the sample. However, the addition of BAO significantly lowered the rise in $\tan\delta$ at higher temperatures. This implies a reduced conductivity of the solid solution. Therefore, the performance of $\tan\delta$ in the solid solution was improved by the addition of BAO.

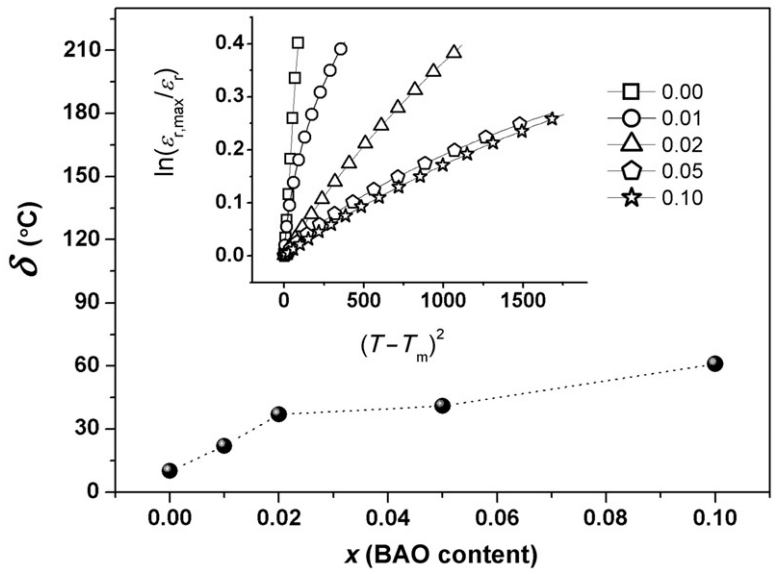

Figure 5. Diffuseness parameter (δ) of $(1-x)$PZT–xBAO ceramics as a function of BAO content. Inset shows plots of $\ln(\varepsilon_{r,max}/\varepsilon_r)$ *vs.* $(T-T_m)^2$ for $(1-x)$PZT–xBAO ceramics.

It has been proposed that the diffuse phase transition in many ferroelectric materials can be described by the following equation [13]:

$$\frac{\varepsilon_{r,max}}{\varepsilon_r} = \exp\left(\frac{(T-T_m)^2}{2\delta_\gamma^2}\right)$$

where δ is the diffuseness parameter of the transition. In the case $(T-T_m)^2/2\delta_\gamma^2 = 0$, the term $\varepsilon_{r,max}/\varepsilon_r = 1$ and the transition shows a completely diffuse transition. The value of δ can be calculated from $\ln(\varepsilon_{r,max}/\varepsilon_r)$ *versus* $(T-T_m)^2$ curve as seen in Figure 5. As clarified by Pilgrim et al. [13], this value is valid for values in the range of $(\varepsilon_{r,max}/\varepsilon_r) < 1.5$. The values of parameter δ for various BAO contents are illustrated in the inset of Figure 5. The parameter δ increased from 10°C for the sample where $x = 0.00$ to 57°C for the sample where $x = 0.10$. The larger value of δ for the higher BAO concentration in the samples indicates and confirms that BAO promoted a diffuse phase transition in the system.

4. Conclusions

Phase formation, dielectric response, and phase transition behavior of the new solid solution $(1-x)$PZT–xBAO, $0.00 \le x \le 0.10$, was investigated for the first time. A single-phase perovskite was observed for compositions where $x \le 0.02$, suggesting that the limit of solubility of BAO in PZT is very small. BAO produced the diffuse phase transition as well as lowered the transition temperature. These results are related to the lattice distortion and compositional fluctuation in the samples.

Acknowledgments

The authors thank The Office of the Higher Education Commission (OHEC) for supporting by grant fund under the program Strategic Scholarships for Frontier Research Network for the

Joint PhD Program Thai Doctoral degree for this research. This study was also supported by The Thailand Research Fund (TRF), Faculty of Science, and Graduate School Chiang Mai University.

References

[1] K. Uchino, *Piezoelectric Actuators and Ultrasonic Motors*, Kluwer Academic Publishers, Boston, MA, 1996.
[2] A.J. Moulson and J.M. Herbert, *Electroceramics; Materials, Properties, Applications*, 2nd ed., John Wiley and Sons, New York, 2003.
[3] N. Vittayakorn, S. Uttiya, G. Rujijanagul, and D.P. Cann, *Dielectric and ferroelectric characteristics of 0.7PZT–0.3PZN ceramics substituted with Sr*, J. Phys. D: Appl. Phys. 38 (2005), pp. 2942–2946.
[4] H. Fan and H.-E. Kim, *Perovskite stabilization and electromechanical properties of polycrystalline lead zinc niobate–lead zirconate titanate*, J. Appl. Phys. 91 (2002), pp. 317–322.
[5] S. Nabunmee, G. Rujijanagul, N. Vittayakorn, and D.P. Cann, *Observation of high dielectric constants in* $x(Pb(Zn_{1/3}Nb_{2/3})O_3$–$(0.2-x)Pb(Ni_{1/3}Nb_{2/3})O_3$–$0.8Pb(Zr_{1/2}Ti_{1/2})O_3$ *ternary solid solutions*, J. Appl. Phys. 102 (2007), p. 094108.
[6] P. Baettig, C.F. Schelle, R. LeSar, U.V. Waghmare, and N.A. Spaldin, *Theoretical prediction ofnew high-performance lead-free piezoelectrics*, Chem. Mater. 17 (2005), pp. 1376–1380.
[7] H. Yu and Z.-G. Ye, *Dielectric properties and relaxor behavior of a new* $(1-x)BaTiO_3$–$xBiAlO_3$ *solid solution*, J. Appl. Phys. 103 (2008), p. 034114.
[8] A. Bouhemadou, R. Khenata, and F. Djabi, *Structural, elastic, electronic and optical properties of the cubic perovskite* $BiAlO_3$, Solid State Sci. 11 (2009), pp. 556–561.
[9] R.V.K. Mangalam, S.V. Bhat, A. Iyo, Y. Tanaka, A. Sundaresan, and C.N.R. Rao, *Dielectric properties, thermal decomposition and related aspects of* $BiAlO_3$, Solid State Commun. 146 (2008), pp. 435–437.
[10] R. Zuo, D. Lv, J. Fu, Y. Liu, and L. Li, *Phase transition and electrical properties of lead free* $(Na_{0.5}K_{0.5})NbO_3$–$BiAlO_3$ *ceramics*, J. Alloys Compd. 476 (2009), pp. 836–839.
[11] J.Q. Qi, W.P. Chen, Y. Wang, and H.L.W. Chan, *Dielectric properties of barium titanate ceramics doped by* B_2O_3 *vapor*, J. Appl. Phys. 96 (2004), pp. 6937–6939.
[12] R. Lal, S.C. Sharma, and P. Ramachandran, *Dielectric behavior of homogeneous PZT ceramics prepared from spray dried powders*, Mater. Res. Bull. 25 (1990), pp. 945–953.
[13] S.M. Pilgrim, A.E. Sutherland, and S.R. Winzer, *Diffuseness as a useful parameter for relaxor ceramics*, J. Am. Ceram. Soc. 73 (1990), pp. 3122–3125.

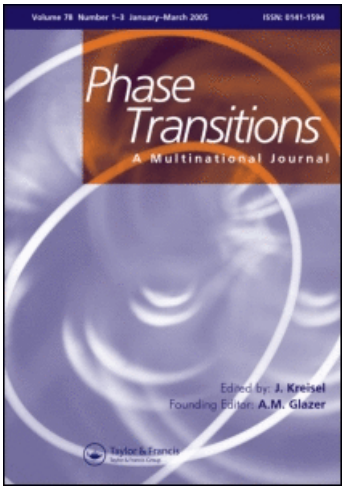

Phase Transitions
Publication details, including instructions for authors and subscription information:
http://www.informaworld.com/smpp/title~content=t713647403

Effects of vibro-milling on relaxor ferroelectric behavior and phase transition of lead-free $Ba(Zr_{0.25}Ti_{0.75})O_3$ ceramics

C. Kruea-In[a]; S. Eitssayeam[a]; K. Pengpat[a]; G. Rujijanagul[ab]; T. Tunkasiri[ac]
[a] Department of Physics and Materials Science, Faculty of Science, Chiang Mai, 50200, Thailand [b] Science and Technology Research Institute, Chiang Mai University, Chiang Mai, 50200, Thailand [c] School of Science, Mae Fah Luang University, Chiang Rai, 57100, Thailand

Online publication date: 20 November 2010

To cite this Article Kruea-In, C. , Eitssayeam, S. , Pengpat, K. , Rujijanagul, G. and Tunkasiri, T.(2010) 'Effects of vibro-milling on relaxor ferroelectric behavior and phase transition of lead-free $Ba(Zr_{0.25}Ti_{0.75})O_3$ ceramics', Phase Transitions, 83: 10, 942 — 949
To link to this Article: DOI: 10.1080/01411594.2010.509604
URL: http://dx.doi.org/10.1080/01411594.2010.509604

Phase Transitions
Vol. 83, Nos. 10–11, October–November 2010, 942–949

Effects of vibro-milling on relaxor ferroelectric behavior and phase transition of lead-free $Ba(Zr_{0.25}Ti_{0.75})O_3$ ceramics

C. Kruea-In[a], S. Eitssayeam[a], K. Pengpat[a], G. Rujijanagul[ab]* and T. Tunkasiri[ac]

[a]*Department of Physics and Materials Science, Faculty of Science, Chiang Mai University, Chiang Mai, 50200, Thailand;* [b]*Science and Technology Research Institute, Chiang Mai University, Chiang Mai, 50200, Thailand;* [c]*School of Science, Mae Fah Luang University, Chiang Rai, 57100, Thailand*

(*Received 24 May 2010; final version received 28 June 2010*)

Lead-free $Ba(Zr_{0.25}Ti_{0.75})O_3$ ceramics were synthesized from powders prepared by a conventional mixed oxide and vibro-milling method to investigate the phase transition, dielectric response, and ferroelectric properties of the prepared samples. Compared to a conventional sample, the samples prepared by the vibro-milling method showed a higher dielectric constant at the ferroelectric-to-paraelectric transition temperature. The vibro-milling method also produced a stronger frequency dependence on the dielectric constant. To confirm the dielectric properties and phase transition behavior, ferroelectric hysteresis measurements were carried out in the temperature range -40°C to 80°C. The microstructural properties of the samples were investigated and the results were then correlated with the characteristics of the milled and calcined powder as well as the grains of the ceramics.

Keywords: phase transition; vibro-milling; ceramics; BZT

1. Introduction

For many years, $Pb(Zr,Ti)O_3$ (PZT) and PZT-based ceramics are the most important piezoelectric materials to be widely used in various fields due to their exceptionally high electrical properties [1,2]. However, it is known that lead oxide (PbO) present in PZT can cause environmental pollution during processing. Due to environmental concerns, it is desirable to find lead-free piezoelectric ceramics to replace PZT and PZT-based ceramics. Recently, many lead-free piezoelectric materials have been developed, such as bismuth sodium titanate ($(Bi_{0.5}Na_{0.5})TiO_3$, BNT), potassium niobate ($KNbO_3$, KN), and barium zirconium titanate ($Ba(Zr_xTi_{1-x})O_3$, BZTs) [3–5]. Among these materials, BZTs have been suggested as interesting lead-free piezoelectric and ferroelectric materials due to their high dielectric and ferroelectric properties [5,6]. Phase transition temperatures of BZT ferroelectrics occur for rhombohedral to orthorhombic (T_1), orthorhombic to tetragonal (T_2), and tetragonal to cubic (T_c) phase transitions and are strongly dependent on Zr concentrations [5]. When the Zr concentration is $\sim$15 at% and more, all the three phase transition temperatures merge into a single diffuse phase transition [5]. At high Zr concentrations ($\geq$30 at%), a relaxor ferroelectric behavior has also been observed [5,7].

*Corresponding author. Email: rujijanagul@yahoo.com

ISSN 0141–1594 print/ISSN 1029–0338 online

DOI: 10.1080/01411594.2010.509604
http://www.informaworld.com

Pure BZTs ceramics are known to be difficult to obtain high electrical properties compared with many PZT based ceramics. Attempts to improve the properties of BZTs ceramics are an important issue to make this material a possible replacement for PZT-based ceramics in the near future. Therefore, various approaches have been proposed to improve the dielectric properties of these ceramics, including doping and processing [8–11]. The properties of BZT ceramics doped with dopants, such as Nb and Yb have been reported [8,9]. For processing effects, many authors have reported that the dielectric responses of BZT ceramics can be affected by the processing parameters [7,11]. Recently, it has been proposed that vibro-milling is an efficient method for producing fine powders [12,13]. Ceramics prepared by this method exhibit better properties compared to the conventional methods. This is due to the fact that vibro-milling produces a high energy which is transferred to the powders [12,13]. To the best of our knowledge, this method has not yet been applied to produce BZT ceramics. This method may help BZT ceramics to show different phase transition behaviors compared to the conventional method, since it can produce a fine powder. Therefore, this work aims to provide a comprehensive study on the process–property relationships of $Ba(Zr_{0.25}Ti_{0.75})O_3$ (BZT25) ceramics. Both the conventional ball-mill mixed oxide and the vibro-milling methods have been used to prepare BZT25 powders. The dielectric relaxor behavior, phase transition, and ferroelectric properties of the samples prepared from the both methods were investigated.

2. Experimental

Powders of BZT25 were prepared *via* conventional and vibro-milling methods where reagent grade $BaCO_3$, ZrO_2, and TiO_2 were used as starting powders for both the methods. For the conventional method, the starting metal powders were weighed and mixed using ball-milling in a polyethylene bottle together with partially stabilized zirconia media for 24 h. For the vibro-milling method, the starting powders were mixed by a vibro-milling machine for 4 h. After that, the resulting powders from both the methods were dried and sieved. The obtained powders were then calcined at 1250°C for 2 h. After grinding and sieving, 3 wt% of a polyvinyl alcohol binder was added. The resulting powders were then cold isostatically pressed into pellets at a pressure of 150 MPa. The pellets were sintered at 1500°C for 2 h. The density of the sintered samples was measured by Archimedes method using distilled water as a fluid medium. Phase formation of the sintered samples was characterized using the X-ray diffraction (XRD) technique. The dielectric properties were determined at various temperatures using a LCR meter coupled to a furnace with a heating rate of $5^{\circ}C\,min^{-1}$. The ferroelectric polarization *versus* electric field (*P–E* hysteresis) measurement was made at various temperatures using a Sawyer–Tower circuit.

3. Results and discussion

Figure 1 shows the XRD results of the ceramics prepared by both the conventional and vibro-milling methods. The XRD result revealed that both samples have a pure perovskite phase, i.e., there was no evidence of impurities in the XRD patterns of both the samples. This result suggests that the method of milling does not influence the phase formation of the samples. The full width at half maximum (FWHM) of the (1 1 1) XRD peak for each sample was calculated. The FWHM was calculated to be 5.13×10^{-3} and 4.06×10^{-3} rad for the conventional and vibro-milled samples, respectively. Generally, the FWHM of the XRD peak can be related to the degree of crystallinity, grain size (particle size) and strain

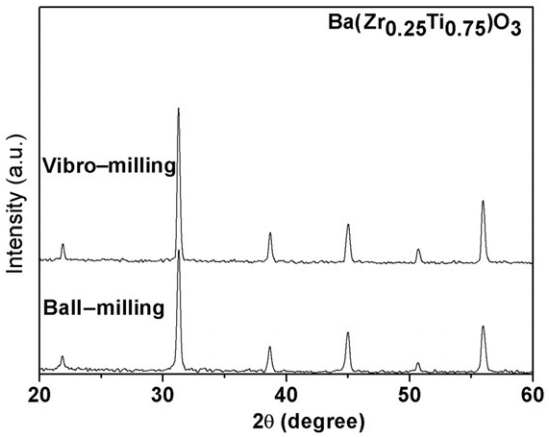

Figure 1. XRD patterns of BZT25 ceramics prepared using the conventional ball-milling and vibro-milling methods.

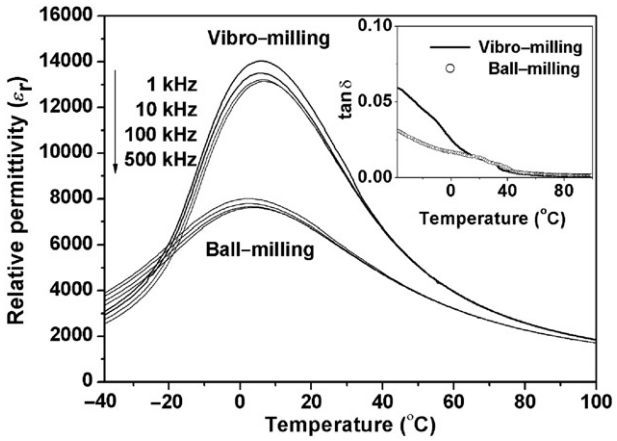

Figure 2. Temperature dependence on the relative permittivity of BZT25 ceramics at frequencies between 1 and 500 kHz, prepared by conventional ball-milling and vibro-milling methods. Inset shows loss tangent ($\tan\delta$) *vs.* temperature at 10 kHz.

of the powder sample, and residue stress in metals [14]. However, in this study, we are concerned only with the degree of crystallinity in the samples. In our case, a lower FWHM value indicates a higher degree of crystallinity in the vibro-milled sample. Furthermore, the density value for the vibro-milled ceramic sample ($6.002 \pm 0.007\,\mathrm{g\,cm^{-3}}$) was higher than that obtained from the conventional ball-milled ceramic sample ($5.992 \pm 0.005\,\mathrm{g\,cm^{-3}}$).

Variations in the dielectric constant of the materials under investigation were measured as a function of temperature between the frequencies 1 and 500 kHz. Figure 2 shows a comparison of the dielectric result between the conventional and vibro-milled samples. The temperature dependence of the dielectric constant depicts a typical relaxor behavior of the dielectric peak at T_m (the temperature of the dielectric maximum) for both the samples. It should be noted that the vibro-milled samples exhibited a stronger frequency dependence

compared to the conventional sample. In addition, the vibro-milled samples had a higher dielectric maximum at the transition temperature ($T_m \sim 4^\circ C$) with maximum permittivity value of ~13,000 (at 10 kHz), while the conventional sample exhibited a rather low dielectric maximum value (~7800 at $T_m \sim 3^\circ C$). The improvement of the maximum permittivity may be attributed to the higher ceramic density and the higher degree of crystallization of the vibro-milled sample. A similar result was reported in the work by Khamman et al. [13] in $Bi_{0.5}Na_{0.5}TiO_3$.

For relaxor ferroelectric materials, the value of the dielectric constant above T_m does not obey the Curie–Weiss law. However, a simple quadratic law can be used to describe the relaxor ferroelectrics, i.e., the ε_r *versus* T relationship follows a function with the additional variables γ and δ_γ as the following equation [15,16]:

$$\frac{\varepsilon_m}{\varepsilon_r} = 1 + \frac{(T - T_m(f))^\gamma}{2\delta_\gamma^2}, \tag{1}$$

where δ_γ is the diffusiveness parameter and γ the degree of dielectric relaxation in the relaxor ferroelectric [15,16]. When $\gamma = 1$, Equation (1) expresses the Curie–Weiss behavior, while for $\gamma = 2$ the equation describes the full relaxor behavior with a quadratic dependence. The values of γ and δ_γ can be calculated from a plot of $\log((\varepsilon_m/\varepsilon_r) - 1)$ *versus* $\log(T - T_m)$. The parameters δ_γ and γ were 24.85 and 1.83 for the conventionally milled sample and 21.85 and 1.91 for the vibro-milled sample, respectively. The higher value of δ_γ for the conventional sample indicates a more diffuse phase transition. In addition, the vibro-milled sample showed a higher degree of dielectric relaxation due to the higher value of γ.

The results of the selected polarization–field (P–E hysteresis loop) at 1 Hz for the ceramics prepared from both methods are shown in Figure 3. The measurement was performed over the temperature range −40°C–80°C, across the transition temperature. The hysteresis data illustrated the dielectric results for the change from a ferroelectric to a paraelectric state. The hysteresis loops showed that remanent polarization is nonzero at temperatures near T_m. For temperatures above T_m, the hysteresis loops transformed to slim loops and the remanent polarization and coercive field values decreased significantly. However, slim ferroelectric hysteresis still occurred for temperatures above T_m, suggesting that these samples exhibited a diffuse phase transition behavior which is the characteristic of a relaxor ferroelectric material. It should be noted that the hysteresis loop at −10°C of the vibro-milled sample deformed from the typical characteristics of the ferroelectric materials. This may contribute to a higher lossy capacitor in the samples which corresponds to its higher loss tangent (inset of Figure 2).

Particle size analysis of the calcined powders was performed by using a laser particle size analyzer (Mastersizer S). The powders were dispersed in distilled water in an ultrasonic bath. The results of particle size analysis are shown in Figure 4. It can be clearly seen that particle size distribution curves for both the powders exhibit a bimodal distribution. This result implies an occurrence of particle agglomeration in the samples. Khamman et al. [12] reported that milling time has an effect on particle agglomeration in lead zirconate powders, as the bimodal distribution was observed in some conditions of the milled powders. Therefore, particle agglomeration observed in this study may be caused by the vibro-milling time (4 h) which has not reached the optimum point to obtain uniform particle size with lower degree of agglomeration. Further work should be attempted to find the optimum milling time.

From the bimodal distribution curves (Figure 4), the first peak at the lower particle diameter is believed to be the primary particle size of the powder, while the second peak at

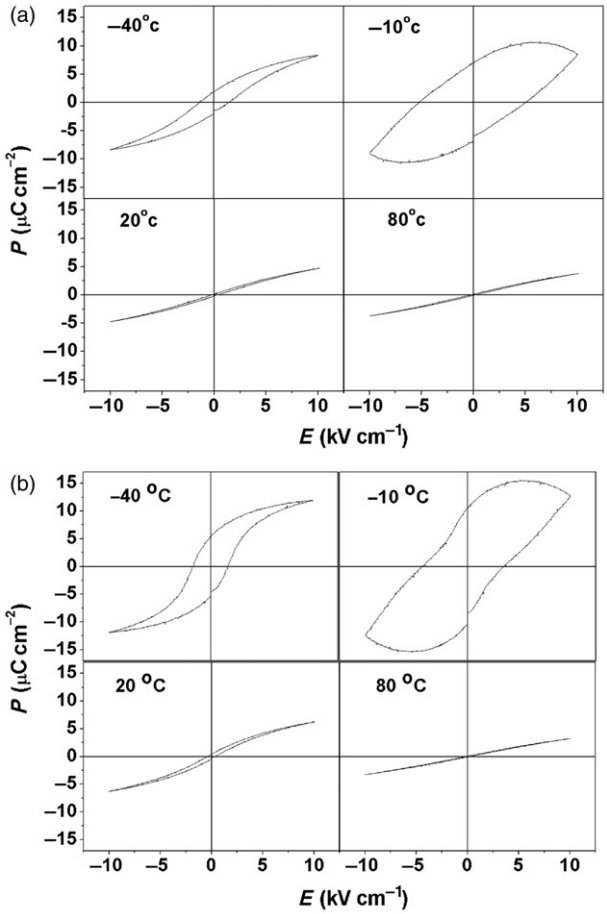

Figure 3. *P–E* hysteresis at different temperatures for BZT25 ceramics prepared by conventional ball-milling (a) and vibro-milling (b) methods.

the higher diameter should be caused by particle agglomeration. It should be noted that the splitting of the two peaks in the bimodal curve is clearly seen for the vibro-milled sample. These results suggest that the vibro-milled powder exhibited a higher degree of particle agglomeration than the conventional sample. In addition, the average particle sizes, as determined from the particle size analyzer, were 4.16 and 3.01 μm for the conventional and vibro-milled powders, respectively.

Figure 5 shows the characteristics of the raw materials after milling. The scanning electron micrographs (SEM) revealed that the powder from the vibro-milling method exhibited finer particle size than that of the conventional one. The average particle sizes, as estimated from the SEM micrographs, were 0.42 and 0.32 μm for the conventional and vibro-milled samples, respectively. Generally, a finer particle powder leads to a higher chemical reaction efficiency, and lowers the calcination temperature. Therefore, higher degree of crystallization for the final product was obtained for the vibro-milled samples.

Figure 6 shows microstructure of the powders after calcination. Values of the average particle size, as estimated from the SEM micrographs, were 0.88 and 0.82 μm for the

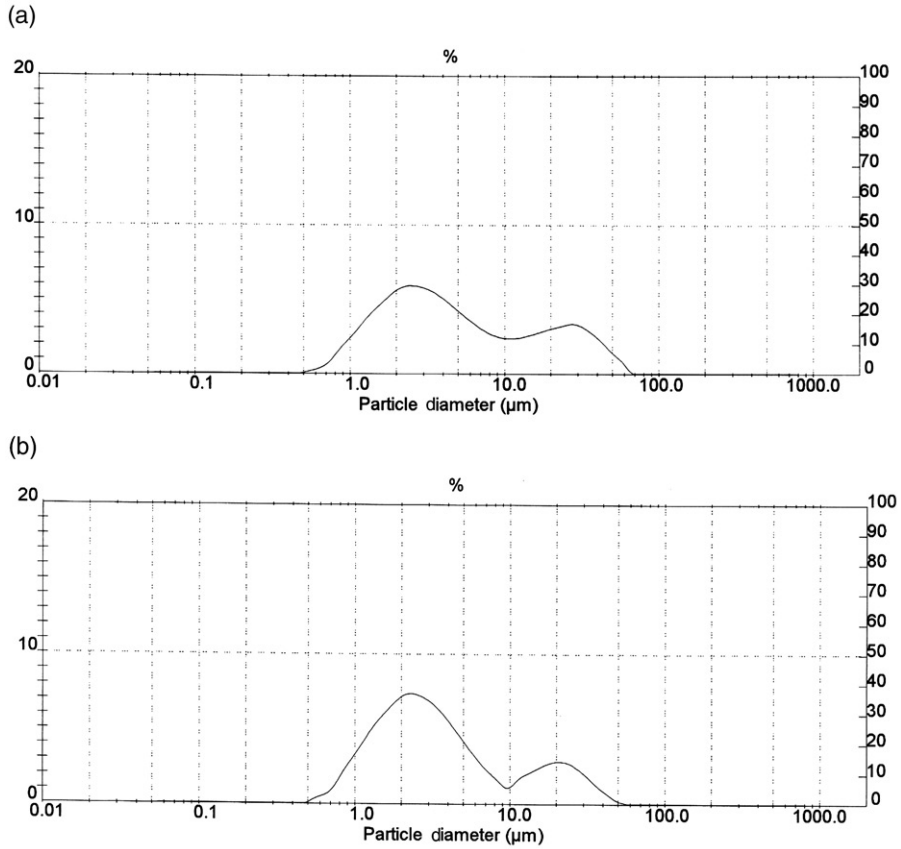

Figure 4. Particle size distribution of the calcined BZT25 powders prepared by ball-milling (a) and vibro-milling (b) methods.

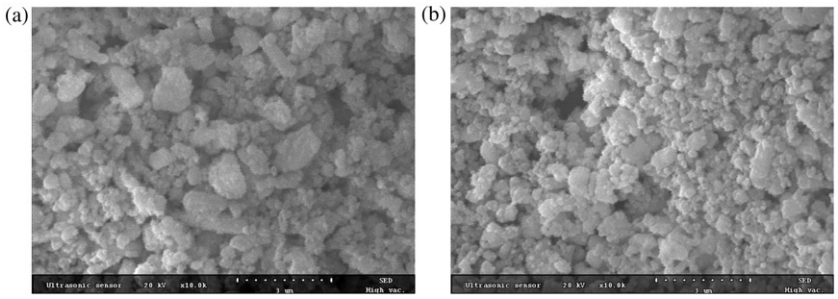

Figure 5. SEM micrographs of raw materials after ball-milling (a) and vibro-milling (b).

conventional and vibro-milled samples, respectively. Although average particle size value of each sample was closely similar, the vibro-milled sample exhibited a more non-uniform particle size. Hence, this characteristic (non-uniform particle size) may produce the higher ceramic density after sintering due to a better particle packing. It should be noted that the

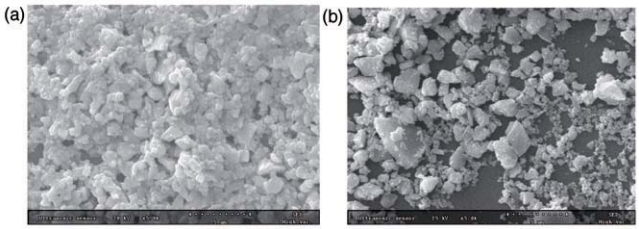

Figure 6. SEM micrographs of ball-milled powder (a) and vibro-milled powder (b) after calcination.

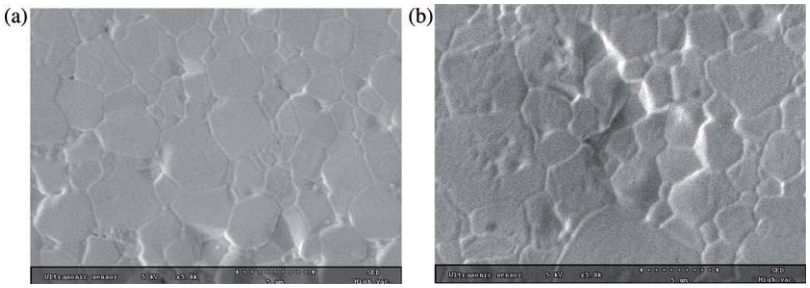

Figure 7. Surface structure of ceramic sample prepared by ball-milling (a) and vibro-milling (b).

average particle size obtained from the particle size analyzer is appreciably larger than that observed from the SEM technique. This may be due to the problem of particle agglomeration.

The microstructures of the ceramic samples are displayed in Figure 7. The average grain sizes for the conventional and vibro-milled samples were 2.4 and 3.2 μm, respectively. This result is unexpected as the vibro-milled sample showed a smaller average value of particle size than that of the conventional one. However, it can be seen from the SEM figures (Figure 7) that the vibro-milled sample exhibited a wider range of ceramic grain sizes compared to the conventional sample. This result can be related to the non-uniform range of particle size in the vibro-milled powder or particle agglomeration (after calcination). Furthermore, the high energy of vibro-milling may produce some impurity generated from the zirconia ball media. Although this impurity could not be detected by the XRD technique, it may produce a fluctuation in the mechanism of grain growth at some area, which results in the occurrence of non-uniform grain size.

In order to explain the relaxor behavior observed in this study, the microstructure of the ceramics was considered. Generally, finer grain ceramics used for relaxor ferroelectric material exhibits a lower dielectric constant (at dielectric–temperature curve), broader dielectric peak, but a higher degree of dielectric relaxation [11]. In the case of vibro-milled sample for our study, however, the evidence is complicated due to the existence of non-uniform grain size. Thus, the microstructure heterogeneity or the non-uniform grain size may produce a different local relaxor behavior resulting in the increase in average degree of dielectric relaxation for the vibro-milled samples.

4. Conclusions

The properties of $Ba(Zr_{0.25}Ti_{0.75})O_3$ ceramics prepared using the conventional and vibro-milling methods were investigated. Phase transition behaviors, dielectric, and ferroelectric

properties were found to be dependent on the method of preparation. Compared to the conventional sample, the vibro-milling sample exhibited a higher dielectric constant (at T_m) and a stronger frequency dependence of the dielectric constant. It is proposed that the characteristics of the milled and calcined powder as well as the grains of the ceramics were responsible for these experimental results.

Acknowledgements

This study was supported by The Office of the Higher Education Commission (OHEC), Faculty of Science and Graduate School, Chiang Mai University, Thailand, and the Thailand Research Fund (TRF).

References

[1] K. Uchino, *Piezoelectric Actuators and Ultrasonic Motors*, Kluwer Academic Publishers, Boston, MA, 1996.
[2] S. Nabunmee, G. Rujijanagul, N. Vittayakorn, and D.P. Cann, *Observation of high dielectric constants in* $x(Pb(Zn_{1/3}Nb_{2/3})O_3$–$(0.2-x))Pb(Ni_{1/3}Nb_{2/3})O_3$–$0.8Pb(Zr_{1/2}Ti_{1/2})O_3$ *ternary solid solutions*, J. Appl. Phys. 102 (2007), pp. 094108-1–094108-4.
[3] H. Nagata, T. Shinya, Y. Hiruma, T. Takennaka, I. Sakaguchi, and H. Haneda, *Piezoelectric properties of bismuth sodium titanate ceramics*, Mater. Electron. Dev. 167 (2004), pp. 213–221.
[4] K. Matsumoto, Y. Hiruma, H. Nagata, and T. Takenaka, *Piezoelectric properties of* $KNbO_3$ *ceramics prepared by ordinary sintering*, Ferroelectrics 358 (2007), pp. 169–174.
[5] Z. Yu, C. Ang, R. Guo, and A.S. Bhalla, *Piezoelectric and strain properties of* $Ba(Ti_{1-x}Zr_x)O_3$ *ceramics*, J. Appl. Phys. 92 (2002), pp. 1489–1493.
[6] P. Jarupoom, K. Pengpat, and G. Rujijanagul, *Enhanced piezoelectric properties and lowered sintering temperature of* $Ba(Zr_{0.07}Ti_{0.93})O_3$ *by* B_2O_3 *addition*, Curr. Appl. Phys. 10 (2010), pp. 557–560.
[7] S.K. Rout, T. Badapanda, E. Sinha, S. Panigrahi, P.K. Barhai, and T.P. Sinha, *Dielectric and phase transition of* $BaTi_{0.6}Zr_{0.4}O_3$ *ceramics prepared by a soft chemical route*, Appl. Phys. A 91 (2008), pp. 101–106.
[8] W. Cao, J. Xiong, and J. Sun, *Dielectric behavior of Nb-doped* $Ba(Zr_xTi_{1-x})O_3$, Mater. Chem. Phys. 106 (2007), pp. 338–342.
[9] Y. Wang, L. Li, J. Qi, and Z. Gui, *Ferroelectric characteristics of ytterbium-doped barium zirconium titanate ceramics*, Ceram. Inter. 28 (2002), pp. 657–661.
[10] Y. Wang, L. Li, J. Qi, and Z. Gui, *Frequency response of ZnO-doped* $BaZr_xTi_{1-x}O_3$ *ceramics*, Mater. Chem. Phys. 76 (2002), pp. 250–254.
[11] X.G. Tang, J. Wang, X.X. Wang, and H.L.W. Chan, *Effects of grain size on the dielectric properties and tunabilities of sol–gel derived* $Ba(Zr_{0.2}Ti_{0.8})O_3$ *ceramics*, Solid State Commun. 131 (2004), pp. 163–168.
[12] O. Khamman, T. Sarakonsri, A. Rujiwatra, Y. Laosiritaworn, R. Yimnirun, and S. Ananta, *Effects of milling time and calcination condition on phase formation and particle size of lead zirconate nanopowders prepared by vibro-milling*, J. Mater. Sci. 42 (2007), pp. 8438–8446.
[13] O. Khamman, A. Watcharapansorn, K. Pengpat, and T. Tunkasiri, *Fine grained bismuth sodium titanate ceramics prepared via vibro-milling method*, J. Mater. Sci. 41 (2006), pp. 5391–5394.
[14] B.D. Cullity, *Elements of X-Ray Diffraction*, 2nd ed., Addison–Wesley Company Inc., Reading, MA, 1978.
[15] H.T. Martirena and J.C. Burfoot, *Grain-size and pressure effects on the dielectric and piezoelectric properties of hot-pressed PZT-5*, Ferroelectrics 7 (1974), pp. 151–152.
[16] K. Uchino and S. Nomura, *Critical exponents of the dielectric constants in diffused-phase-transition crystal*, Ferroelectr. Lett. 44 (1982), pp. 55–61.

Current Applied Physics 10 (2010) 557–560

Contents lists available at ScienceDirect

Current Applied Physics

journal homepage: www.elsevier.com/locate/cap

Enhanced piezoelectric properties and lowered sintering temperature of $Ba(Zr_{0.07}Ti_{0.93})O_3$ by B_2O_3 addition

P. Jarupoom, K. Pengpat, G. Rujijanagul *

Department of Physics and Materials Science, Faculty of Science, Chiang Mai University, Chiang Mai 50200, Thailand

ARTICLE INFO

Article history:
Received 12 March 2009
Received in revised form 21 July 2009
Accepted 23 July 2009
Available online 28 July 2009

PACS:
77.65.Bn
77.80.Dj
81.20.Ev

Keywords:
BZT
Lead-free piezoelectric ceramic
Piezoelectric coefficient

ABSTRACT

The effects of B_2O_3 doping on densification, ferroelectric, and piezoelectric properties of $Ba(Zr_{0.07}Ti_{0.93})O_3$(BZT) ceramics were investigated. The addition of B_2O_3 to the ceramics lowered the sintering temperature by ~200 °C as well as changed their microstructures. Higher B_2O_3 concentration caused a decrease in remanent polarization and coercive field, while the piezoelectric coefficient d_{33} remained at a high value of 291 pC/N for the ceramic sample with 2 wt.% B_2O_3. The relationship between piezoelectric properties and ferroelectric constant was examined.

1. Introduction

$Pb(Zr,Ti)O_3$ (PZT) materials are the most widely use piezoelectric materials due to their superior piezoelectric properties, but they are not environmental friendly due to lead oxide toxicity. For this reason, it is desirable to find lead-free piezoelectric ceramics with equivalent properties, which could be used as a replacement for lead-based ceramics such as PZT. One of the most studied lead-free ceramics is barium zirconium titanate (BZT) [1–5]. This material is of interest as a candidate to replace lead-based materials due to its high dielectric, ferroelectric and piezoelectric properties [1]. The BZT ceramic can be formed by the substitution of Zr ions at the B site in $BaTiO_3$ lattices. This substitution significantly changes the electrical and structural properties of $BaTiO_3$ [2] including a diffuse phase transition and relaxor ferroelectric behavior [1,3].

In recent years, many researchers have focused on decreasing the sintering temperatures and improving electrical properties by adding sintering aid reagents into lead-free ceramics for many electronic applications such as multilayer capacitors [6–12]. Valant and Suvorov studied the effect of Li_2O on the properties of the $Ba_{0.6}Sr_{0.4}TiO_3$ ceramics and found an improvement of densification [6]. Rhim et al. [8,9] reported that B_2O_3 helped to improve the dielectric constant of $Ba_{0.7}Sr_{0.3}TiO_3$ ceramics. Qi et al. [10] reported that the dielectric properties of $BaTiO_3$ ceramics can be improved by B_2O_3 vapor doping. They also proposed that the boron interstitial introduced into the $BaTiO_3$ lattice resulted in an expansion of the unit-cell volume. With standard BZT ceramics, the temperature used for sintering is quite high (~1450 °C) [3]. Thus, it is interesting to lower the sintering temperature and to achieve the high electrical properties for this ceramic by adding selected sintering aids such as B_2O_3. Since ferroelectric and piezoelectric properties of B_2O_3 doped BZT ceramics have not been studied, the effects of B_2O_3 on the properties of BZT ceramics were investigated in this work.

2. Experimental

$Ba(Zr_{0.07}Ti_{0.93})O_3$ (BZT) ceramics were prepared via a conventional mixed-oxide method. Reagent-grade oxide powders of $BaCO_3$, ZrO_2, TiO_2 were used as raw materials. The metal oxide powders were weighed based on the stoichiometric formula of $Ba(Zr_{0.07}Ti_{0.93})O_3$. The weighed batch was ball-milled in alcohol and zirconia milling media for 24 h. The mixed powder was calcined at 1200 °C for 2 h. Boron oxide (B_2O_3) was added with concentrations ranging between 1 and 3 wt.% and mixed with 3 wt.% polyvinyl alcohol (PVA) binder by a ball milling method for 24 h in ethanol. The obtained powders were pressed into disc-shape pellets 10 mm in diameter. The green pellets were sintered at temperatures ranging from 1150 °C to 1450 °C for 2 h. Phase formation

* Corresponding author. Tel.: +66 53 943 376; fax: +66 53 357 512.
E-mail address: rujijanagul@yahoo.com (G. Rujijanagul).

1567-1739/$ - see front matter © 2009 Elsevier B.V. All rights reserved.
doi:10.1016/j.cap.2009.07.020

of the prepared ceramics was studied by X-ray diffraction (XRD). The bulk density of the sintered samples was measured using the Archimedes method, ASTM C 373-88. A microstructural study of the sintered samples was performed under a scanning electron microscope (SEM). For the electrical study, silver paste was painted on both sides of the samples. The hysteresis loops were measured at room temperature using a hysteresis circuit. The ceramics were poled for piezoelectric measurement in silicone oil bath at room temperature for 30 min and field strength of 3–4 kV/mm. The piezoelectric coefficients d_{33} of the samples, which were left for 24 h after poling, were measured using a d_{33} meter.

3. Results and discussion

The densities of the B_2O_3 doped BZT ceramics sintered under various sintering temperatures are shown in Fig. 1. It can be seen that concentration of B_2O_3 influenced the sintered density. A decrease in optimum density was observed for the doped BZT ceramics. It should also be noted that the 2 wt.% B_2O_3 doped ceramic had the optimum density closest to that of the unmodified ceramic. The plot of the optimum sintering temperature as a function of B_2O_3 content is shown in Fig. 2. The decrease in optimum density indicates that B_2O_3 can be used as a sintering aid to reduce the sintering temperature for BZT ceramics. In this work, it was found that the sintering temperature could be lowered by ~200 °C.

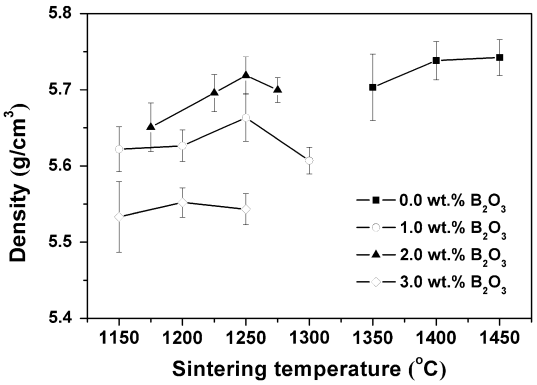

Fig. 1. Variation of density and the sintering temperature of B_2O_3 doped BZT ceramics.

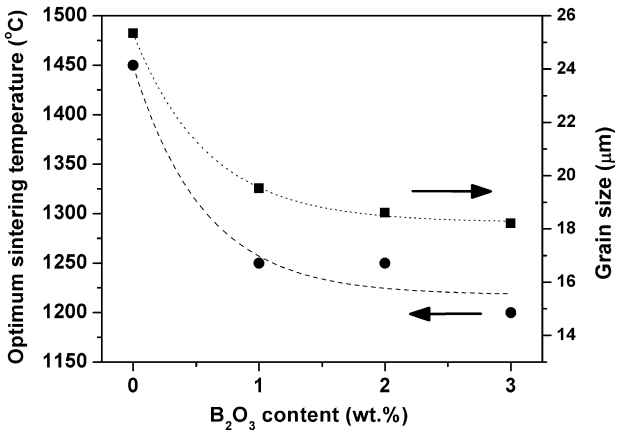

Fig. 2. Optimum sintering temperature and grain size as a function of the B_2O_3 content for B_2O_3 doped BZT ceramics.

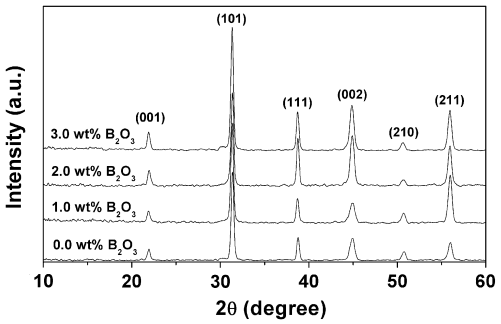

Fig. 3. X-ray diffraction patterns of B_2O_3 doped BZT ceramics sintered at the optimum sintering temperature.

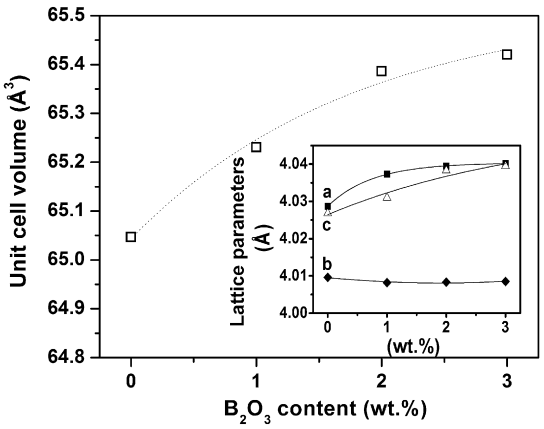

Fig. 4. Unit-cell-volume and lattice parameters of B_2O_3 doped BZT ceramics.

To investigate the phase formation, the ceramics with optimum density were examined by XRD at room temperature. Fig. 3 shows XRD patterns of B_2O_3 doped BZT ceramics. From the XRD patterns, all of the main diffraction peaks correspond to an orthorhombic perovskite phase. Plots of lattice parameters and unit-cell volume as a function of B_2O_3 content are shown in Fig. 4. An increase in unit-cell volume was observed with increasing B_2O_3 content. This increasing may be due to the introduction of boron ions in the BZT lattice [10].

SEM micrographs of the ceramic surfaces sintered at the optimum sintering temperature are shown in Fig. 5. The porosity levels in the SEM micrographs of the pellet surfaces are consistent with the trend in optimum density values. The microstructural analysis also showed that B_2O_3 additions resulted in a change in grain size (Fig. 2). Average values of grain size, as measured by the linear intercept method, decreased from 25 μm for the unmodified BZT to 18 μm for the 3 wt.% ceramics. The decrease in grain size may be due to the reduction of the optimum sintering temperature of the ceramics with increasing B_2O_3 content. However, it is believed that a partial amount of B_2O_3 could segregate to the grain boundaries, leading to the inhibition of grain growth [6].

Ferroelectric hysteresis loop measurements at room temperature were performed using a Sawyer–Tower circuit. The hysteresis loops (P–E) for various B_2O_3 contents are shown in Fig. 6. Ferroelectric properties such as saturate polarization (P_s), remanent polarization (P_r) and coercive field (E_c) are listed in Table 1. All samples show the ferroelectric behavior. However, it seems that the higher doped samples exhibit unsaturated hysteresis loops with a lower P_s Fig. 7 shows the influence of B_2O_3 doping on the leakage current density of the samples. Higher leakage current densities were observed in the higher doped samples. Therefore,

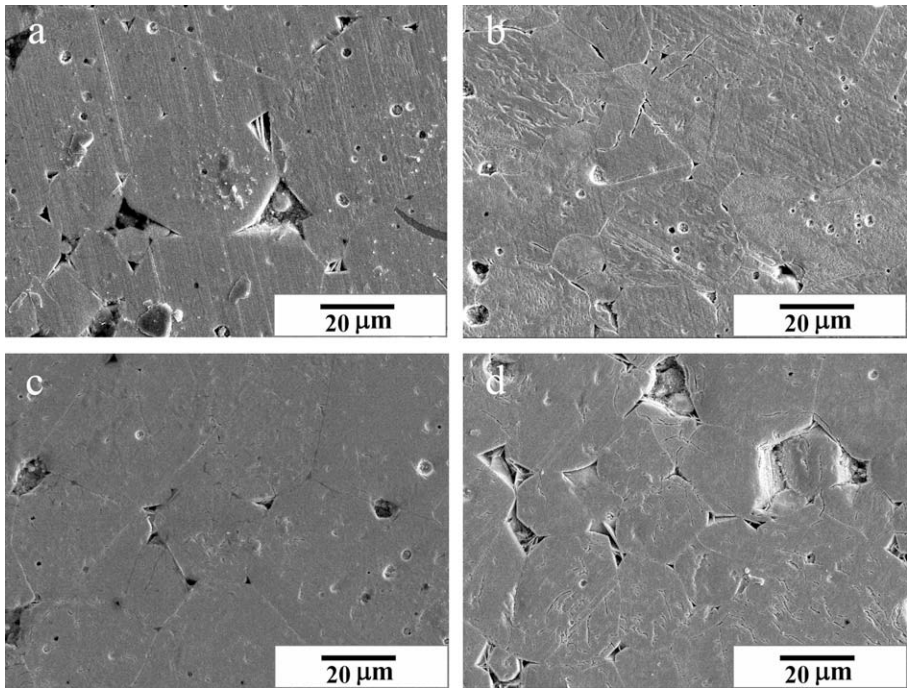

Fig. 5. SEM micrographs of ceramic surfaces of (a) pure BZT, (b) BZT – 1 wt.% B_2O_3, (c) BZT – 2 wt.% B_2O_3, and (d) BZT – 3 wt.% B_2O_3.

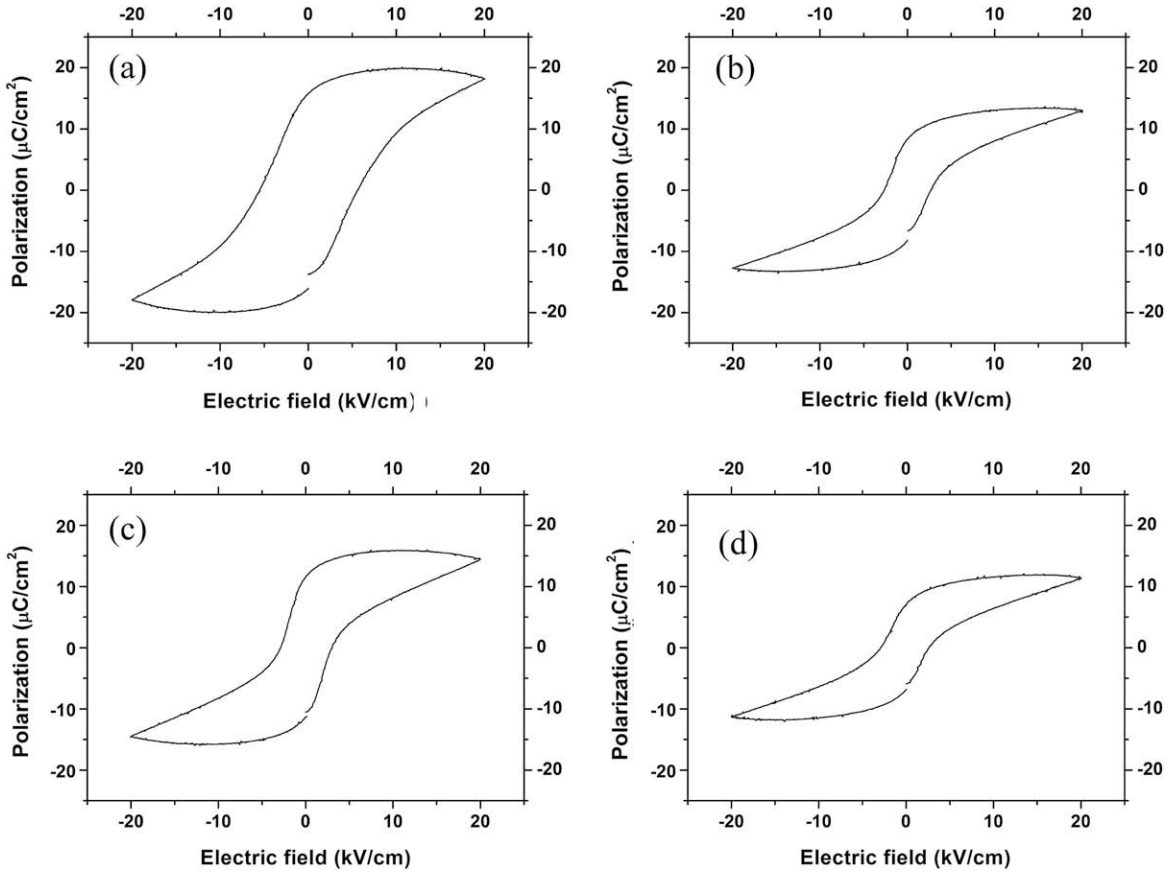

Fig. 6. Dependence of the polarization versus electric field (*P*–*E*) loop of (a) pure BZT, (b) BZT – 1 wt.% B_2O_3, (c) BZT – 2 wt.% B_2O_3, and (d) BZT – 3 wt.% B_2O_3.

the unsaturated hysteresis loops may be caused by the high leakage current density [13,14]. In addition, a decrease in E_c was found for the doped ceramics. It has been was suggested that B^{3+} ions can act as interstitial ions in ABO_3 lattice ($BaTiO_3$), due to their very small ion size [10]. In our work, it is possible that some B^{3+} ions have incorporated into the lattice of BZT as a result of a slight

Table 1
Electrical properties at room temperature of B_2O_3 doped BZT ceramics.

wt.% B_2O_3	ε_r (at 1 kHz)	P_s (μC/cm^2)	P_r (μC/cm^2)	E_c (kV/cm)	R_{sq}
0.0	2040	18.2	15.7	5.78	0.957
1.0	1910	13.5	10.4	2.82	0.797
2.0	1630	14.4	11.6	3.01	0.874
3.0	1370	11.1	7.90	4.41	0.772

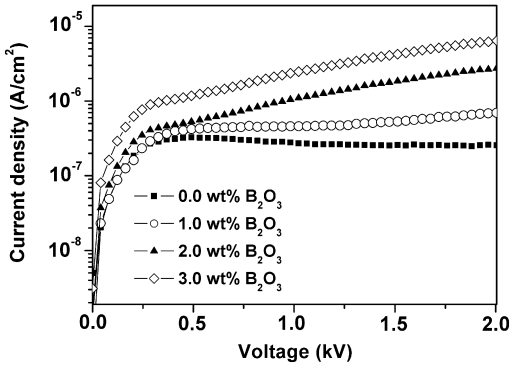

Fig. 7. Leakage current density as a function of voltage for B_2O_3 doped BZT ceramics.

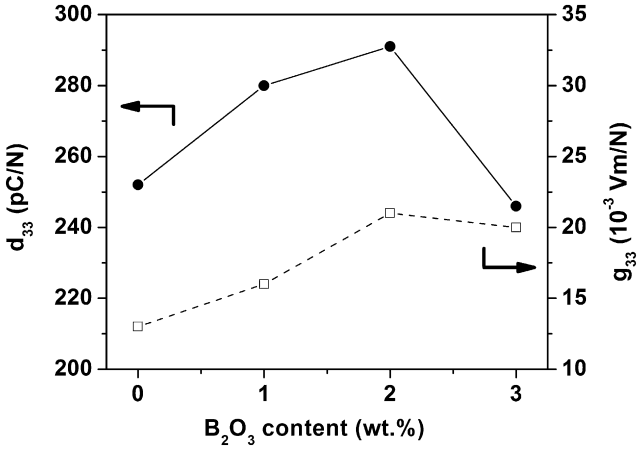

Fig. 8. Piezoelectric coefficients of B_2O_3 doped BZT ceramics.

increase in unit-cell volume (Fig. 4). In this case, some vacancies at A sites could appear in the crystal. These vacancies may reduce the inner stress and make the domain wall easy to move as a result of the reduction in E_c [12].

To check the quantification of changes in the hysteresis behavior, Haertling and Zimmer [15] derived an empirical relationship between remanent polarization, saturation polarization, and the polarization beyond the coercive field through the following equation:

$$R_{sq} = \frac{P_r}{P_s} + \frac{P_{1.1Ec}}{P_r} \quad (1)$$

where R_{sq} is the squareness of the hysteresis loop, P_r is the remanent polarization, P_s is the saturate polarization, and $P_{1.1Ec}$ is the polarization at an electric field equal to 1.1 times of the coercive field. The R_{sq} values as listed in Table 1 are in the range of ~0.85–0.9. A slightly low value of R_{sq} was found for the doped ceramics. The R_{sq} value for the 2.0 wt.% ceramic is 0.874 which is closed to the R_{sq} value of about 0.957 obtained in the unmodified ceramic, indicating that the quantification of hysteresis loop behavior is slightly changed by B_2O_3 addition.

Plots of piezoelectric coefficient d_{33} and piezoelectric voltage coefficient g_{33} as a function of B_2O_3 content are shown in Fig. 8. The coefficient g_{33} was calculated via the equation [16]:

$$g_{33} = \frac{d_{33}}{\varepsilon_0 \varepsilon_r} \quad (2)$$

where ε_0 is the permittivity of free space and ε_r is the relative permittivity. The values of ε_r measured at room temperature are listed in Table 1. The additions studied here were found to have a significant effect on the piezoelectric coefficients. An increase in the piezoelectric coefficients was observed for ceramics doped with B_2O_3 (0.0–2.0 wt.% B_2O_3). It should be noted that the 2 wt.% ceramic has a d_{33} value of 291 pC/N, which is considered as high value for lead-free piezoceramics [17]. The increased d_{33} value may be due to the low E_c value which might enable an easier poling process [18]. However, the presence of high porosity observed in the highly doped ceramic (3 wt.%) have resulted in the lowering of the d_{33} value.

4. Conclusion

Densification, ferroelectric, and piezoelectric properties of BZT ceramics added with B_2O_3 (0.0–3.0 wt.%) were investigated. The sintering temperature of the ceramics could be lowered by adding the addition. A decrease in grain size and ferroelectric properties were observed with increasing the B_2O_3 content. The modified ceramics also showed the increase in unit-cell volume. However, a high piezoelectric coefficient d_{33} was observed for the ceramics added with 2 wt.% B_2O_3. The results indicated that B_2O_3 addition could act as both sintering aid and dopant for enhancing the piezoelectric properties of the BZT ceramics.

Acknowledgements

This work was supported by The Thailand Research Fund (TRF), The Royal Golden Jubilee Ph.D. Program, Faculty of Science and Graduate School Chiang Mai University, and Commission on Higher Education (CHE) Thailand. The authors would like to thank Prof. Dr. Tawee Tunkasiri for his help in many facilities.

References

[1] Z. Yu, C. Ang, R. Guo, A.S. Bhalla, Appl. Phys. Lett. 81 (2002) 1285.
[2] C.E. Ciomaga, M.T. Buscaglia, M. Viviani, V. Buscaglia, L. Mitoseriu, A. Stancu, P. Nanni, Phase. Transit. 79 (2006) 389.
[3] Z. Yu, R. Guo, A.S. Bhalla, J. Appl. Phys. 88 (2000) 410.
[4] S. Bhaskar Reddy, K. Prasad Rao, M.S. Ramachandra Rao, Appl. Phys. A 89 (2007) 1011.
[5] P. Kantha, K. Pengpat, P. Jarupoom, U. Intatha, G. Rujijanagul, T. Tunkasiri, Curr. Appl. Phys. 9 (2009) 460.
[6] M. Valant, D. Suvorov, J. Am. Ceram. Soc. 87 (2004) 1222.
[7] D. Prakash, B.P. Sharma, T.R. Rama Mohan, P. Gopalan, J. Solid State Chem. 155 (2000) 86.
[8] S.M. Rhim, S. Hong, H. Bak, O.K. Kim, J. Am. Ceram. Soc. 83 (2000) 1145.
[9] S.M. Rhim, H. Bak, S. Hong, O.K. Kim, J. Am. Ceram. Soc. 83 (2000) 3009.
[10] J.Q. Qi, W.P. Chen, Y. Wang, H.L.W. Chan, J. Appl. Phys. 96 (2004) 6937.
[11] J.Q. Qi, Z. Gui, Y. Wang, Y. Wu, L. Li, Mater. Sci. Eng. B 95 (2002) 283.
[12] X.X. Wang, H.L.W. Chan, C.L. Choy, Appl. Phys. A 80 (2005) 333.
[13] S.K. Singh, K. Maruyama, H. Ishiwara, Appl. Phys. Lett. 91 (2007) 112913.
[14] X. Wang, H. Liu, B. Yan, J. Eur. Ceram. Soc. 29 (2009) 1183.
[15] G.H. Haertling, W.J. Zimmer, Am. Ceram. Soc. Bull. 45 (1966) 1084.
[16] A.J. Moulson, J.M. Herbert, Electroceramics Materials, Properties, Applications, second ed., J. Wiley and Sons, New York, 2003.
[17] T.R. Shrout, S.J. Zhang, J. Electroceram. 19 (2007) 111.
[18] Q. Xu, X. Chen, W. Chen, S. Chen, B. Kim, J. Lee, Mater. Lett. 59 (2005) 2437.

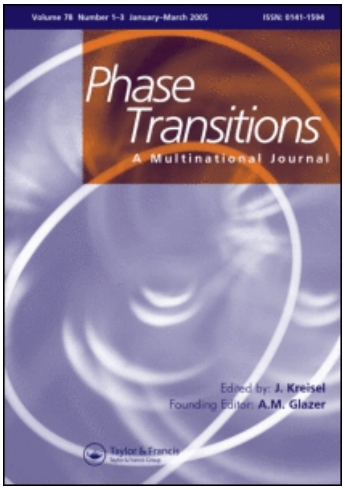

Phase Transitions
Publication details, including instructions for authors and subscription information:
http://www.informaworld.com/smpp/title~content=t713647403

Influence of B_2O_3 on electrical properties and phase transition of lead-free $Ba(Ti_{0.9}Sn_{0.1})O_3$ ceramics

N. Tawichai[a]; U. Intatha[b]; S. Eitssayeam[a]; K. Pengpat[a]; G. Rujijanagul[a]; T. Tunkasiri[a]
[a] Faculty of Science, Department of Physics, Chiang Mai University, Chiang Mai 50200, Thailand [b] School of Science, Mae Fah Luang University, Chiang Rai 57000, Thailand

Online publication date: 27 January 2010

To cite this Article Tawichai, N. , Intatha, U. , Eitssayeam, S. , Pengpat, K. , Rujijanagul, G. and Tunkasiri, T.(2010) 'Influence of B_2O_3 on electrical properties and phase transition of lead-free $Ba(Ti_{0.9}Sn_{0.1})O_3$ ceramics', Phase Transitions, 83: 1, 55 — 63
To link to this Article: DOI: 10.1080/01411590903549005
URL: http://dx.doi.org/10.1080/01411590903549005

Phase Transitions
Vol. 83, No. 1, January 2010, 55–63

Taylor & Francis
Taylor & Francis Group

Influence of B_2O_3 on electrical properties and phase transition of lead-free $Ba(Ti_{0.9}Sn_{0.1})O_3$ ceramics

N. Tawichai[a], U. Intatha[b], S. Eitssayeam[a], K. Pengpat[a], G. Rujijanagul[a]* and T. Tunkasiri[a]

[a]*Faculty of Science, Department of Physics, Chiang Mai University, Chiang Mai 50200, Thailand;* [b]*School of Science, Mae Fah Luang University, Chiang Rai 57000, Thailand*

(*Received 5 November 2009; final version received 11 December 2009*)

The phase transition and electrical properties of $Ba(Ti_{0.9}Sn_{0.1})O_3$ ceramics with B_2O_3 added were investigated to explore the effect of B_2O_3 addition on enhanced densification and dielectric constant of these ceramics. With increasing B_2O_3 content, a linear reduction of ferroelectric to paraelectric transition temperature was observed. In addition, higher B_2O_3 concentrations enhanced a ferroelectric relaxor behavior in the ceramics. Changes in this behavior were related to densification, second-phase formation and compositional variation of the ceramics.

Keywords: phase transition; dielectric properties; ceramics; sintering

1. Introduction

In recent years, $BaTiO_3$-based ceramics have received considerable attention from many researchers due to their enhanced electrical performances and environmentally friendly nature leading to their use as a replacement for lead-based ceramics such as $Pb(Zr, Ti)O_3$(PZT) [1–6]. Among the $BaTiO_3$-based ceramics, barium stannate titanate ($BaTi_{1-x}Sn_xO_3$, BTS) ceramics are of particular importance for electronic materials and have been heavily investigated for many years [7–10]. This material has a perovskite-type structure and beneficial electrical properties such as a large dielectric constant and high dielectric tunability [8,11]. The transition temperature from a ferroelectric (FE) to paraelectric (PE) state of barium titanate stannate (BTS) can be controlled by varying the Sn concentration [7]. This material also exhibits a diffuse phase transition and shows a relaxor ferroelectric behavior for some compositions [8–9]. Since BTS also has a non-toxic composition, it is a promising candidate as an environmentally friendly alternative to the traditional more toxic materials.

For multilayer capacitor applications, many researchers have focused on improving the sintering behaviors and the dielectric properties by adding additives to such $BaTiO_3$-based ceramics [12–16]. Valant and Suvorov [15] studied the effect of Li_2O on the properties of $Ba_{0.6}Sr_{0.4}TiO_3$ ceramics. Although the densification of their ceramics was improved, Li_2O had only a small effect on the transition temperature. Rhim et al. [13,14] reported

*Corresponding author. Email: rujijanagul@yahoo.com

ISSN 0141–1594 print/ISSN 1029–0338 online

DOI: 10.1080/01411590903549005
http://www.informaworld.com

that B_2O_3 helped to increase the dielectric constant of $Ba_{0.7}Sr_{0.3}TiO_3$ ceramics. Further, Qi et al. [16] found that the positive temperature coefficient resistivity (PTCR) effect in $BaTiO_3$-based ceramics was improved by B_2O_3 vapor doping. However, the effects of B_2O_3 addition on phase transition and electrical properties such as dielectric, ferroelectric, and piezoelectric properties of BTS ceramics have not been widely investigated. It is expected that the electrical properties of BTS ceramics should be improved by B_2O_3 doping. Therefore, the present work was aimed at studying the effects of B_2O_3 on the properties of BTS ceramics. BTS ceramics of the composition $Ba(Ti_{0.9}Sn_{0.1})O_3$ were doped with B_2O_3 and prepared by a solid state reaction to investigate their electrical properties.

2. Experimental

Ceramics of $Ba(Ti_{0.9}Sn_{0.1})O_3$ were prepared via the conventional method. $Ba(Ti_{0.9}Sn_{0.1})O_3$ powder was produced by the mixed-oxide technique using reagent grade $BaCO_3$, SnO_2, and TiO_2. The starting powders were then mixed and ball-milled in isopropanol for 24 h using zirconia grinding media. After mixing, the slurry was dried, sieved and calcined for 2 h at 1300°C. B_2O_3 powder, equivalent to 1.0, 2.0, and 3.0 wt.%, was then blended to calcined $Ba(Ti_{0.9}Sn_{0.1})O_3$ powder. The mixed powders, with the addition of polyvinyl alcohol as an organic binder, were then ball-milled in isopropanol for 24 h. This slurry was dried at 150°C and sieved to form a fine powder which was pressed at 100 MPa into 15 mm diameter pellets. The pellets were then sintered at 1350°C for 4 h with a heating/cooling rate of $5^\circ C\,min^{-1}$ after binder burnout at 500°C for 1 h. Phase formation of the sintered samples was checked using a Bruker D8 Advance diffractometer with a Cu-Kα source. The sintered ceramics were also crushed into powders for an X-ray diffraction (XRD) experiment. The dielectric properties and phase transition behaviors were studied at frequencies of 1–500 kHz in the temperature range from −20°C to 100°C using a dielectric measurement system consisting of a HP 4276A LCZ meter and a furnace tube. Polarization was also measured as a function of electric field, using a Sawyer–Tower circuit. Finally, the piezoelectric coefficients (d_{33}) were measured using a PM-3001 d_{33} piezometer. Before the d_{33} measurement was performed, the samples were left for 24 h after poling at $1.5\,kV\,cm^{-1}$.

3. Results and discussion

3.1. *Phase formation and densification*

The XRD patterns for the sintered ceramic powders containing B_2O_3 up to 3.0 wt.% are shown in Figure 1(a). The XRD results reveal that the main phase of the samples has a perovskite structure. However, a single-phase perovskite was observed for unmodified and 1.0 wt.% samples and small amounts of $BaTi_4O_9$ and $BaTi_5O_{11}$ were found in the 2.0 wt.% sample. In the case of higher B_2O_3 concentrations (3.0 wt.%), another phase of $Ba_2Ti_9O_{20}$ occurred. These results indicate that increased B_2O_3 addition promoted the formation of secondary phases which may in turn produce a change in composition of the samples. Wang et al. [17] reported that $Ba_2Ti_9O_{20}$ could be formed by adding B_2O_3 in a mixture phase of $BaTi_4O_9$ and $BaTi_5O_{11}$. In the present work, the higher B_2O_3 addition may help the $BaTi_4O_9$ and $BaTi_5O_{11}$ components (occurred in the 2.0 wt.% sample) transform to $Ba_2Ti_9O_{20}$, which presented the 3.0 wt.% sample.

From Figure 1(a), the shift in the XRD peak position with increasing B_2O_3 addition indicates a change in lattice parameter. Variation in cell dimensions with B_2O_3 addition

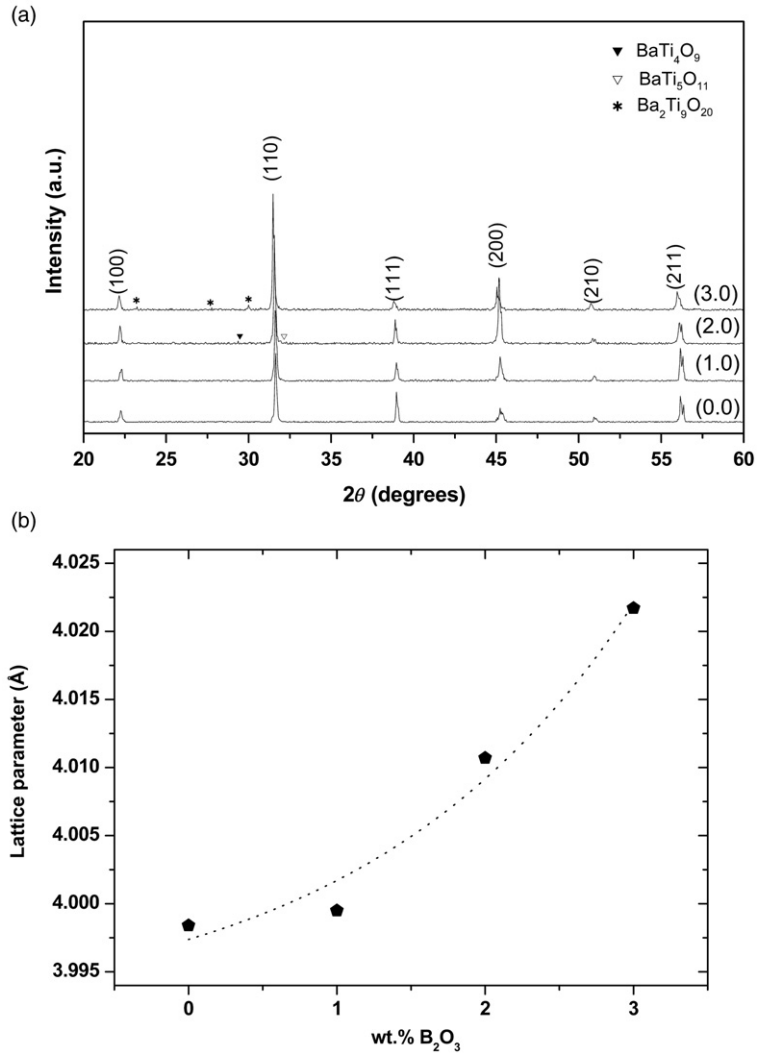

Figure 1. (a) XRD patterns at room temperature of $Ba(Ti_{0.9}Sn_{0.1})O_3$ ceramics as a function of B_2O_3 content, (b) Variation of lattice parameter as a function of B_2O_3 content.

was calculated using an equivalent cubic cell parameter (Figure 1(a)) corresponding to the unit cell volume as a pseudo-cubic [10,18]. A plot of the lattice parameter as a function of B_2O_3 addition is shown in Figure 1(b). An increase in lattice parameter with increasing B_2O_3 addition was observed. This implies a lattice distortion in the modified samples.

The sintered density values of the samples for various B_2O_3 content are shown in Figure 2. The density increases from $5.231\,g\,cm^{-3}$ for the unmodified sample to $5.681\,g\,cm^{-3}$ for the 2.0 wt.% sample then decreased to $5.380\,g\,cm^{-3}$ for the 3.0 wt.% sample. It is known that B_2O_3 can be melted at a low temperature (~450°C). Therefore, the B_2O_3 may have formed a liquid phase at a relative low temperature, which promoted sintering [17]. However, it is believed that solid-state sintering becomes dominant and assists the densification at a high temperature. In this work, the optimized amount of B_2O_3 addition for obtaining an optimum density is 2.0 wt.%. An overdoping of B_2O_3 (3.0 wt.%)

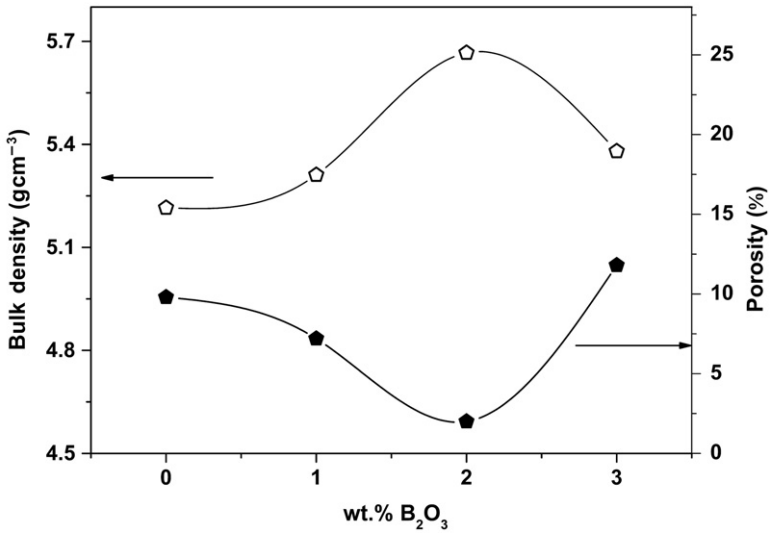

Figure 2. Density and porosity of sintered samples as a function of B_2O_3 content.

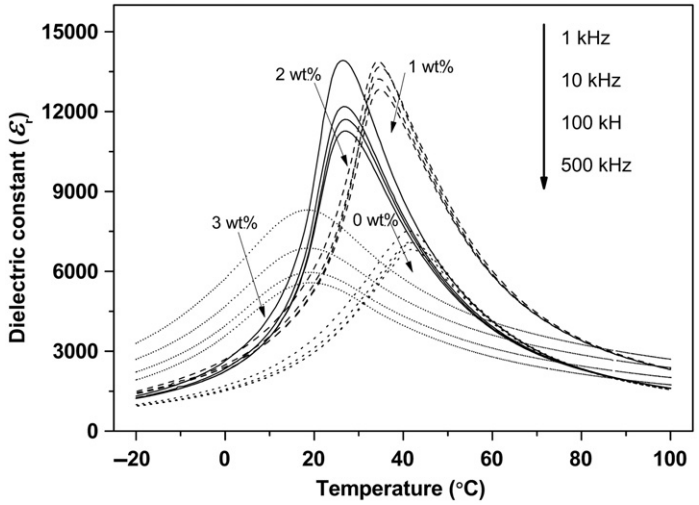

Figure 3. Dielectric constant versus temperature for $Ba(Ti_{0.9}Sn_{0.1})O_3$ ceramics with differing amounts of B_2O_3 contents.

may have caused a higher porosity due to the formation of the another phase. A similar result was reported in a previous work [19].

3.2. *Dielectric properties*

Figure 3 shows the dielectric constant and dielectric loss of the samples as a function of temperature. The dielectric data reveals that B_2O_3 addition has a significant effect on the dielectric constant. The values of the dielectric constant at the dielectric peak ($\varepsilon_{r,\max}$) as a function of B_2O_3 content are shown in Figure 4. The maximum value of $\varepsilon_{r,\max}$ of 13,900

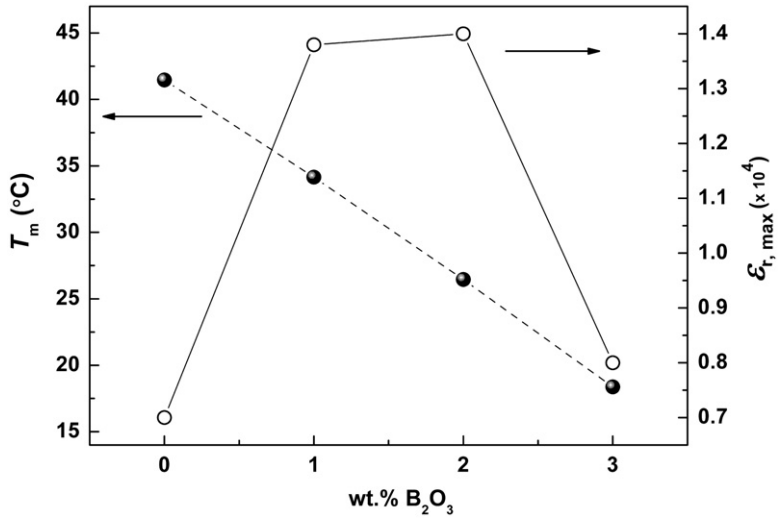

Figure 4. Transition temperature (T_m) and maximum dielectric constant ($\varepsilon_{r,max}$) of the ceramics as a function of B_2O_3 content.

Table 1. Electrical properties of B_2O_3 doped $Ba(Ti_{0.9}Sn_{0.1})O_3$ ceramics.

Amount of B_2O3 (wt.%)	$\varepsilon_{r,room}$	$\tan\delta_{room}$	$\varepsilon_{r,max}$	$\tan\delta_{max}$	δ_γ (°C)	P_r ($\mu C\,cm^2$)	E_c (kV cm)	d_{33} ($pC\,N^{-1}$)
0.0	4400	0.085	7500	0.045	15.8	1.1138	0.271	104
1.0	8400	0.069	13,800	0.035	16.1	1.6600	0.383	107
2.0	13,800	0.123	13,900	0.115	14.0	1.6968	0.542	Break down
3.0	7700	0.155	8300	0.178	28.1	0.9448	0.568	Break down

was recorded for the 2.0 wt.% sample, which is ~46% higher than that of the undoped sample. The temperature dependences of the dielectric constant in the samples depict a frequency dispersion of the dielectric peak. For the unmodified sample, weak frequency dispersion behavior was observed. However, an enhancement of frequency dependence of the dielectric constant was found for higher B_2O_3 contents. The frequency dependence of higher doped samples (2–3 wt.% samples) is also stronger than that in [9] for the same composition. This implies that ferroelectric relaxor behavior was enhanced. It should be noted that the value of the dielectric constant for the 1.0 wt.% sample was found to be close to the value obtained for the 2.0 wt.% sample, which is unexpected because the 2.0 wt.% sample has the maximum density. This result may be due to the existence of a second phase in the 2.0 wt.% sample which deteriorated the dielectric constant. For higher B_2O_3 concentrations (3.0 wt.%), the sample presented a lower dielectric constant, which may be due to the presence of another phase and higher porosity.

Values of the dielectric loss ($\tan\delta$) of undoped and doped ceramics are shown in Table 1. The $\tan\delta$ at room temperature (denote as $\tan\delta_{room}$) and at $\varepsilon_{r,max}$ (denote as $\tan\delta_{max}$) has a trend to increase with B_2O_3 content. However, high $\tan\delta_{room}$ and $\tan\delta_{max}$ (>0.1) was observed for 2.0 and 3.0 wt.% sample, implying that these samples have lower resistivity.

3.3. *Phase transition studies*

The transition temperature (T_m) at the dielectric maximum peak of the dielectric curve ($\varepsilon_{r,max}$) as a function of B_2O_3 concentration is shown in Figure 4. The T_m at the dielectric peak was observed to decrease linearly from 41°C for the unmodified sample to 18°C for the 3.0 wt.% sample. This result indicates that the T_m of this system can be controlled by the addition of B_2O_3. In this work, lattice distortion and compositional variation may be the major reasons for this behavior. It was suggested from the literature that B ions can act as interstitial ions in $BaTiO_3$ lattice due to their very small ionic radius which can cause a lattice distortion [16]. Although the structure of $Ba(Ti_{0.9}Sn_{0.1})O_3$ in this work is complex compared to $BaTiO_3$ and it has a symmetry close to cubic, it is believed that some B ions can be incorporated into lattices. The incorporation of B ions may produce lattice distortion and defects at A sites in the samples [16]. Furthermore, a second-phase formation in the sample may cause the compositional variation. These changes may also have produced a difference in local transition temperatures, resulting in the shift of T_m [20]. It has been suggested that the paraelectric side of the permittivity curve, having diffuse phase transition, can be written as [21]

$$\frac{\varepsilon_{r,max}}{\varepsilon_r} = \exp\left(\frac{(T - T_m)^2}{2\delta_\gamma^2}\right)$$

where $\varepsilon_{r,max}$ is maximum value of the relative permittivity at transition temperature ($T = T_m$); ε_r is the dielectric constant of sample; and δ_r is diffuseness parameter of the transition. The value of δ_r can be calculated from $\ln(\varepsilon_{r,max}/\varepsilon_r)$ *versus* $(T - T_m)^2$ curve [22]. This value is valid for the range of $(\varepsilon_{r,max}/\varepsilon_r) < 1.5$, as clarified by Pilgrim et al. [21]. The values of parameter δ_r for various B_2O_3 contents are listed in Table 1. The parameter δ_r was laid between 14.0 and 28.1 K. The lower value of δ_r was observed in the 2.0 wt.% sample, indicating that 2.0 wt.% B_2O_3 addition promoted a sharper phase transition in the $Ba(Ti_{0.9}Sn_{0.1})O_3$ system.

3.4. *Ferroelectric and piezoelectric properties*

In the present work, the ferroelectric properties of the ceramics were measured using a Sawyer–Tower circuit at room temperature. The hysteresis loops (P–E) for various B_2O_3 contents are shown in Figure 5. All samples showed a slim ferroelectric hysteresis loop. Ferroelectric properties including the saturated polarization (P_r), and coercive field (E_c) are listed in Table 1. A slight change in the ferroelectric properties was observed for the 1.0–2.0 wt.% samples. For the 3.0 wt.% sample, the hysteresis loop became more slanted with a lower P_r value. The existence of a ferroelectric hysteresis loop above the transition temperature (~18°C) for the 3.0 wt.% sample, indicates a relaxor behavior which confirms the dielectric result [23]. It should be noted that higher B_2O_3 samples showed an unsaturated hysteresis loop. Previous work suggested that [24–25] the unsaturated hysteresis loop could be related to a high leakage current. To check this possibility, the leakage current densities of the samples were measured. A plot of leakage current density as a function of applied voltage and annealing time is displayed in Figure 6. Higher leakage current densities were observed for longer annealed samples, as expected. This result is thus confirmed that the high B_2O_3 content samples have lower resistivity. Therefore, samples with 2.0 and 3.0 wt.% B_2O_3 exhibited lower dielectric strengths. These samples can easily break down in the poling process. However, the d_{33}

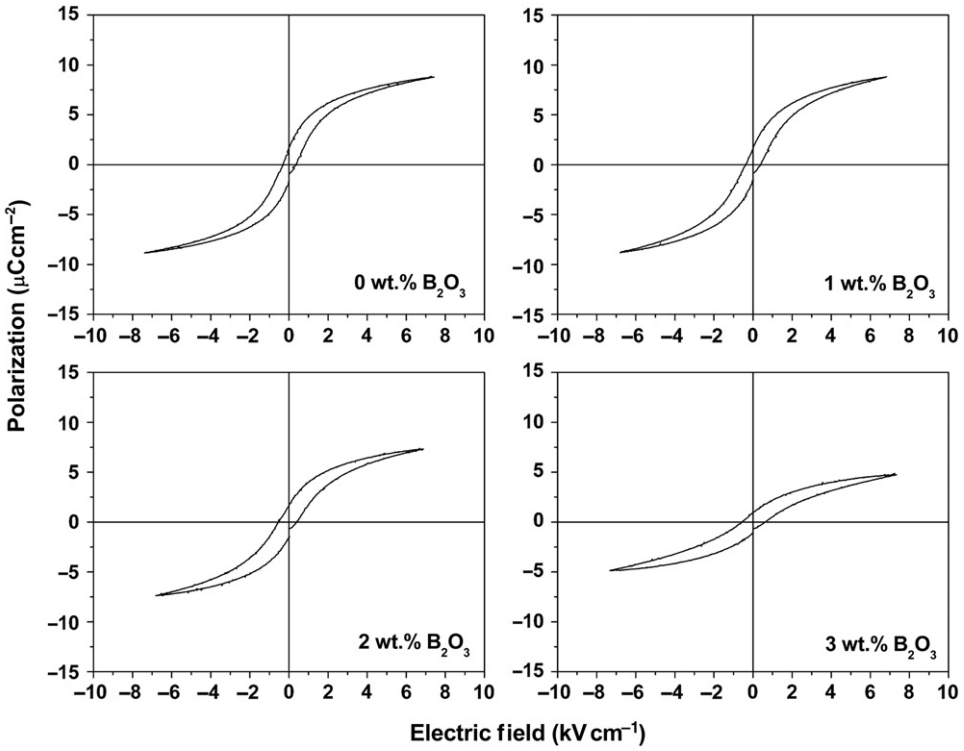

Figure 5. Dependence of the polarization versus electric field (P–E) loop on the B_2O_3 dopant concentration.

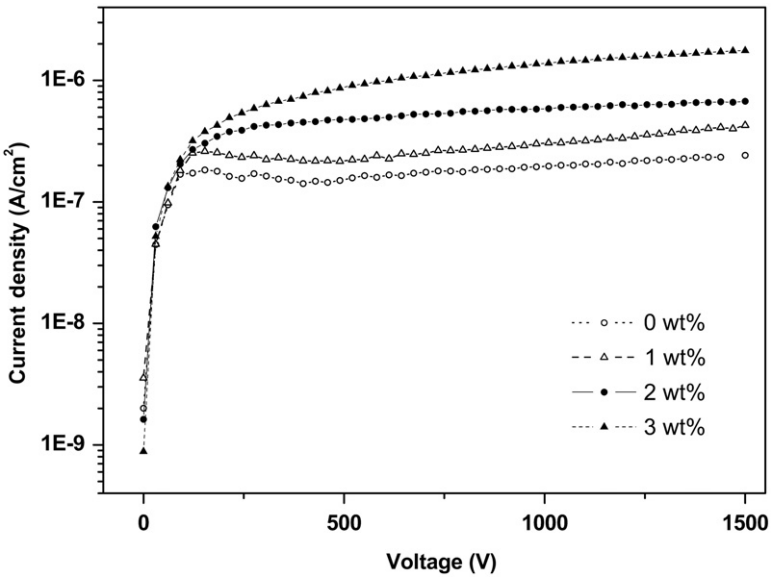

Figure 6. Leakage current density as a function of voltage for B_2O_3-doped $Ba(Ti_{0.9}Sn_{0.1})O_3$ ceramics.

values were measured to be 104 and 107 pC N^{-1} for the undoped and 1.0 wt.% samples, respectively (Table 1).

4. Conclusions

In the present work, we demonstrated that B_2O_3 has significant effects on the electrical properties and phase transition behavior of $Ba(Ti_{0.9}Sn_{0.1})O_3$ ceramics. The density and dielectric constant were enhanced by adding B_2O_3 up to 2.0 wt.%. This dielectric result indicates that high B_2O_3 content produced a reduction in the FE–PE transition temperatures. In addition, B_2O_3 addition enhanced the ferroelectric relaxor behavior in the ceramics.

Acknowledgements

The authors would like to thank the Commission on Higher Education (CHE) for supporting by grant fund under the program Strategic Scholarships for Frontier Research Network for the Join PhD Program Thai doctoral degree for this research. This work was also supported by the Faculty of Science and Graduate School Chiang Mai University, The Thailand Research Fund (TRF), National Nanotechnology Center (NANOTEC), NSTDA, Thailand.

References

[1] A.J. Moulson and J.M. Herbert, *Electroceramics; Materials, Properties, Applications*, 2nd ed., J. Wiley and Sons, New York, 2003.
[2] T.R. Shrout and S.J. Zhang, *Lead-free piezoelectric ceramics: Alternatives for PZT*, J. Electroceram. 19 (2007), pp. 111–124.
[3] M. Kumar, A. Garg, R. Kumar, and M.C. Bhatnagar, *Structural, dielectric and ferroelectric study of $Ba_{0.9}Sr_{0.1}Zr_xTi_{1-x}O_3$ ceramics prepared by the sol–gel method*, Physica B 403 (2008), pp. 1819–1823.
[4] C.R.K. Mohan and P.K. Bajpai, *Effect of sintering optimization on the electrical properties of bulk $Ba_xSr_{1-x}TiO_3$ ceramics*, Physica B. 403 (2008), pp. 2173–2188.
[5] P. Jarupoom, K. Pengpat, N. Pisitpipathsin, S. Eitssayeam, U. Intatha, T. Tunkasiri, and G. Rujijanagul, *Development of electrical properties in lead-free bismuth sodium lanthanum titanate–barium titanate ceramic near the morphotropic phase boundary*, Curr. Appl. Phys. 8 (2008), pp. 253–257.
[6] K. Pengpat, S. Hanphimol, S. Eitssayeam, U. Intatha, G. Rujijanagul, and T. Tunkasiri, *Morphotropic phase boundary and electrical properties of lead-free bismuth sodium lanthanum titanate–barium titanate ceramics*, J. Electroceram. 16 (2006), pp. 301–305.
[7] J.N. Lin and T.B. Lu, *Effects of isovalent substitutions on lattice softening and transition character of $BaTiO_3$ solid solutions*, J. Appl. Phys. 68 (1990), pp. 985–993.
[8] W. Xiaoyong, F. Yujun, and Y. Xi, *Dielectric relaxation behavior in barium stannate titanate ferroelectric ceramics with diffused phase transition*, Appl. Phys. Lett. 83 (2003), pp. 2031–2033.
[9] V.V. Shvartsman, J. Dec, Z.K. Xu, J. Banys, P. Keburis, and W. Kleemann, *Crossover from ferroelectric to relaxor behaviour in $BaTi_{1-x}Sn_xO_3$ solid solutions*, Phase Transitions. 81 (2008), pp. 1013–1021.
[10] J. Zhai, B. Shen, X. Yao, L. Zhang, and H. Chen, *Dielectric properties of $Ba(Sn_xTi_{1-x})O_3$ thin films grown by a sol–gel process*, J. Am. Ceram. Soc. 87 (2004), pp. 2223–2227.
[11] Z. Jiwei, S. Bo, Y. Xi, and Z. Liangying, *Dielectric and ferroelectric properties of $Ba(Sn_{0.15}Ti_{0.85})O_3$ thin films grown by a sol–gel process*, Mater. Res. Bull. 39 (2004), pp. 1599–1606.

[12] D. Prakash, B.P. Sharma, T.R.R. Mohan, and P. Gopalan, *Flux additions in barium titanate: Overview and prospects*, J. Solid State Chem. 155 (2000), pp. 86–95.
[13] S.M. Rhim, S. Hong, H. Bak, and O.K. Kim, *Effects of B_2O_3 addition on the dielectric and ferroelectric properties of $Ba_{0.7}Sr_{0.3}TiO_3$ ceramics*, J. Am. Ceram. Soc. 83 (2000), pp. 1145–1148.
[14] S.M. Rhim, H. Bak, S. Hong, and O.K. Kim, *Effects of heating rate on the sintering behavior and the dielectric properties of $Ba_{0.7}Sr_{0.3}TiO_3$ ceramics prepared by boron-containing liquid-phase sintering*, J. Am. Ceram. Soc. 83 (2000), pp. 3009–3013.
[15] M. Valant and D. Suvorov, *Low-temperature sintering of $(Ba_{0.6}Sr_{0.4})TiO_3$*, J. Am. Ceram. Soc. 87 (2004), pp. 1222–1226.
[16] J.Q. Qi, Z. Qing, W. Yongli, W. Yajing, and L. Longtu, *Enhancement of positive temperature coefficient resistance effect of $BaTiO_3$-based semiconducting ceramics caused by B_2O_3 vapor dopants*, Solid State Commun. 120 (2001), pp. 505–508.
[17] S.F. Wang, C.C. Chung, C.H. Wang, and J.P. Chu, *Effects of B_2O_3 on the phase stability of $Ba_2Ti_9O_{20}$ microwave ceramic*, J. Am. Ceram. Soc. 85 (2002), pp. 1619–1621.
[18] Y.-L. Tu, J.M. Herbert, and S.J. Milne, *Fabrication and characterization of high permittivity ceramics in the $Ba(Ti_{1-x-y}Sn_xZr_y)O_3$ system*, J. Mater. Sci. 29 (1994), pp. 4152–4156.
[19] C. Huan, Y. Chen, and C. Tasi, *Influence of B_2O_3 additions to $0.8(Mg_{0.95}Zn_{0.05})TiO_3$–$0.2Ca_{0.61}Nd_{0.26}TiO_3$ ceramics on sintering behavior and microwave dielectric properties*, J. Ally. Comp. 460 (2008), pp. 675–679.
[20] P.V. Divya and V. Kumar, *Crystallization studies and properties of $(Ba_{1-x}Sr_x)TiO_3$ in borosilicate glass*, J. Am. Ceram. Soc. 90 (2007), pp. 472–476.
[21] S.M. Pilgrim, A.E. Sutherland, and S.R. Winzer, *Diffuseness as a useful parameter for relaxor ceramics*, J. Am. Ceram. Soc. 73 (1990), pp. 3122–3125.
[22] G. Rujijanagul and N. Vittayakorn, *Influence of fabrication processing on phase transition and electrical properties of $0.8Pb(Zr_{1/2}Ti_{1/2})O_3$–$0.2Pb(Ni_{1/3}Nb_{2/3})O_3$ ceramics*, Curr. Appl. Phys. 8 (2008), pp. 88–92.
[23] Z. Wang, X. Li, X. Long, and Z.G. Ye, *Characterization of relaxor ferroelectric behavior in the $(1-x)Ba(Yb_{1/2}Nb_{1/2})O_3$–$xPbTiO_3$ solid solution*, Scr. Mater. 60 (2009), pp. 830–833.
[24] S.K. Singh, K. Maruyama, and H. Ishiwara, *Reduced leakage current in La and Ni codoped $BiFeO_3$ thin films*, Appl. Phys. Lett. 91 (2007), pp. 112–913.
[25] B. Yan, H. Liu, and X. Wang, *Enhanced ferroelectric properties of Ce-substituted $BiFeO_3$ thin films on $LaNiO_3$/Si substrates prepared by sol–gel process*, J. Eur. Ceram. Soc. 29 (2009), pp. 1183–1187.

Materials and Design xxx (2009) xxx–xxx

Contents lists available at ScienceDirect

Materials and Design

journal homepage: www.elsevier.com/locate/matdes

Short Communication

Processing and properties of nanoporous hydroxyapatite ceramics

A. Raksujarit [a], K. Pengpat [b], G. Rujijanagul [b,*], T. Tunkasiri [b]

[a] Department of Science, Faculty of Science and Technology, Chiang Mai Rajabhat University, Chiang Mai 50300, Thailand
[b] Department of Physics, Faculty of Science, Chiang Mai University, Chiang Mai 50200, Thailand

ARTICLE INFO

Article history:
Received 10 September 2008
Accepted 2 June 2009
Available online xxxx

ABSTRACT

Method for fabrication and properties of nanoporous hydroxyapatite (HA) ceramic were described in the present work. The nanoporous hydroxyapatite was derived from nano hydroxyapatite powder and polyvinyl alcohol (as a pore former). The HA nanopowder was obtained from vibro-milling for 4 h. The nanoporous ceramics were sintered at 1200 °C. Properties of the nanoporous ceramics were investigated using various methods. Average porosity of the final product was found to be 64.6 ± 1.4%. Open and interconnected pores were obtained with an average pore size less than 100 nm, confirming the nanoporous structure of this ceramic. A high bending strength of 14.7 ± 3.2 MPa for the nanoporous ceramic, shows significant promise as a potential bone repairing material.

1. Introduction

For many years, bioceramics, especially hydroxyapatite (HA) have shown significant promise in the biomedical industry as a material to improve the quality of human life. Hydroxyapatite, $Ca_{10}(PO_4)_6(OH)_2$, is a bioceramic with excellent biocompatibility and bioactivity with the human body [1–4] which makes it a material of considerable interest for medical applications. In addition to structural applications, porous HA ceramics can be used as a platform for controlled drug delivery systems, such as in the delivery of anti-tumor agents and antibodies for the treatment of osteomyelilis [4]. To optimize HA material porosity for drug delivery, the control of the three-dimensional (3-D) pore structure is of critical importance [5]. Such an optimized pore structure could enhance the possibility of tissue in-growth of natural bone, and offer greater drug-loaded regions with a large surface to volume ratio [4,5]. However, HA porous ceramics have traditionally exhibited poor mechanical performance, which has restricted their use in many applications [1–3]. Recently, it was found that nanocrystalline HA offers an approach to overcome some of the limitations of conventional HA materials. Nanostructured HA materials can improve sinterability and densification due to their greater surface area, which could improve fracture toughness and other critical mechanical properties [1–3]. Consequently nano HA ceramics are expected to have a better bioactivity than that of coarser HA crystals [2].

In the present work, a nanoporous HA ceramic was fabricated from the mixed powders of natural bovine bone and polyvinyl alcohol (PVA). To obtain the nanopowder, a vibro-milling method was used in the fabrication process. Properties including porosity, phase, microstructures and bending strength of the samples were investigated and reported.

2. Materials and methods

The hydroxyapatite powder under study here was derived from natural bovine bone by a sequence of thermal processes. The fresh bones were cut into small pieces and well cleaned to remove macroscopic adhering impurities. The bone samples were then boiled in distilled water for 8 h to simplify the removal of the bone marrow and tendons. After that the bone was deproteinized by continued boiling in water. The boiling treated bone samples were then dried overnight at 200 °C. The deproteinized bone was further calcined at 800 °C for 3 h to sterilize the samples so that no prions or disease-causing agents could contaminate the samples. The resulting product was crushed into small pieces and milled in a ball mill pot for 24 h. The bone powder was mixed with polyvinyl alcohol (PVA) of 40 wt.% and ball milled in ethanol for 24 h. To obtain the HA nanopowder, the mixture was then milled by a vibro-milling method for 4 h. The obtained powder was pressed into a disc shape with an uniaxial pressing machine. To obtain the best condition for sintering, many sintering conditions were examined. The densities of the sintered samples were measured by the Archimedes method using distilled water as the fluid medium. X-ray diffraction analysis (XRD) was also performed to study the phase formation of the samples. Bending strength was investigated using a ball-on-ring test [6] and the microstructure of the sample was examined using a scanning electron microscopy (SEM).

* Corresponding author. Tel.: +66 53 943376; fax: +66 53 357512.
E-mail address: rujijanagul@yahoo.com (G. Rujijanagul).

0261-3069/$ - see front matter © 2009 Elsevier Ltd. All rights reserved.
doi:10.1016/j.matdes.2009.06.050

3. Results and discussions

The XRD pattern of the powder obtained after vibro-milling is shown in Fig. 1. A standard HA phase was observed which corresponds to that of the standard JCPDS File No. 9432. No impurity in the powder was detected by XRD, confirming the purity of this prepared HA powder within the limitation of the XRD method. Comparing the generated materials with a calcined powder (Fig. 1), there are no obvious changes in structure and phase composition. However, drop in XRD intensity peaks indicates that the vibro-milling process produced a smaller HA particle size.

Fig. 2 shows a SEM micrograph of the HA nanoparticles after vibro-milling at 4 h. It can clearly be seen that the hydroxyapatite powder is composed of a nanorod-like shape with diameter less than 100 nm. HA ceramics were fabricated using this HA nanopowder. Various sintering temperatures ranging from 1150 to 1300 °C were used. Fig. 3 shows the XRD patterns of the HA ceramics from various sintering temperatures. The XRD results reveal that the main phase of these ceramics is HA. However, beta-tricalcium phosphate (β-TCP) was observed in all samples. In addition, alpha-tricalcium phosphate (α-TCP) was found in the sample sintered at 1300 °C. The existence of α-TCP and β-TCP are due to a gradual loss of the radical OH^- in the structure when HA is heated in air to above 800 °C [7]. This process called dehydroxylation is an irreversible process. It has been also suggested that during heating, HA materials tend to lose H_2O above the critical point [7]. The densities of samples sintered at various sintering temperatures are listed in Table 1. The ceramics sintered at 1200 °C and 1250 °C showed a maximum density of 3.01 gm/cm^3.

The bending strength of the ceramics was determined using a ball-on-ring tester [6]. The strength was calculated via the equation;

$$\sigma = \frac{3F(1+\nu)}{4\pi t^2}\left[\frac{(1-\nu)}{(1+\nu)}\cdot\frac{2a^2-b^2}{2R^2}+2\ln\left(\frac{a}{b}\right)+1\right] \quad (1)$$

where σ is the strength in MPa; F the breaking load in Newton; ν the Poisson ratio; a the radius of the support; R the radius of the samples; t the thickness of the sample; and b is the $t/3$. The values for the bending strength of the samples sintered at various sintering temperatures are listed in Table 1. A sharp increase in the sample strength was observed at sintering temperatures of 1150–1200 °C, and strength values were found to decrease as the temperature was increased above this range. A maximum bending strength of 88.6 MPa was observed in the sample sintered at 1200 °C. The improvement in bending strength might be due to the formation of nanorod structures in the matrix of the ceramics as seen in Fig. 4. The mechanism for the nanorod formation is unclear, but the results indicate that nanorod reinforcement may attribute to the increase in strength. For higher sintering temperatures, the reduction of strength may be caused by the increased formation of β-TCP and α-TCP as observed by XRD [8–10].

In order to fabricate nanoporous hydroxyapatite ceramics, 40 wt.% of PVA was added into the HA powder and then milled with a vibro-milling machine. The mixed powder was then pressed

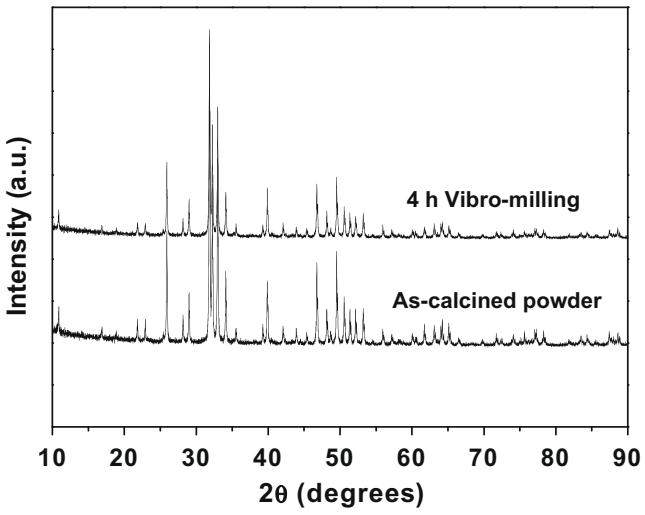

Fig. 1. XRD patterns of as-calcined and nano HA powders.

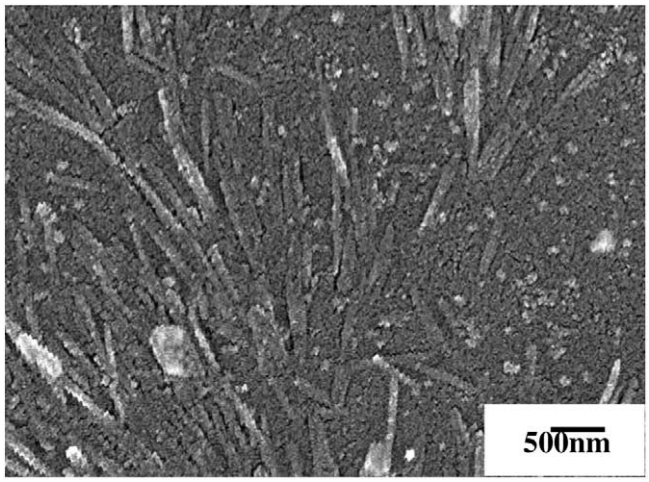

Fig. 2. SEM micrograph of HA nanopowder.

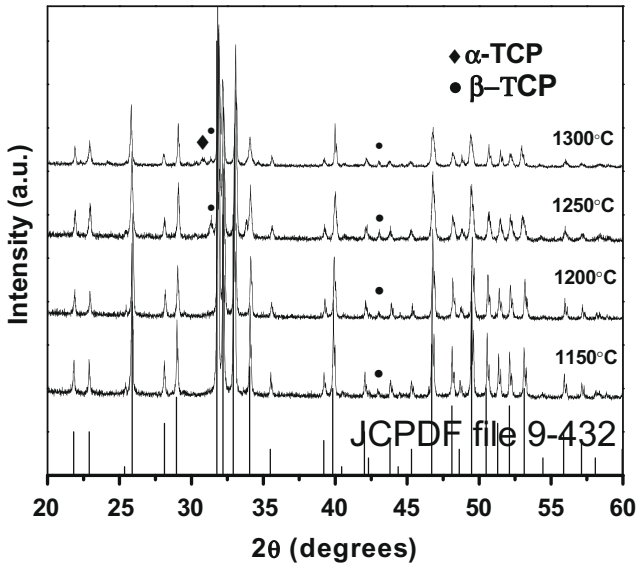

Fig. 3. X-ray diffraction patterns of various HA ceramics sintered at 1150–1300 °C.

Table 1
Density and bending strength of the ceramics sintered at various sintering temperatures.

Sintering temperature (°C)	Bulk density (g/cm^3)	Bending strength (MPa)
1150	2.32 ± 0.01	45.6 ± 4.6
1200	3.01 ± 0.01	88.6 ± 3.0
1250	3.01 ± 0.01	55.5 ± 2.8
1300	2.97 ± 0.01	36.4 ± 3.6

Please cite this article in press as: Raksujarit A et al. Processing and properties of nanoporous hydroxyapatite ceramics. J Mater Design (2009), doi:10.1016/j.matdes.2009.06.050

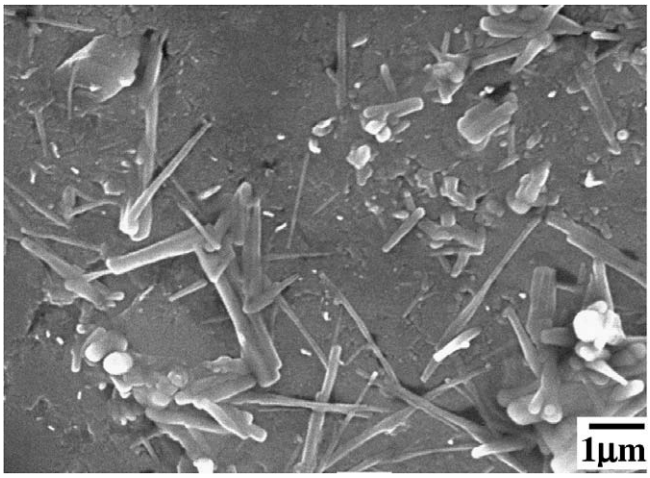

Fig. 4. SEM micrograph of fracture surface of sample sintered HA at 1200 °C.

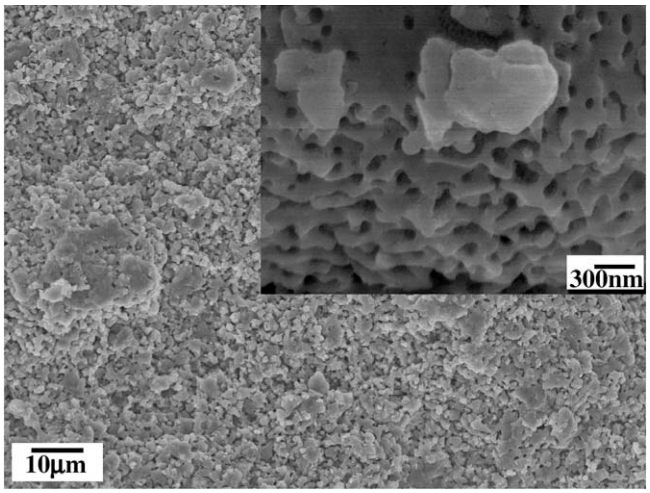

Fig. 5. SEM micrographs of fracture surfaces of nanoporous HA ceramics. Inset shows at high magnification.

into a disc shape and sintered at standard atmospheric pressure. The sintering temperature of 1200 °C was selected because this condition produced the optimum ceramics properties, as described in the previous section. Fig. 5 shows the SEM micrographs of these porous ceramics. These ceramics were permeated with a matrix of interconnected pores. The SEM image at higher magnifications illustrate that the porous structure looks quite strong and crack free (Fig. 5b). The average pore size were found to be less than ~100 nm. The porosity was determined to be 64.6 ± 1.4% which confirmed the high porosity of the sample. Using a ball-on-ring test, the bending strength value of the sample was found to be 14.7 ± 3.2 MPa. This value is high enough for easy handing and shaping of porous samples for implantation as well as having a decent load bearing capacity after surgery [11]. It has been proposed that the nanoporous structure of some biomaterials could enhance cell adhesion, proliferation and differentiation [1,2,12]. Therefore, our nanoporous ceramic having the optimum strength could have a high potential to support bone tissue in-growth upon implantation in the future and to improved load bearing properties.

4. Conclusions

In this work, we demonstrate a method to fabricate the nanoporous ceramics derived from nano HA powder and PVA. The nano HA power was obtained from natural bovine bone after being subjected to vibro-milling for 4 h. The optimized sintering temperature of 1200 °C was found to best generate dense HA ceramics. This sintering temperature was then used to fabricate nanoporous HA ceramics for further study. These nanoporous HA ceramics showed an interconnected nanopous structure with pore sizes less than 100 nm. A high bending strength of ~15 MPa was obtained. This nanoporous ceramic has a potential for using in many areas of medical applications.

Acknowledgement

This work was supported by Faculty of Science and Graduate School Chiang Mai University, and Commission on Higher Education (CHE) Thailand.

References

[1] Murugan R, Ramakrishna S. Development of nanocomposites for bone grafting. Compos Sci Technol 2005;65:2385–406.
[2] Kalita SJ, Bhardwaj A, Bhatt HA. Nanocrystalline calcium phosphate ceramics in biomedical engineering. Mater Sci Eng C 2007;27:441–9.
[3] Banerjee A, Bandyopadhyay A, Bose S. Hydroxyaapatite nanopowder: synthesis, densification and cell-materials interaction. Mater Sci Eng C 2007;27:729–35.
[4] Li Y, Tjandra W, Tam KC. Synthesis and characterization of nanoporous hydroxyapatite using cation surfactants as templates. Mater Res Bull 2008;43:2318–26.
[5] Jie W, Yubao L. Tissue engineering scaffold materials of nano-apatite crystal and polyamide composite. E Polym J 2004;40:509–15.
[6] Dewith G, Wagemans HHM. Ball-on-ring test revisited. J Am Ceram Soc 1989;72(8):1538–41.
[7] Fang W, Mu-sen L, Yu-peng L, Yong-xin Q. A simple sol–gel technique for preparing hydroxyapatite nanopowders. Mater Lett 2005;59:916–9.
[8] Suchanek W, Yashimura M. Processing and properties of hydroxyapatite-based biomaterials for use as hard tissue replacement implants. J Master Res 1998;13:94–117.
[9] Lopes MA, Monterio FJ, Santos JD. Glass–reinforced hydroxyapatite composites: fracture toughness and hardness dependence on microstructural characteristics. Biomaterials 1999;20:2085–90.
[10] Goller G, Demirkiran H, Oktar FN, Demirkesen E. Processing and characterization of bioglass reinforces hydroxyapatite composite. Ceram Int 2003;29:721–4.
[11] Landi E, Tampieria A, Celottia G, Langenatib R, Monica S, Sprio S. Nucleation of biomimetic apatite in synthetic body fluids: dense and porous scaffold development. Biomaterials 2005;26:2835–45.
[12] Murugan R, Ramakrishna S, Panduranga Rao K. Nanoporous hydroxycarbonate apatite scaffold made of natural bone. Mater Lett 2006;60:2844–7.

Please cite this article in press as: Raksujarit A et al. Processing and properties of nanoporous hydroxyapatite ceramics. J Mater Design (2009), doi:10.1016/j.matdes.2009.06.050

Current Applied Physics 9 (2009) 993–996

Contents lists available at ScienceDirect

Current Applied Physics

journal homepage: www.elsevier.com/locate/cap

Effect of the solid-state synthesis parameters on the physical and electronic properties of perovskite-type $Ba(Fe,Nb)_{0.5}O_3$ ceramics

S. Eitssayeam [a,*], U. Intatha [b], K. Pengpat [a], G. Rujijanagul [a], K.J.D. MacKenzie [c], T. Tunkasiri [a]

[a] Department of Physics, Faculty of Science, Chiang Mai University, Chiang Mai 50200, Thailand
[b] School of Science, Mae Fah Luang University, Chiang Rai 57100, Thailand
[c] School of Chemical and Physical Science, Victoria University of Wellington, P.O. Box 600, Wellington, New Zealand

ARTICLE INFO

Article history:
Received 13 May 2008
Received in revised form 7 July 2008
Accepted 27 October 2008
Available online 5 November 2008

PACS:
77.22.−d
77.84.Dy
81.40.Rs

Keywords:
Solid-state reaction
Dielectric properties
Barium iron niobate

ABSTRACT

Single-phase cubic $Ba(Fe,Nb)_{0.5}O_3$ (BFN) powder was synthesized by solid-state reaction at 900, 1000, 1100, 1200 °C for 4 h in air. X-ray diffraction indicated that the BFN oxide mixture calcined at 1200 °C crystallizes to the pure cubic perovskite phase. The crystallite size of the BFN increases slightly with increasing temperature, while the lattice strain progressively decreases. BFN ceramics were produced from this powder by sintering at 1350–1400 °C for 4 h in air. Samples prepared under these conditions achieved up to 97.4% of the theoretical density. The temperature dependence of their dielectric constant and loss tangent, measured at difference frequencies, shows an increase in the dielectric constant with sintering temperature and measurement frequency which is probably due to disorder on the B site ion of the perovskite. The Mössbauer spectra of these sintered BFN ceramics suggests the presence of a superstructure on the B-cation sublattice.

1. Introduction

Perovskite – type ceramics ABO_3 are widely used in the electronics industry. Of these materials, the complex perovskites $A(B_IB_{II})O_3$, are particularly attractive for applications such as microwave frequency resonators, capacitors or various types of detectors. The high value of the dielectric constant of perovskites over a very wide temperature interval is due to disorder in the distribution of the B-site ions in the perovskite unit cell. This may lead to composition fluctuations and, as a consequence, to different local Curie temperatures in the different regions of the ceramic [1]. High values of the dielectric constant (ε_r) over a wide temperature range have recently been reported by Yokosuka [2], Tezuka et al. [3], Raevskite et al. [1], and Saha and Sinha [4,5] in ceramic samples of the ternary perovskite $Ba(Fe,Nb)_{0.5}O_3$ (BFN). Some of these workers have assumed that BFN is a relaxor ferroelectric, but the phenomenon of its dielectric behavior is not clearly understood. In general, BFN ceramics require very high sintering temperatures to achieve satisfactory density and high dielectric constant. Sintering at about 1350–1400 °C produces materials with a dielectric constant (ε_r) of 30,000. This study focuses on the solid-state preparation of BFN ceramics, with particular reference to the effect of the calcination and sintering conditions on the dielectric behavior and physical properties of the ceramic, with the aim of achieving optimal properties at moderate processing temperatures.

2. Experimental

Barium iron niobate ($Ba(FeNb)_{0.5}O_3$: BFN) was synthesized by solid-state reaction of appropriate mixtures of barium carbonate, $BaCO_3$ (Fluka, 99.0% purity), iron oxide, Fe_2O_3 (Riedel – deHaën, 99.0% purity) and niobium oxide, Nb_2O_5 (Aldrich, 99.9% purity). The powders were milled together in ethanol for 24 h in a polyethylene container with zirconia balls, dried at 120 °C and calcined at temperatures ranging from 900 to 1200 °C, with a dwell time of 4 h and a heating/cooling rate of 5 °C/min. The thermal reactions of these powder mixtures were investigated by thermogravimetry and differential thermal analysis, using a heating rate of 10 °C/min in air from room temperature to 1250 °C. The calcined powders were subsequently examined at room temperature by X-ray diffraction using Cu Kα radiation (XRD; Siemens D500/D501) to identify the phase composition of each calcined sample. The powder produced under the optimum calcining conditions was pressed into discs using polyvinyl alcohol as a binder and sintered at various temperatures from 1250 to 1400 °C, with a dwell time of 4 h at

* Corresponding author. Tel.: +66 5394 3376; fax: +66 5335 7512.
E-mail address: sukum99@yahoo.com (S. Eitssayeam).

1567-1739/$ - see front matter © 2008 Elsevier B.V. All rights reserved.
doi:10.1016/j.cap.2008.10.003

a heating and cooling rate of 5 °C/min. The densities of the sintered discs were determined using the Archimedes principle. The sintered samples were polished to obtain plane and parallel surfaces and silver paste electrodes were applied for the purpose of the dielectric measurements which were made at 1 KHz to 1 MHz and temperatures of −50 to 300 °C using a precision impedance analyzer (Agilent 4294A). The room temperature Mössbauer spectra of the powdered sintered samples were recorded using a conventional microcomputer-controlled spectrometer in the sinusoidal mode. The ^{57}Co/Rh source had a maximum activity of 1.85 GBq and the isomer shifts are quoted with respect to the midpoint of the magnetic spectrum of natural iron. The spectra were fitted to Lorentzian lineshapes using the commercially available fitting program NORMOS written by R.A. Brand (distributed by Wissenschaftliche Elektronik GmbH, Germany).

3. Results and discussion

TGA and DTA curves of the BFN precursor mixture are shown in Fig. 1. The solid-state reactions in this precursor are marked by two distinct weight losses, one above ≈600 °C and the other above 1000 °C. In the temperature range from room temperature to ≈600 °C, the sample shows a small broad exothermic DTA peak at 524 °C, attributed to the decomposition of the organic species from the milling process and the carbonate reactant. The calculated loss of CO_2 corresponds well with the weight loss indicated by the TGA curve. The endothermic peak at 814 °C corresponds to the transition of α-Fe_2O_3 to β-Fe_2O_3 as reported by Cahn and Lifshin [6]. The exothermic peak at ≈1000 °C arises from the solid-state reaction between barium oxide, iron oxide and niobium oxide. Another small exothermic peak at ≈1200 °C probably corresponds to a phase transition.

The X-ray diffraction (XRD) patterns of the calcined powders (Fig. 2) indicate that the formation of pure cubic $Ba(FeNb)_{0.5}O_3$ (BFN) begins at about 900 °C and is complete at about 1200 °C (ICSD file number 52835 [7]), consistent with the DTA peak at 1200 °C (Fig. 1). Therefore, the optimum calcination temperature of 1200 °C was chosen to subsequently produce BFN powder in this work in order to confirm the complete reaction and high purity. The cubic cell parameter (a) of this compound is 4.080 Å, in the space group $Pm3m$. Our results are in agreement with Rama et al. [8] and Tezaka et al. [3] who also prepared this compound by solid-state reaction. However, Saha and Sinha [4] deduced a monoclinic-type BFN structure by using a standard computer program (POWD) analysis. Based on the DTA and XRD data we conclude that over a wide range of calcination conditions, pure BFN can be formed by a solid-state mixed oxide synthetic route. The present results suggest that the optimal calcination conditions for producing single-phase BFN are 1200 °C for 4 h with heating/cooling rates of 5 °C/min.

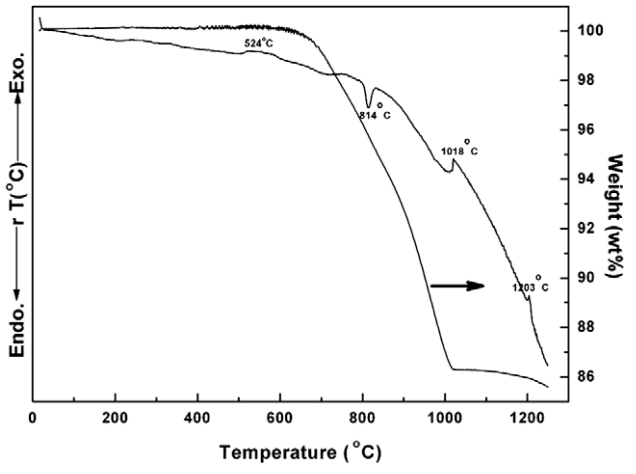

Fig. 1. DTA and TGA curves of the BFN precursor.

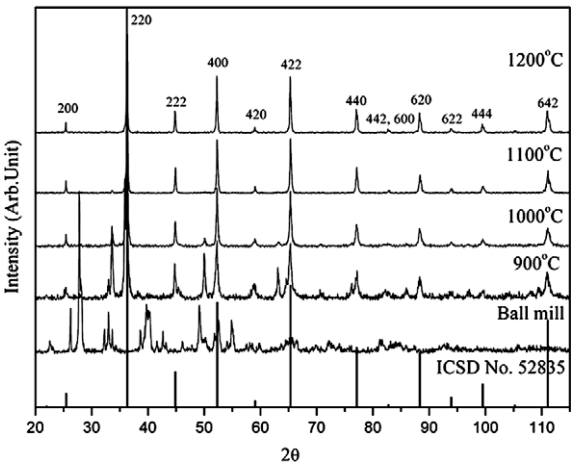

Fig. 2. XRD patterns of calcined BFN powder.

The crystallite size and lattice strain of powder were also estimated from the XRD profiles. The crystallite size thus measured is the size of coherently diffracting domains and is not necessarily the same as the size of the polycrystalline aggregates. The crystallite size was estimated from the Scherrer formula [9]:

$$t = \frac{0.89\lambda}{B\cos\theta} \quad (1)$$

where B is the broadening of diffraction line (in radians), t is the diameter of the crystal particle, θ is the maximum intensity peak angle and λ is the wavelength of the X-rays used. The lattice strain, defined as the change in length per unit length, is determined as the change in the d spacing of the strained sample by comparison with the unstrained state. The relationship between the strain (ε) and the line broadening β is defined as [10]:

$$\varepsilon = \frac{\beta}{4\tan\theta} \quad (2)$$

where β is the integral breadth of line profile ($\beta = A/I_{max}$, A is the peak area and I_{max} is the maximum height of the peak). The calculated crystallite sizes and lattice strain of the powders produced under different calcination conditions are shown in Table 1. In general, the crystallite size of the BFN powder increases slightly with increasing temperature, while the lattice strain progressively decreases, in good agreement with Tunkasiri and Lewis [11]. The strain in the diffracting planes originates from microstresses caused by structural imperfections which may be related to the grain size [12]. At lower temperatures the kinetic energy is not sufficient to decompose the powder, whereas at high temperatures the kinetic and chemical driving forces increase sufficiently to promote diffusional processes and influence the reaction kinetics, reducing the imperfections in the crystal [13].

Table 1
Effect of calcination temperature on the variation of crystallite size and strain of BFN powder.

Calcination Temperature (°C)	Crystallite size (nm)	Lattice strain (%)
900	62	1.13
1000	83	0.55
1100	97	0.44
1200	105	0.38

The densities of the BFN ceramics increase with sintering temperature, these are 4.6, 4.8, 6.1 and 6.2 g/cm^3 for sintering at 1250, 1300, 1350 and 1400 °C, respectively, the maximum density being recorded for a sample sintered at 1400 °C (6.2 g/cm^3, or 94.7% of the theoretical density (reported in ICSD) [7]). It is known that the relative density is the most important factor for a dielectric material since the dielectric constants are in good correlation with relative density, hence the highly dense samples sintered at 1350 and 1400 °C were selected for the dielectric property measurements, made as a function of temperature from −50 to 300 °C at different frequencies. The variation of dielectric constant and dielectric loss with temperature is shown in Figs. 3 and 4. Both dielectric constant (ε_r) and dielectric loss (tan δ) were found to decrease for a given frequency. There are two possible explanations for the systematic increase in dielectric constant with sintering temperature. One possibility is that it is due to increased conductivity in the samples, suggested by Ananta and Thomas [14] to result from the presence of Fe^{2+} in sintered BFN ceramics. The concentration of such species is known to be highly sensitive to the sintering temperature, increasing with increasing temperature [15]. It is known that the co-existence of Fe^{2+} and Fe^{3+} on equivalent crystallographic sites can give rise to an electron-hopping conduction mechanism, which, owing to its finite hopping (or jump) probability, tends to come into effect at lower frequencies. An alternative explanation is related to disorder in the B site cations, as suggested by Majumder et al. [16] to occur in complex perovskites. In $A(B_IB_{II})O_3$-type perovskites such as $Pb(Fe^{+3}_{0.5}Nb^{+5}_{0.5})O_3$, the $Fe^{+3}(B_I)$ and $Nb^{+5}(B_{II})$ ions randomly occupy the octahedral *B* sites

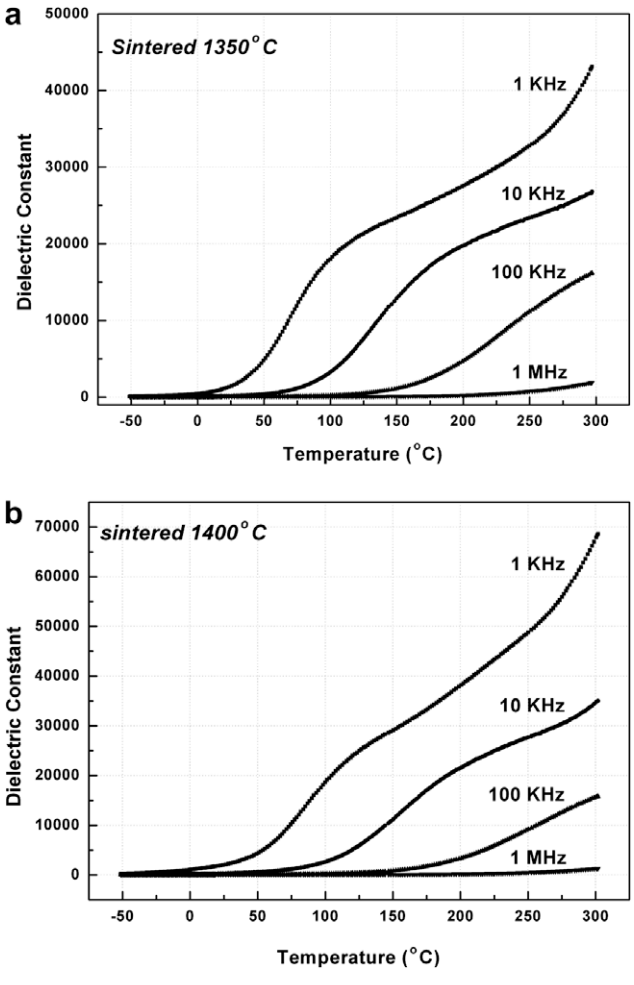

Fig. 3. Dielectric constant of BFN ceramics at various frequencies.

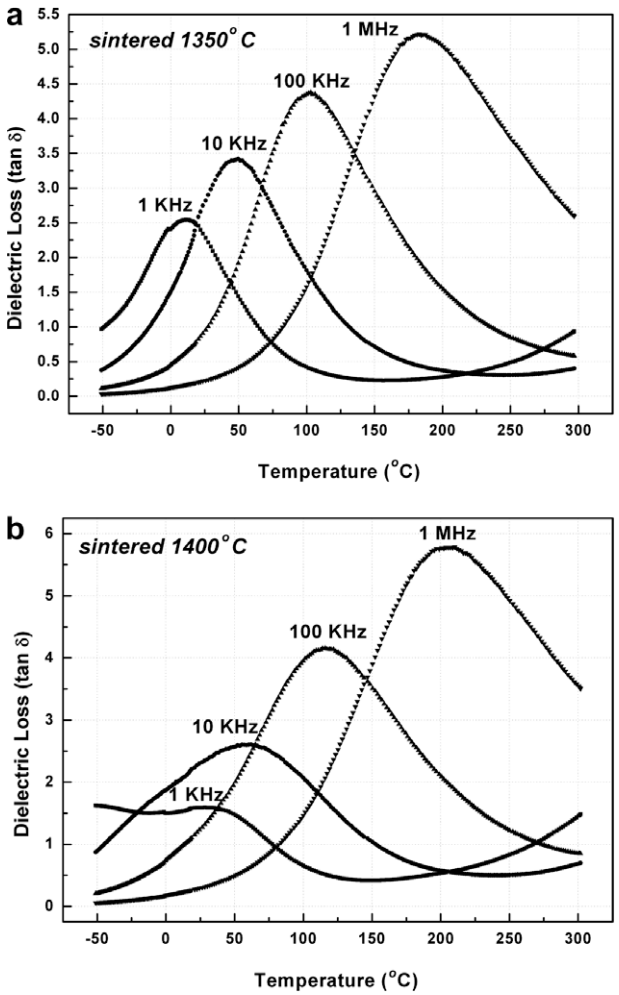

Fig. 4. Comparison of the 1 KHz dielectric properties of BFN ceramics sintered at 1350 °C and 1400 °C.

surrounded by O^{-2} anions. Due to the presence of larger $Fe^{+3}(B_I)$ cations, a larger "rattling space" is available for the relatively smaller $Nb^{+5}(B_{II})$ cations. When an oscillating ac signal is applied to such disordered systems, the smaller B_{II} cations (with a large rattling space) can readily move without distorting the oxygen framework. In an ordered perovskite, a comparatively smaller rattling space is available for B site cations. Therefore a larger dielectric constant is expected in disordered complex perovskites such as PFN compared with ordered perovskites (e.g., $PbTiO_3$).

To attempt to distinguish between these two possible explanations, the room temperature Mossbauer spectra were determined of the present BFN ceramics sintered at 1350 and 1400 °C (Fig. 5). The spectra of BFN prepared at both temperatures can be fitted to two quadrupole doublets with isomer shifts (δ) and quadrupole splitting (ΔE_Q) values shown in Table 2. In both sintered samples, the occupancy of the site corresponding to the wider-spaced doublet 2, as determined from the fitted peak area, is considerably less than the site occupancy of doublet 1, and decreases slightly with increased sintering temperature (24.3% and 22.7% in the samples sintered at 1350 °C and 1400 °C, respectively). The isomer shift values for both doublets in both samples are similar, falling in the range for high-spin ferric iron [17]. However, these values also overlap with the values for low-spin ferrous ion, making it impossible to distinguish between these two valency states on the basis of isomer shifts alone. The doublets of site 1 with quadrupole splitting values in the range 0.43–0.45 mm/s fall

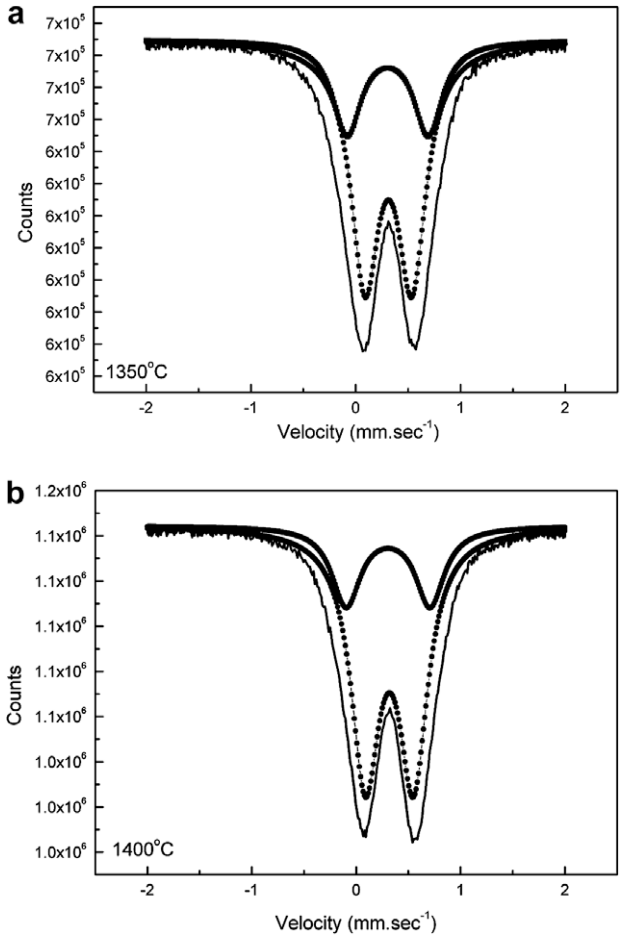

Fig. 5. Mössbauer spectra of (a) BFN sintered 1350 °C and (b) BFN sintered 1400 °C at 293 K.

Table 2
Mössbauer hyperfine parameters of BFN samples.

Sample	Isomer shift (δ), mm s^{-1}	Quadrupole splitting (ΔE_Q), mm s^{-1}
BFN sintered at 1350 °C		
Doublet site 1	0.312	0.462
Doublet site 2	0.306	0.803
BFN sintered at 1400 °C		
Doublet site 1	0.316	0.487
Doublet site 2	0.301	0.865

within the range for high-spin ferric iron in an octahedral configuration, and are assigned as such. The doublets of site 2, with slightly wider separation fall within the range of high-spin ferric iron, but the possibility that they arise from low-spin ferrous iron cannot be ruled out on the basis of their quadrupole splitting, since the parameters of these two species also overlap to some extent. However, the *decrease* in the concentration of sites corresponding to doublet 2 with increasing sintering temperature is contrary to the reported behavior of Fe^{2+}, which *increases* in concentration with increasing sintering temperature [15]. It is therefore more likely that both doublets arise from high-spin ferric iron, since the nearest and next-nearest neighbors are the same in both samples, explaining the similarity of the isomer shifts of each site. The differences in the quadrupole splitting values could arise from differences in the site occupation of the nearest and next-nearest neighbor sites, possibly related to the presence of a superstructure on the B-cation sublattice.

4. Conclusions

$BaFe_{0.5}Nb_{0.5}O_3$ ceramics were prepared by solid-state reaction, producing single-phase cubic $BaFe_{0.5}Nb_{0.5}O_3$ powders when calcined at 1200 °C. The sintering temperature affects the density and dielectric properties of $BaFe_{0.5}Nb_{0.5}O_3$, densities 94.7% of theoretical being achieved upon sintering at 1400 °C. The plot of dielectric constant as a function of temperature exhibits a broad curve with the highest value of dielectric constant (ε_r). The increase of dielectric constant with sintering temperature and frequency is likely to be due to increased conductivity in the samples. The Mössbauer spectra of these sintered BFN ceramics suggest that the behavior of the dielectric properties with temperature is not due to the presence of Fe^{2+}.

Acknowledgements

The authors would like to express their sincere thanks to Financial support from the Thailand Research Fund including the support giving through the Royal Golden Jubilee Ph.D. Program. Graduate school and Faculty of Science, Chiang Mai University, THAILAND. Industrial Research Limited and the School of Chemical and Physical Science, Victoria University of Wellington, Wellington. New Zealand. And Dr. K. D. Becker of the Technical University of Braunschweig, Germany, for determining the Mössbauer spectra.

References

[1] I.P. Raevski, S.A. Prosandeev, A.S. Bogatin, M.A. Malitskaya, L. Jastrabik, J. Appl. Phys. 93 (2003) 4130.
[2] M. Yokosuka, Jpn. J. Appl. Phys. 34 (1995) 5338.
[3] K. Tezuka, K. Henmi, Y. Hinatsu, N.M. Masaki, J. Solid State Chem. 154 (2000) 591.
[4] S. Saha, T.P. Sinha, Phys. Rev. B 65 (2002) 134103.
[5] S. Saha, T.P. Sinha, J. Phys.: Condens. Mat. 14 (2002) 249.
[6] R.W. Cahn, E. Lifshin, Concise Encyclopedia of Materials Characterization, Pergamon Press, 1993.
[7] The Inorganic Crystal Structure database (ICSD) code, 52835.
[8] N. Rama, J.B. Philipp, M. Opel, K. Chandrasekaran, V. Sankaranarayanan, R. Gross, M.S.R. Rao, J. Appl. Phys. 95 (2004) 7528.
[9] B.D. Cullity, Elements of X-ray Diffraction, second ed., Addison-Wesley Publishing Company Inc, 1978.
[10] H.P. Klug, L.E. Alexander, X-ray Diffraction Procedures for Polycrystalline and Amorphous Materials, second ed., A Wiley-Interscience Publication, 1954.
[11] T. Tunkasiri, D. Lewis, J. Mater. Sci. Lett. 11 (1976) 1751.
[12] Y.H. Zhao, U. Welzel, J.V. Lier, E.J. Mittemeijer, Thin Solid Films 514 (2006) 110.
[13] W.D. Kingery, H.K. Bowen, D.R. Uhlmann, Introduction to Ceramics, second ed., John Wiley and sons, 1975.
[14] S. Ananta, N.W. Thomas, J. Eur. Ceram. Soc. 19 (1999) 1873.
[15] K. Singh, S.A. Band, W.K. Kinge, Ferroelectrics 306 (2004) 179.
[16] S.B. Majumdar, D. Bhattacharyya, R.S.Katiyar.A. Manivannan, P. Dutta, M.S. Seehra, J. Appl. Phys. 99 (2006) 024108.
[17] B. Srinivasulu, M. Vithal, J. Mat. Sci. Lett. 18 (1999) 1771.

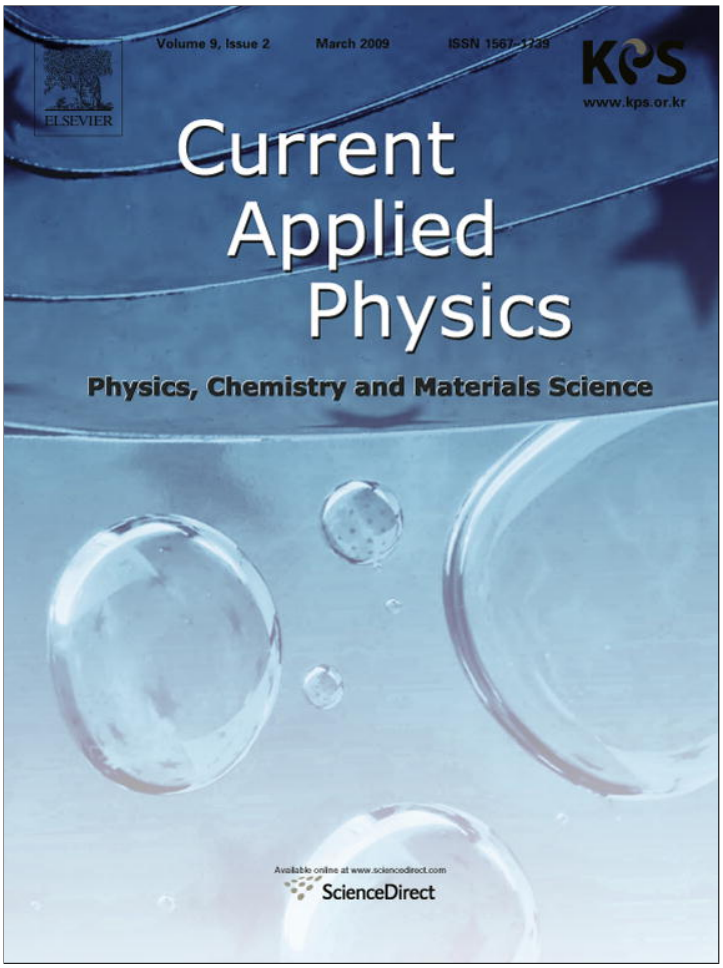

Available online at www.sciencedirect.com
ScienceDirect
Current Applied Physics 9 (2009) 460–466
Current Applied Physics
An official journal of the KPS
www.elsevier.com/locate/cap
www.kps.or.kr

Phase formation and electrical properties of BNLT–BZT lead-free piezoelectric ceramic system

P. Kantha [a], K. Pengpat [a,*], P. Jarupoom [a], U. Intatha [b], G. Rujijanagul [a], T. Tunkasiri [a]

[a] Department of Physics, Faculty of Science, Chiang Mai University, Chiang Mai 50202, Thailand
[b] School of Science, Mae Fah Luang University, Chiang Rai 57000, Thailand

Received 16 March 2008; received in revised form 7 April 2008; accepted 8 April 2008
Available online 15 April 2008

Abstract

Phase formation study in lead-free piezoelectric ceramics based on lanthanum doped bismuth sodium titanate ($Bi_{0.4871}Na_{0.4871}La_{0.0172}TiO_3$:BNLT) and zirconium doped barium titanate ($BaZr_{0.05}Ti_{0.95}O_3$:BZT), has been carried out in the system of $(1-x)$BNLT–xBZT where $x = 0.0$–1.0, by two-step mixed oxide method. It was observed that the addition of BZT in the BNLT ceramics developed the dielectric and piezoelectric properties of the ceramics with the optimum piezoelectric constant (d_{33}) and dielectric constant (ε_r) at room temperature of about 138 pC/N and 1651, respectively, from the 0.2 BNLT to 0.8 BZT ceramic sample. The Curie temperature (T_C) of this ceramic was found at 295 °C which is 195 °C higher than that of pure BZT ceramics, promising the use of this ceramic in a higher range of temperature.

PACS: 77.22.ch; 77.65.Bn; 77.84.Bw; 61.05.cp

Keywords: BNLT; BZT; Lead-free piezoelectric ceramic; Two step mixed-oxide method

1. Introduction

The most widely used piezoelectric materials are lead-based ceramics due to their superior piezoelectric properties, but they are not environmental friendly for their lead oxide toxicity. Recently, lead-free materials are increasingly desired, especially in consumer products such as cars and sound generators. Thus, it is necessary and urgent to search for the lead-free piezoelectric ceramics with excellent properties, which should be comparable with those found in the lead-based ceramics.

Bismuth sodium titanate (BNT) is one of the most important lead-free piezoelectric materials to replace the widely used lead-based perovskite materials, because of the free control of sintering atmosphere and the lack of lead pollution during the preparation process of BNT. However, the electrical properties of the BNT ceramic are quite poor. To improve its properties, several solid solutions of BNT based materials, such as BNT–$BaTiO_3$, have been extensively studied [1–4]. Another way to improve the electrical properties of BNT is the addition of a modifier element by cation, such as K^+ and La^{3+} etc. Herabut and Safari [5] reported the effect of La additive on piezoelectric properties of $(Bi_{0.5}\ Na_{0.5})_{(1-1.5x)}La_x$-$TiO_3$:BNLT ceramics. They found that the dielectric constant (ε_r) and piezoelectric constant (d_{33}) increased up to 550 and 91 pC/N, respectively, when the La doping content was only about 1.72%.

Due to the excellent dielectric properties of barium titanate (BT), the BT ceramics are generally used as high dielectric capacitors. Moreover, studies have been focusing on the temperature dependence of the dielectric constant and the nature of phase transition, but piezoelectric behavior was scarcely observed. Yu et al. [6] have reported that

* Corresponding author. Tel.: +66 81 884 1859; fax: +66 53 357 512.
E-mail address: kpengpat@gmail.com (K. Pengpat).

1567-1739/$ - see front matter © 2008 Elsevier B.V. All rights reserved.
doi:10.1016/j.cap.2008.04.004

Zr-doped $BaTiO_3$ (BZT) ceramics with 5% Zr content showed fairly satisfactory piezoelectric response, with the piezoelectric constant value of 236 pC/N at room temperature. The large temperature dependence of BZT ceramics, combined with the low Curie temperature, however, limits their practical applications as the piezoelectric devices [7]. To overcome this problem, the new system such as BNT $(1-x)(Bi_{1/2}Na_{1/2})TiO_3$–$xBa(Ti,Zr)O_3$ by Peng et al. [8] was investigated. They reported that the highest piezoelectric response, with the maximum piezoelectric constant of about 147 pC/N with higher Curie temperature than that of the BZT ceramics, was successfully obtained from the $(1-x)$BNT–xBZT ceramic where $x = 0.09$.

In this work, the fabrication of the ceramics from $(1-x)Bi_{0.4871}Na_{0.4871}La_{0.0172}TiO_3$ (BNLT)–$xBaZr_{0.05}Ti_{0.95}O_3$ (BZT) system, where x was varied between 0.0 and 1.0 mole, has been carried out, in order to study phase evolution of the entire system of BNLT–BZT ceramics and find out the optimum conditions for obtaining the ceramics with improved electrical properties.

2. Experimental

High purity (purity > 99.0%) powders of bismuth oxide (Bi_2O_3), sodium carbonate (Na_2CO_3), lanthanum oxide (La_2O_3), titanium dioxide (TiO_2), barium carbonate ($BaCO_3$) and zirconium dioxide (ZrO_2) were used as starting materials for producing the ceramics from $(1-x)(Bi_{0.4871}Na_{0.4871}La_{0.0172}TiO_3)$–$x(BaZr_{0.05}Ti_{0.09}O_3)$ system where $x = 0.0$, 0.2, 0.4, 0.6, 0.8 and 1.0 mole. The batch compositions of BNLT and BZT were weighed and mixed by ball-milling method for 24 h. Then both mixtures of BNLT and BZT were dried and calcined separately at 900 °C and 1250 °C for 2 h, respectively. Both calcined powders were then mixed with respect to the above formula by ball-milling method for 24 h with ethanol as a milling media.

After drying and sieving the mixtures, the BNLT–BZT batches of different compositions were made into pellets of 10 mm in diameter using uniaxial pressing in stainless steel mold. The pellets were subsequently sintered between 1075 °C and 1500 °C in an electric furnace and air atmosphere under controlled heating and cooling rate of 5 °C/min with soaking time for 4 h. X-ray diffractometer (XRD, Siemens D500) and scanning electron microscope (SEM, JEOL JSM5910LV) were used to evaluate the crystal structure and to observe the microstructures of the sintered ceramics, respectively. The mean linear intercept was used to determine grain size of the ceramics and the bulk densities of the sintered samples were measured by Archimedes method using distilled water as a medium.

The two circular surfaces of the sintered ceramics were polished and coated with silver paste as electrodes for electrical contact. The room temperature dielectric constant (ε_r) and dielectric loss ($\tan\delta$) of ceramics were measured at various frequencies from 1 to 100 kHz using an LCZ meter (HP4276 A). Temperature dependence of dielectric constant and dielectric loss ($\tan\delta$) of selected sample were observed in order to determine the Curie temperature (T_C) at 1 kHz by using LCR meter (HIOKI3532-50). To measure piezoelectric charge constant (d_{33}) and ferroelectric hysteresis loops, the prepared ceramic samples were polarized in silicone oil bath at 50 °C under 4.0 KV/mm for 15 min and the samples were aged at room temperature for 24 h after poling. After that the piezoelectric measurements were performed using a piezoelectric-d_{33}-meter (Model 8000, Penne baker). Finally, the measurements of ferroelectric hysteresis loops were conducted at room temperature by using a ferroelectric tester (Radiant Technologies Inc.) at 20 kV/cm.

3. Results and discussion

The X-ray diffraction study was performed in order to study phase formation of the lead-free piezoelectric ceramics based on BNLT–BZT prepared by two-step mixed oxide method. The X-ray results of $(1-x)$BNLT–xBZT ceramics

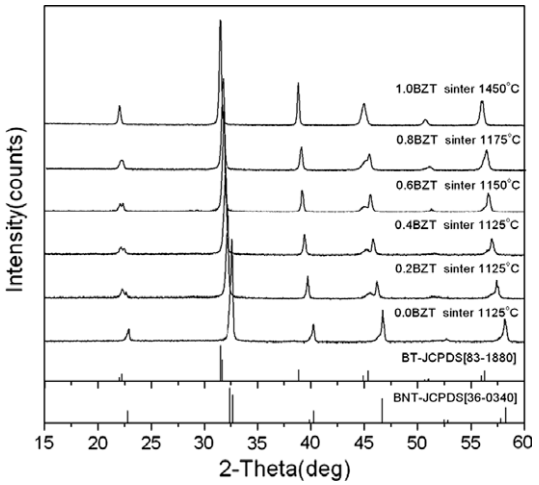

Fig. 1. XRD patterns of sintered BNLT–BZT ceramics.

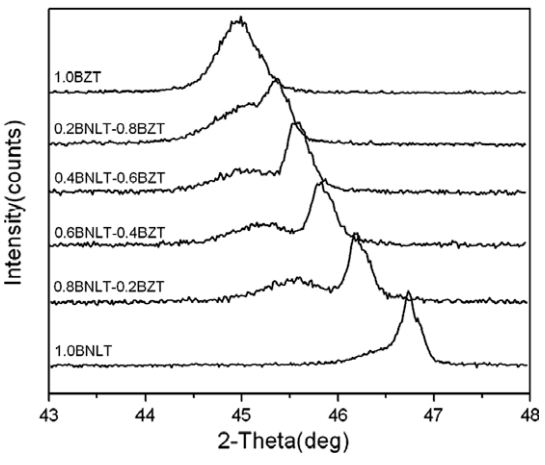

Fig. 2. XRD patterns of sintered BNLT–BZT ceramics in the 2θ range between 43° and 48°.

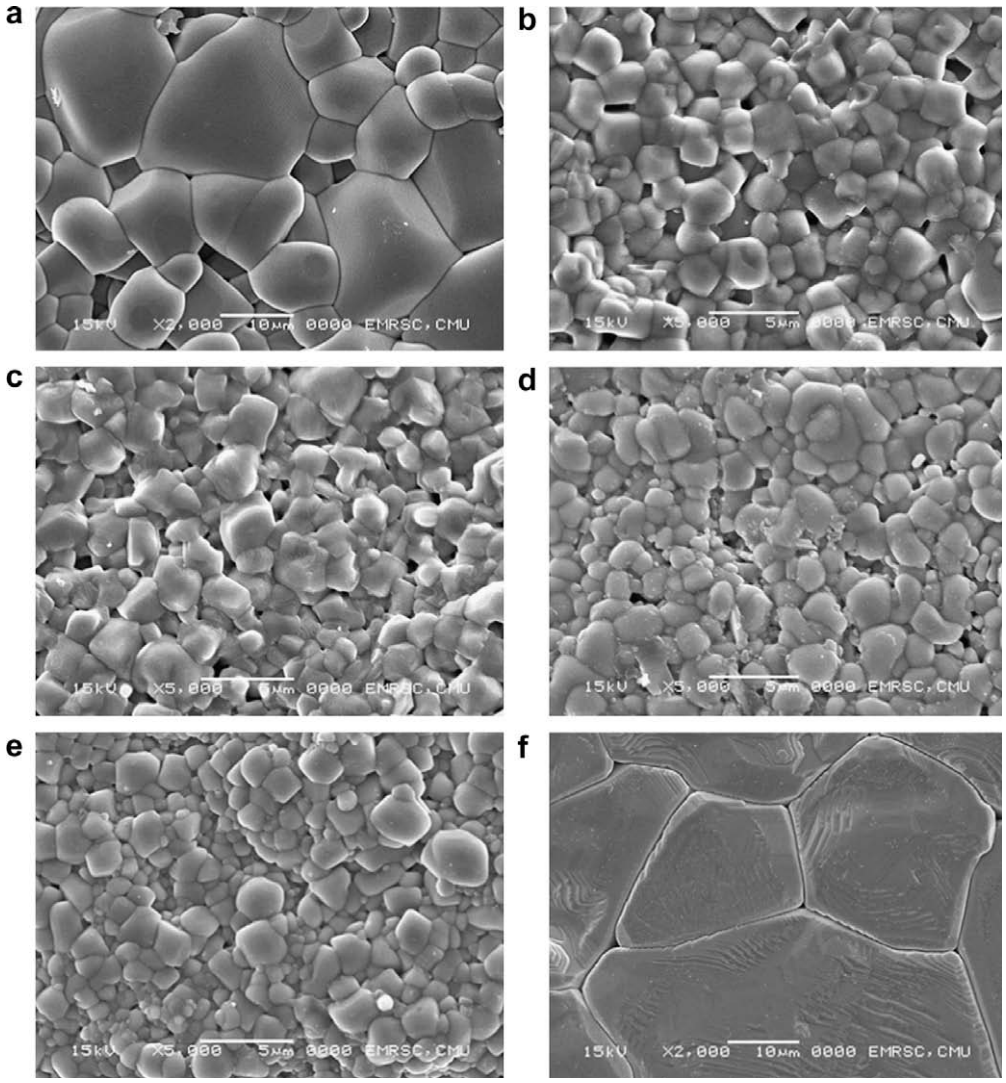

Fig. 3. SEM micrographs of $(1-x)$BNLT–xBZT ceramics where $x =$ (a) 0, (b) 0.2, (c) 0.4, (d) 0.6, (e) 0.8 and (f) 1.0.

where x was varied from 0.0 to 1.0 are shown in Fig. 1. The peak shift started to appear in XRD patterns of the ceramics where $x > 0.2$, indicating the changes in lattice parameter of these ceramics compared with the pure BNLT phase. A single phase perovskite could be obtained in this system with rhombohedral, tetragonal symmetry or mixing of both symmetries in each X-ray diffraction pattern at various BZT content which can be distinguished by the splitting of XRD peak at 2θ range between 43° and 48° as shown in Fig. 2. The structural symmetry of BNLT ($x = 0.0$) sample is rhombohedral which is corresponding to the single peak at about 47° in its XRD pattern. A splitting of (002) and (200) peak started to appear at $x = 0.2$, indicating the tetragonality of the ceramic. This tetragonality of the BNLT–BZT ceramics was found to increase with increasing BZT content. As the minimum amount of BZT added in this study equals to $x = 0.2$, therefore, the morphotropic phase boundary (MPB) composition was not revealed. As from the previous study in BNT–BZT system [8], the MPB ceramic was found at 9% BZT addition. Thus, the future work in our $(1-x)$BNLT–xBZT system will concentrate closely to the expected MPB region of around $x = 0.1$.

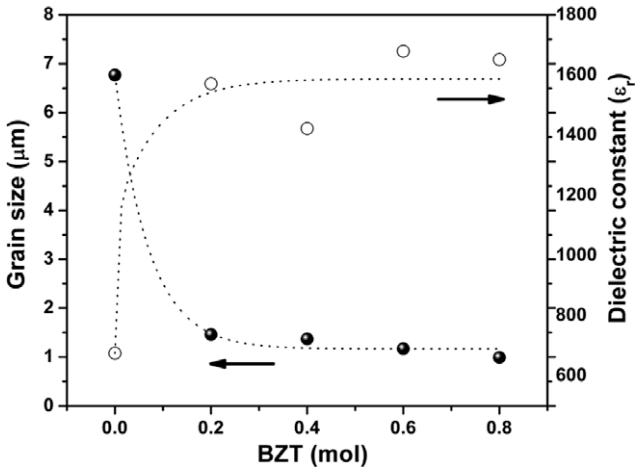

Fig. 4. The comparison between grain size and dielectric constant as a function of BZT content.

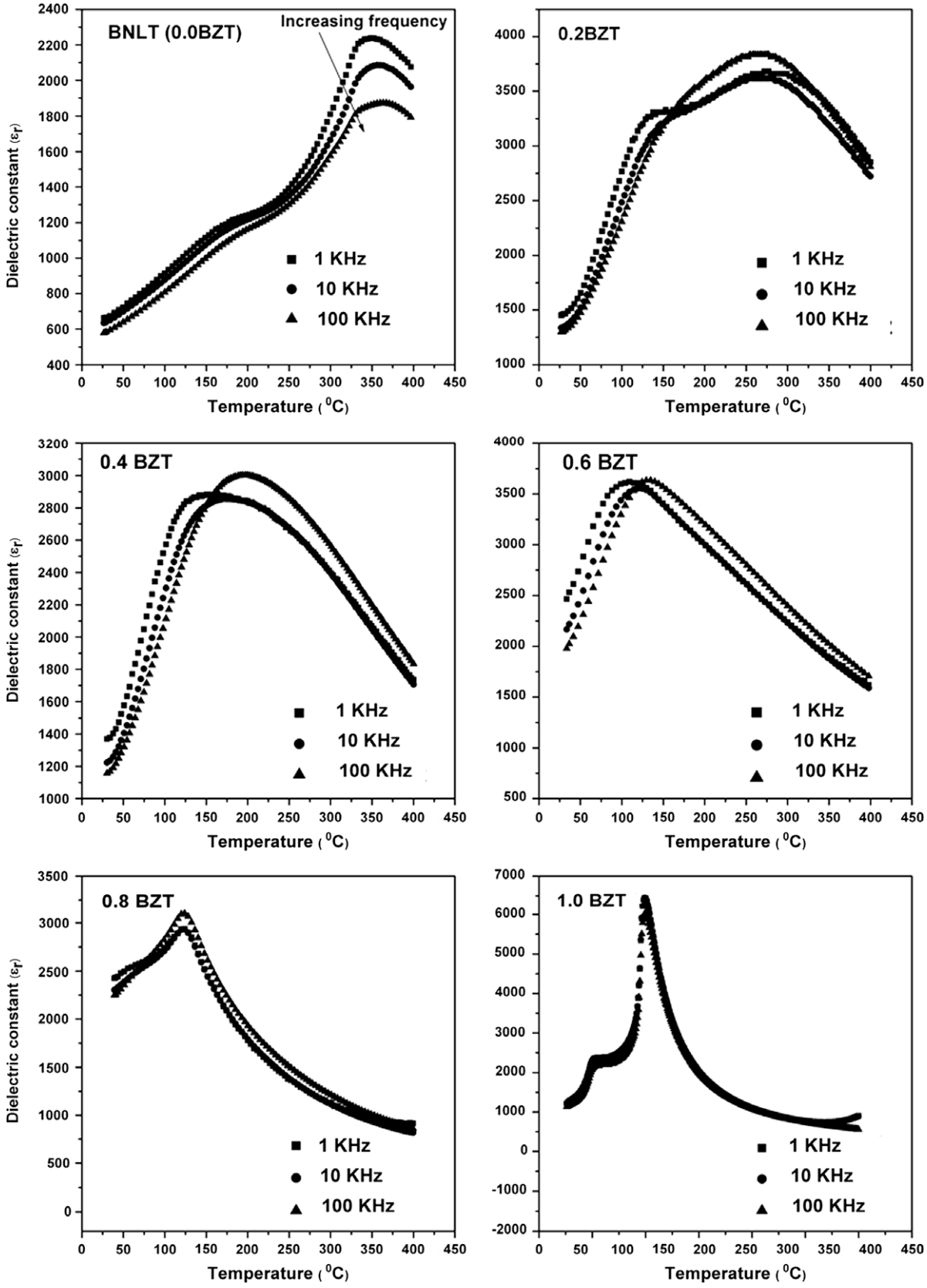

Fig. 5. Temperature dependence of dielectric constant BNLT–BZT ceramics.

The SEM micrographs of BNLT–BZT ceramics were obtained in Fig. 3. The SEM observation confirms that the BNLT–BZT ceramics are densely sintered with the density value ranging from 5.74 to 5.80 g/cm^3. No abnormal

grain was observed in the samples, indicating an absence of pyrochlore formation. The microstructures in SEM micrographs of the ceramics are thus consistent with the XRD results. It can be clearly seen that the amount of BZT additions has no significant change in shape in the BNLT–BZT ceramics. However, microstructural analysis also revealed that BZT additions produced a notable decrease in grain size. Average values of grain size, as measured by the linear intercept method, decreased from ~7 μm for the 0.0BZT or the pure BNLT sample to ~1 μm for 0.8 BZT sample. The plot of grain size as a function of BZT content is shown in Fig. 4. The reduction in grain size may be due to the difference in ionic radius and valency of A-site cations of Bi^{3+} (131 pm) and Ba^{2+} (156 pm) which plays an important role in grain growth mechanism, as beyond the solubility limit of BZT, it may be accumulated at the grain boundary which would result in the inhibition of grain growth. This result agreed pretty well with the work done by Pengpat et al. [9] and Eitssayeam et al. [10], who found the similar result in the BNLT–$BaTiO_3$ system and $PbZr_{0.52}Ti_{0.48}O_3$–$BaFe_{0.5}Nb_{0.5}O_3$, respectively. From the plot of dielectric constant at room temperature as a function of BZT content, it can be clearly seen that the dielectric constant increased dramatically when BZT was added to the BNLT ceramics from 675 ($x = 0$) to 1571 ($x = 0.2$). Further increase in BZT content from $x = 0.2$ to 0.8 has, however, affected insignificantly on the dielectric constant as well as grain size of the BZT added ceramics (Fig. 4). Thus, the tetragonality seems to play an important role in enhancing the dielectric constant of the BZT added ceramics which is consistent with the XRD result as the structure of the BNLT ceramic is rhombohedral.

Temperature dependence on dielectric constant is shown in Fig. 5. For $x = 0$ sample (pure BNLT), the temperature dependences of dielectric constant depict a strong frequency dependence of the dielectric peak at $T = T_m$ (T_m, the temperature of dielectric maximum). BNLT is ferroelectric (FE) with a rhombohedral structure at room temperature. The rhombohedral phase transforms to a ferroelectric (FE) tetragonal at the temperature (T_2), which occurs at ~180 °C and the transforms of the tetragonal to the paraelectric (PE) cubic phase occurs at 340 °C [11]. In the present BNLT samples, the measured T_2 and T_m values were ~176 and 345 °C, respectively. The maximum dielectric constant at T_m of BNLT was found to be 2200 and this value is close to the result in the literature. The similar transition was reported by Yu et al. [6] who observed the T_2 at 50 °C in the $Ba(Ti_{1-x}Zr_x)O_3$ where $x = 0.05$. For $x = 0.2$–0.8 samples, the dielectric–temperature curves showed a board dielectric peaks as well as the transition temperature at T_2 exhibited an unclear phase transformation especially at high frequency. However, the optimum of the maximum dielectric constant at T_m of 3600 was observed at the $x = 0.2$ sample. In the present work, we prepared $(1-x)$BNLT–xBZT by mixing BNLT and BZT together before sintering. Therefore, it is believed that a microscopic compositional fluctuation might occur in the BNLT–BZT ceramics, especially in the $x = 0.2$ sample. This may cause the evidence of unclear phase transition and broadening dielectric–temperature curves, indicating relaxor behavior of these ceramics. This is agreed pretty well with other previous works. [11–13] For $x = 1.0$ sample (pure BZT sample), the two clear phase transitions was observed again at 51 and 110 °C, which may be corresponding to antiferroelectric (AFE) orthorhombic phase transforms to a ferroelectric (FE) tetragonal phase transition and a ferroelectric (FE) tetragonal transforms to a paraelectric (PE) cubic phase transition, respectively [8]. Sharp dielectric peak with dielectric constant of 6500 was observed at 110 °C for the FE to PE transformation in the BZT sample. In addition, weak frequency dependence of the dielectric curve was also observed in this sample. It can be noticed that the dielectric curves of the BZT added samples ($x = 0.2$–0.6) show unusual behavior where the dielectric constant at high frequency of 100 kHz was larger than that of lower frequency in the high temperature region. The similar result was also found in the work done by Tian et al. [14], who studied the dielectric behavior of their BNT–BZT ceramic sample. It is also observed in the dielectric loss versus frequency curves of those ceramics (figures not shown) that the dielectric loss increases dramatically at 100 kHz, comparing to that of lower frequency, causing the increase in dielectric constant of the ceramics as described above. One of the possible reasons may be due to the perturbation of thermal motion of ionic or molecular dipoles, leading to an abnormal change in conduction mechanism at this frequency of 100 kHz. It is worth further study in the electrical phenomena of these ceramics by an impedance spectroscopy. Fig. 6 shows the dielectric loss ($\tan\delta$) versus temperature of all ceramic samples. It can be seen that $\tan\delta$ values of the BZT added samples are lower than that of the pure BNLT (0.0BZT) sample especially when the temperature are higher than their T_2. This may be caused by the change in their structures from the FE tetragonal phase to AFE orthorhombic phase.

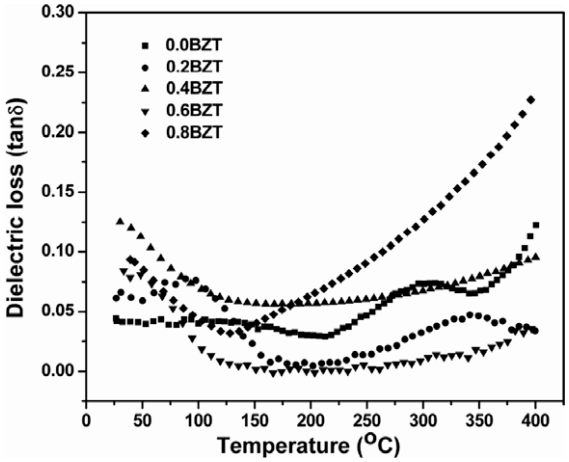

Fig. 6. Temperature dependence of dielectric loss of BNLT–BZT ceramics.

In order to study the ferroelectric properties, measurements of polarization hysteresis were performed at room temperature using a Sawyer–Tower circuit. The results are shown in Fig. 7. For $x = 0.0$–0.8, slim hysteresis loops with small remanent polarization (P_r) were observed. Among those ceramic samples, the $x = 0.2$ sample has a good ferroelectric property with high P_r value of about 10 μC/cm^2 and $E_c = 13$ kV/cm. This may be resulted from a good homogeneity of the solid solution between BNLT and BZT at this composition. For $x = 1.0$ sample (the pure BZT), its hysteresis loop exhibits a nearly square with a little bit slant. The values of P_r and E_c for $x = 1.0$ sample are approximately 10 μC/cm^2 and 13 kV/cm, respectively. The result indicates that the best piezoelectric properties should be observed in this composition.

Fig. 8 shows the changes in the piezoelectric constant (d_{33}) as a function of the BZT content. The d_{33} coefficient of this BNLT–BZT system was found to be in the range of 79–224 pC/N. As expected, the highest d_{33} of 224 pC/N was observed in the $x = 1.0$ sample due to its excellent ferroelectric property as mentioned above. For $x = 0.0$–0.8 sample, the highest d_{33} coefficient of 159 pC/N was observed in $x = 0.8$ samples, but it also has quite low T_m (127 °C) as summarized in Table 1. The sample with $x = 0.2$, however, exhibits the optimum properties with high T_m of about 295 °C and acceptable d_{33} value of

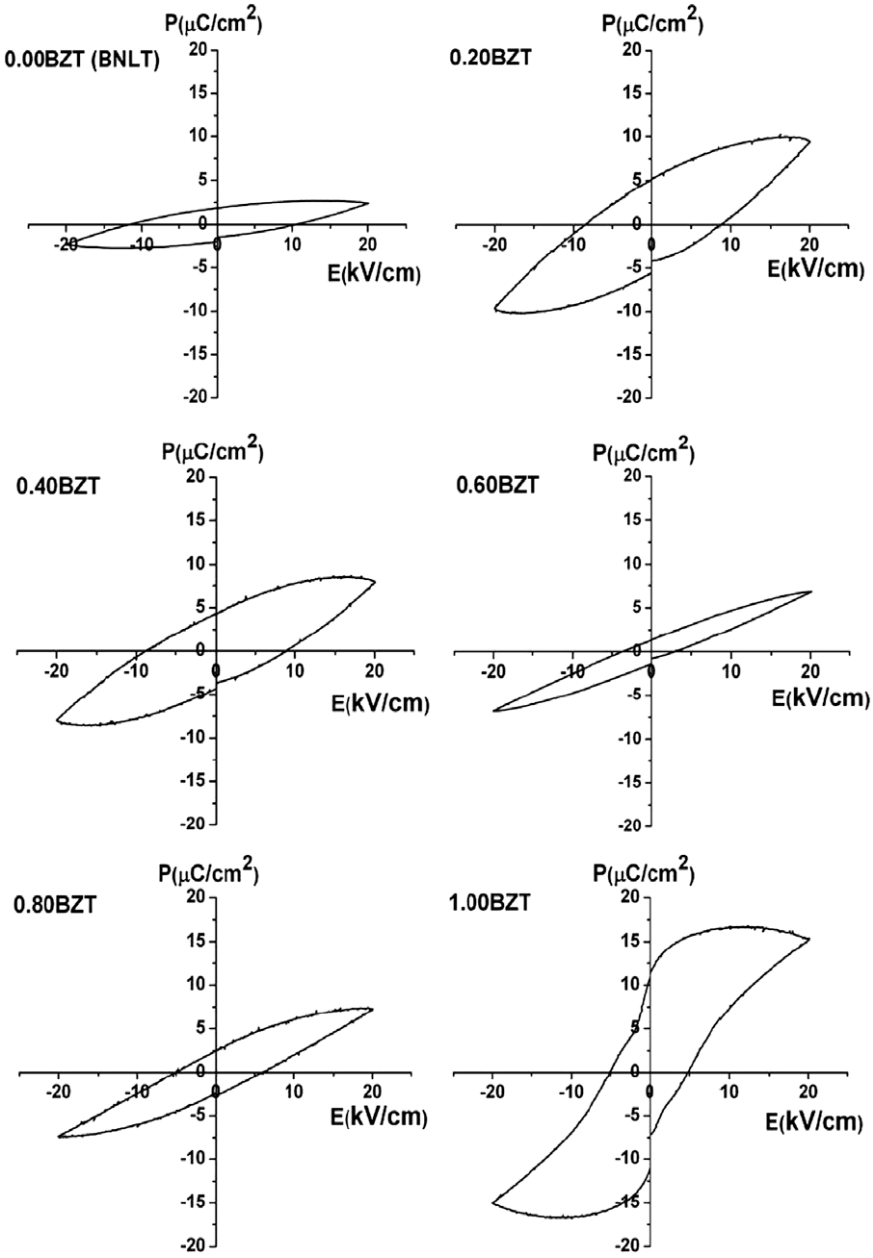

Fig. 7. Ferroelectric hysteresis loops of the BNLT–BZT ceramics at various BZT contents.

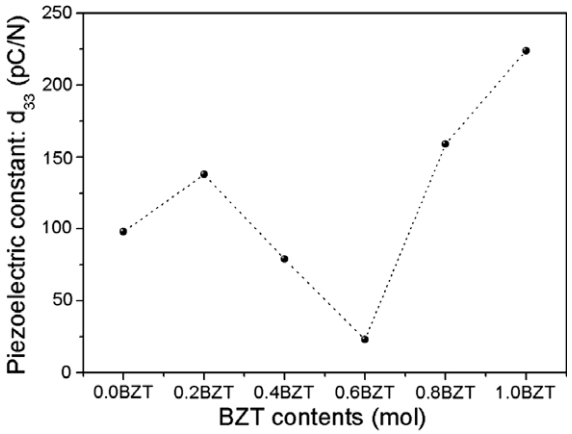

Fig. 8. Piezoelectric constant (d_{33}) as a function of BZT content.

Table 1
Density, piezoelectric and dielectric properties of BNLT–BZT ceramics

Sample	ρ (g/cm3)	d_{33} (pC/N)	ε_r at 1 kHz[a]	$\tan\delta$	T_m (°C)
1.0BNLT	5.77	98	675	0.04	345
0.8BNLT–0.2BZT	5.79	138	1571	0.08	295
0.6BNLT–0.4BZT	5.76	79	1422	0.09	131
0.4BNLT–0.6BZT	5.74	23	1679	0.10	112
0.2BNLT–0.8BZT	5.78	159	1651	0.04	127
1.0BZT	5.80	224	1227	0.03	100
BNLT [5]	–	91	550	0.04	345
BNT–BT [4]	–	125	580	0.01	288
BNT–BZT [8]	5.82	147	881	0.03	244
BNLT–BT [11]	5.86	130	1060	0.05	275

[a] At room temperature.

138 pC/N. It can also be seen from Table 1 that BZT addition has improved the dielectric and piezoelectric properties of the ceramics comparing to the pure BNLT ceramics. [5] The more the BZT added, the lower the T_m value could be obtained as the pure BZT ceramic has a low T_m of about 100 °C. To retain a high T_m value with acceptable d_{33} and dielectric constant, the $x = 0.2$ sample is, therefore, considered to be the optimum composition in this study. Comparing to other systems of BNT–BT [4], BNT–BZT [8] and BNLT–BT [15], the $x = 0.2$ sample offers better dielectric constant and higher T_m value. Moreover, it also has board dielectric peak, promising the wider temperature range for using in electronic applications.

4. Conclusions

The BNLT–BZT ceramics have been prepared by two-step mixed oxide method. The pure BNLT and BZT powders were produced with calcination temperature of 900 and 1250 °C, respectively. Both powders of various amounts of BZT from 0 to 100 mol.% were then pressed and sintered to form the dense ceramics with the density value ranging from 5.74 to 5.80 g/cm^3. After electrical characterization had been employed to the selected ceramics, it was found that the addition of BZT developed the piezoelectric and dielectric properties of $(1-x)$BNLT–xBZT ceramics with the optimum condition of $x = 0.2$ where piezoelectric coefficient (d_{33}), dielectric constant at room temperature under 1 kHz and Curie temperature are of about 138 pC/N, 1571 and 295 °C, respectively.

Acknowledgements

The authors would like to thank the Thailand Research Fund and Faculty of Science, Chiang Mai University for financial supports. We also thank the Research Laboratory for Excellent in Electronic Materials, Department of Physics, and Graduate School, Chiang Mai University Thailand.

References

[1] H. Li, C. Feng, W. Yao, Mater. Lett. 58 (2004) 1194.
[2] J.V. Zvigzds, P.P. Kapostins, L.A. Zvigzds, Ferroelectric 40 (1982) 75.
[3] T. Takennaka, K. Sakata, K. Toda, Ferroelectric 95 (1989) 153.
[4] T. Takennaka, K. Maruyama, K. Sakata, Jpn. J. Appl. Phys. 30 (1991) 2236.
[5] A. Herabut, A. Safari, J. Am. Ceram. Soc. 80 (1997) 2954.
[6] Z. Yu, C. Ang, B. Guo, A.S. Bhalla, J. Appl. Phys. 92 (2002) 1489.
[7] M. Matsubara, T. Yamaguchi, W. Sakamoto, K. Kikuta, T. Yogo, S. Hirano, J. Am. Ceram. Soc. 88 (2005) 1190.
[8] C. Peng, J.F. Li, W. Gong, Mater. Lett. 59 (2005) 1576.
[9] K. Pengpat, S. Hanphimol, S. Eitssayeam, U. Intatha, G. Rujijanagul, T. Tunkasiri, J. Electroceram. 16 (2006) 301.
[10] S. Eitssayeam, U. Intatha, K. Pengpat, T. Tunkasiri, Appl. Phys. A 83 (2006) 295.
[11] R. Ganesh, E. Goo, J. Am. Ceram. Soc. 79 (1996) 225.
[12] B.S. Chiou, R.W. Vest, Bull. Am. Ceram. Soc. 63 (1984) 811.
[13] B.S. Chiou, IEEE Trans. Comp., Hybrid Manu. 12 (1989) 798.
[14] H.Y. Tian, K.W. Kwok, H.L.W. Chan, C.E. Buckley, J. Mater. Sci. 42 (2007) 9750.
[15] P. Jarupoom, K. Pengpat, N. Pisitpipathsin, S. Eitssayeam, U. Intatha, G. Rujijanagul, T. Tunkasiri, Curr. Appl. Phys. 8 (2008) 253.

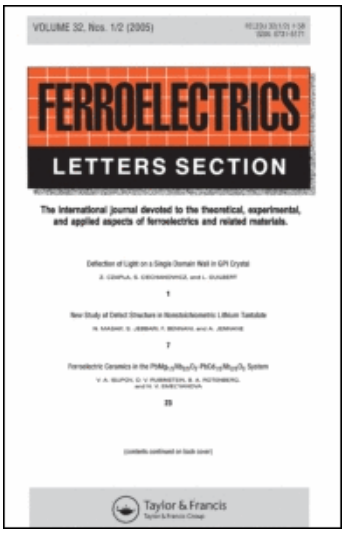

Ferroelectrics Letters Section
Publication details, including instructions for authors and subscription information:
http://www.informaworld.com/smpp/title~content=t713871498

Effect of Particle Size on the Dielectric Properties of Sodium Potassium Niobate -Portland Cement Composites

R. POTONG [a]; R. RIANYOI [a]; P. JARUPOOM [a]; K. PENGPAT [a]; A. CHAIPANICH [a]
[a] Department of Physics and Materials Science, Faculty of Science, Chiang Mai University, Chiang Mai, Thailand

Online Publication Date: 01 January 2009

To cite this Article POTONG, R., RIANYOI, R., JARUPOOM, P., PENGPAT, K. and CHAIPANICH, A.(2009)'Effect of Particle Size on the Dielectric Properties of Sodium Potassium Niobate -Portland Cement Composites',Ferroelectrics Letters Section,36:3,76 — 81
To link to this Article: DOI: 10.1080/07315170903152748
URL: http://dx.doi.org/10.1080/07315170903152748

Ferroelectric Letters, 36:76–81, 2009

ISSN: 0731-5171 print / 1563-5228 online
DOI: 10.1080/07315170903152748

Taylor & Francis
Taylor & Francis Group

Effect of Particle Size on the Dielectric Properties of Sodium Potassium Niobate -Portland Cement Composites

R. POTONG, R. RIANYOI, P. JARUPOOM, K. PENGPAT, and A. CHAIPANICH*

Department of Physics and Materials Science, Faculty of Science, Chiang Mai University, Chiang Mai 50200, Thailand

Communicated by Dr. George W. Taylor

(Received April 1, 2009)

In this research, the effect of sodium potassium niobate, $(Na_{0.5}K_{0.5})NbO_3$ (NKN) particle size on the dielectric properties of 0-3 non lead based piezoelectric cement based composites were investigated. NKN of various particle sizes (75, 225 and 450 μm) were used at 50% by volume to produce the composites. Dielectric properties at various frequencies (0.1–20 kHz) were investigated. The results showed that the dielectric values of NKN-PC composites increased with increasing NKN particle size where ε_r at 1 kHz are 158.60 and 191.21 for composites with 75 μm and 450 μm NKN particle size respectively. The dielectric loss (tanδ) was found to reduce with increasing NKN particle size and the tan δ value was lowest at 0.39 for composite with 450 μm NKN particle size.

Keywords: NKN; Composites; Particle size; Dielectric Properties.

1. INTRODUCTION

Nowadays, the piezoelectric materials are widely used for capacitors and various application such as lead zirconate titanate (PZT) as it has excellent dielectric constant (ε_r) and piezoelectric coefficient (d_{33}) [1–4]. Cement based composites consisting of PZT have been developed for applications where the composites can be inserted into concrete structures to detect loading after they were fabricated [5–11]. Moreover, the use of such piezoelectric-cement

*Corresponding author. E-mail: arnon@chiangmai.ac.th

based composite would provide an advantage in the matching of structural concrete compared to other piezoelectric composites. However, lead oxide from processing of lead-based piezoelectric materials has high toxic and used of the lead-based materials has caused lead pollution and crucial environmental problems. Therefore, lead-free piezoelectric materials received attention from environmental protection. Recently, sodium potassium niobate, $NaKNbO_3$ (NKN) have begun to attract attention because of high piezoelectric coefficient (d_{33}) [12]. Dielectric measurements were first reported by Mathias and Remeika [13]. In addition, dielectric constant of $Na_{0.5}K_{0.5}NbO_3$ is 218.87 at 1 kHz and low dielectric loss by Kuldeep Singh et al. [14]. In this research, NKN-PC composite material was produced from sodium potassium niobate, $Na_{0.5}K_{0.5}NbO_3$ (NKN) with Portland cement of normal type (PC), commonly known as ordinary Portland cement to form 0-3 connectivity NKN-PC composites. The dielectric properties of the new composite material of lead-free piezoelectric materials, NKN, made with Portland cement were then investigated.

2. EXPERIMENTAL

$Na_{0.5}K_{0.5}NbO_3$ (NKN) ceramic of different median particle size (75 μm, 225 μm and 450 μm) were used. These NKN ceramic particles were then mixed with normal Portland cement (The American Society for Testing and Materials Type I cement) to produce 0-3 connectivity NKN-PC composite of 50:50 by volume using a hydraulic press to form disk samples of 15 mm diameter and 2 mm thickness. Thereafter, the composites were placed for curing at 60°C and 98 % relative humidity for 3 days before measurements. For measurement of the dielectric properties, silver paste electrodes were formed at the two surfaces of disk-shaped specimens. An impedance meter (Hewlett Packard 4194A) was use to obtain the capacitance and the dissipation factor ($\tan\delta$) of the composites at room temperature and at very frequency. The relative dielectric constant (ε_r) was the calculated from the following equation:

$$\varepsilon_r = \frac{Ct}{\varepsilon_0 A}$$

Where C is the sample capacitance, t is the thickness, ε_0 is the permittivity of free space constant (8.854×10^{12} Fm^{-1}), and A is the electron area.

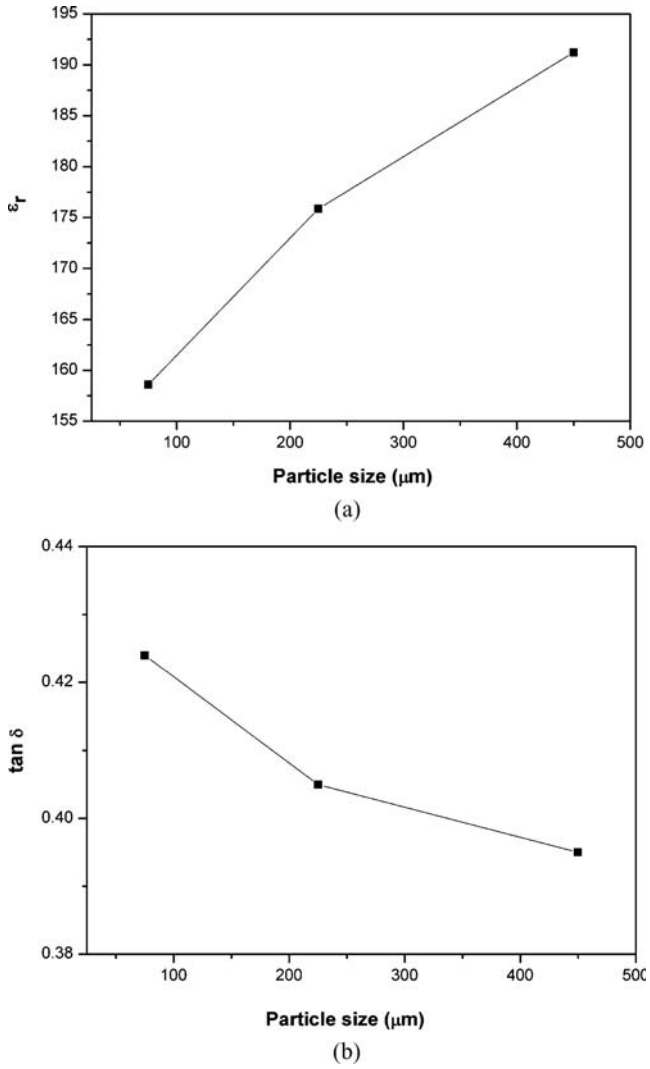

Figure 1. Effect of particle size on dielectric properties results of NKN-Portland cement composites (a) dielectric constant and (b) dielectric loss.

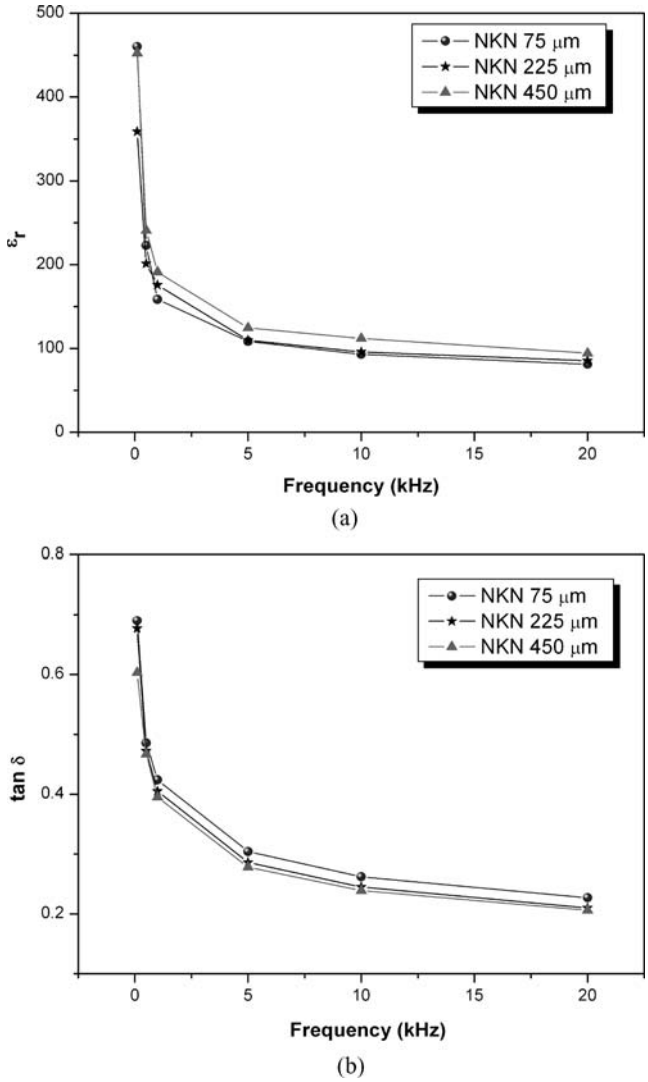

Figure 2. Effect of frequency on dielectric properties results of NKN-Portland cement (a) dielectric constant and (b) dielectric loss.

3. RESULTS AND DISCUSSION

The effect of NKN-PC composites on the dielectric constant (ε_r) is plotted against the NKN particle size in Fig. 1 (a) where the effect of NKN particle size on the dielectric constant can be seen. The dielectric constant of the composites can be seen to increase with increasing NKN particle size and that the dielectric constant was highest at 191.21 of 450 μm NKN particle size at 1 kHz.

Measured dielectric loss (tanδ) results of composites showing the effect of NKN particle size can be seen in Fig. 1 (b). The dielectric loss (tanδ) was found to reduce with increasing NKN particle size and the tan δ value at 1 kHz was lowest at 0.39 for composite at 450 μm NKN particle size.

At varying frequency, the effect of NKN-PC composites on the dielectric constant (ε_r) is shown against the frequency in Fig. 2 (a) where the effect of frequency on the dielectric constant can be seen. The dielectric constant of the composites can be seen to reduce with increasing frequency where 0.1 kHz and 20 kHz with dielectric constant = 452.31 and 94.24 for composites at 450 μm NKN particle size. In addition, the dielectric loss (tanδ) was found to reduce with increasing frequency where 0.1 kHz and 20 kHz with dielectric loss = 0.60 and 0.20 for composites at 450 μm NKN particle size. Moreover, the dielectric constant of the composites decrease sharply with increasing frequency and with an increasing frequency, some polarization, especially interfacial polarizations cannot follow the change of the electric field due to lengthy time for the construction of space charge polarization. The result, dielectric constants are lower at high frequency [15].

Furthermore, from the above results, high dielectric constant (ε_r) and low dielectric loss (tanδ) of 0-3 NKN-Portland cement composites were obtained with a particle size of NKN as large as 450 μm using the method described.

4. CONCLUSIONS

The results showed that the dielectric properties of 0-3 NKN-Portland cement composites reduced with increasing frequency. The dielectric constant (ε_r) was found to increase with increasing NKN particle size. Moreover, particle size of NKN ceramic as large as 450 μm can be produced and it gave the highest dielectric values (ε_r = 191.21). The dielectric loss (tanδ) was found to reduce with increasing NKN particle size and the tan δ value was lowest at 0.39 for composite at 450 μm NKN particle size. At varying

frequency, the dielectric constant and dielectric loss of the composites was found to reduce with increasing frequency.

ACKNOWLEDGMENTS

The authors are grateful to members of staff at the Electroceramics Research Laboratory for the research facilities made possible for this research work and also to the Thailand Research Fund (TRF)and the Commission on Higher Education (Thailand) for financial support.

REFERENCES

[1] S. T. Lau, K.W. Kwok, H. L. W. Chan, and C. L. Choy, Piezoelectric Composite Hydrophone Array. *Sens. Actuators A.*, **96**, 14–20 (2002).
[2] R. E. Newnham and A. Amin, Smart systems: Microphones, fish farming, and beyond—Smart materials, acting as both sensors and actuators, can mimic biological behavior. *Chem. Tech.* **29**, 38–47 (1999).
[3] R. Ranjan, R. Kumar, B. Behera, and R. N. P. Choudhary, Effect of Sm on structural, Dielectric and conductivity properties of PZT ceramics. *Mater Chem Phys.* **115**, 473–477 (2009).
[4] J. F. Tressler, S. Alkoy, and R. E. Newnham, *J. Electroceram: Piezoelectric Sensors and Sensor Materials*. **2**, 257–272 (1998).
[5] N. Jaitanong and A. Chaipanich, Effect of polling temperature on piezoelectric properties of 0-3 PZT-Portland cement composite. *Ferr. Lett.* **35**, 17–23 (2008).
[6] A. Chaipanich and N. Jaitanong, Effect of polling time on piezoelectric properties of 0-3 PZT-Portland cement composite. *Ferr. Lett.* **35**, 73–78 (2008).
[7] Z. Li, D. Zhang, and K. Wu, J. Am., Cement-Based 0-3 piezoelectric composites. *Ceram. Soc.* **85**, 305–313 (2002).
[8] S. Huang, J. Chang, R. Xu, F. Liu, L. Lu, Z. Ye, and X. Cheng, Piezoelectric properties of 0-3 PZT/sulfoaluminate cement composites. *Smart Mater. Struct.* **13**, 270–274 (2004).
[9] Z. Li, B. Dong, and D. Zhang, Influence of polarization on properties of 0–3 cement-based PZT composites. *Cem. Concr. Compos.* **27**, 27–32 (2005).
[10] B. Dong and Z. Li, Cement-based piezoelectric ceramic smart composites. *Compos. Sci. Technol.* **65**, 1363–1371 (2005).
[11] C. Xin, S. Huang, C. Jun, X. Ronghua, L. Futian, and L. Lingchao, Piezoelectric and dielectric properties of piezoelectric ceramic–sulphoaluminate cement composites. *J. Eur. Ceram. Soc.* **25**, 3223–3228 (2005).
[12] Y. Saito, H. Takao, T. Tani, T. Nonoyama, K. Takatori, T. Homma, T. Nagaya, and M. Nakamura, Lead-free piezoceramics, *Nature*, **43**, 84–87 (2004).
[13] B. T. Mathias and J. Remeika, Dielectric Properties of Sodium and Potassium Niobates. *Phys. Rev.* **82**, 727–729 (1951).
[14] K. Singh, V. Lingwal, S. C. Bhatt, N. S. Panwar, and B. S. Semwal, Dielectric properties of potassium sodium niobate mixed system. *Mater. Res. Bull.* **36**, 2365–2374 (2001).
[15] C. Xin, S. Huang, C. Jun, and L. Zongjin, Piezoelectric, dielectric, and ferroelectric properties of 0-3 ceramic/cement composite. *J. Appl. Phys.* 101 (2007)

Materials Letters 63 (2009) 1027–1029

Contents lists available at ScienceDirect

Materials Letters

journal homepage: www.elsevier.com/locate/matlet

Nanocrystallization of ferroelectric lithium niobate in $LiNbO_3$-SiO_2 glasses

P. Prapitpongwanich [a,c], R. Harizanova [b], K. Pengpat [a], C. Rüssel [c,*]

[a] Department of Physics, Faculty of Science, Chiang Mai University, Thailand
[b] University of Chemical Technology and Metallurgy, Sofia, Bulgaria
[c] Otto-Schott-Institut, Friedrich-Schiller-University Jena, Germany

ARTICLE INFO

Article history:
Received 28 August 2008
Accepted 28 January 2009
Available online 10 February 2009

Keywords:
Crystallization
Nano-crystals
Ferroelectric
Lithium niobate
Glass-ceramics

ABSTRACT

Transparent glasses in the (100-x)$LiNbO_3$-xSiO_2 system where $20 \leq x \leq 35$, were produced by conventional melt-quenching technique. The quenched samples were amorphous as proved by X-ray diffraction (XRD) technique. Annealing of the quenched samples at temperatures ranging from 580 to 975 °C resulted in the precipitation of lithium niobate nano-crystals. Scanning electron microscopy (SEM) showed the presence of randomly oriented $LiNbO_3$ nano-crystals dispersed in a continuous glass matrix. The relative dielectric constant (ε_r) was in the range of 80 to 180 and increased with increasing $LiNbO_3$ concentration. The glass ceramic samples annealed at temperatures up to 600 °C are fully transparent.

1. Introduction

In the past few years, the preparation of numerous ferroelectric materials by glass crystallization has been described in the literature [1–4]. This method has been applied for various ferroelectric crystals, such as $BaTiO_3$, $PbTiO_3$, $NaNbO_3$, $LiTaO_3$ and $LiNbO_3$. This method is simple, cheap and potentially suitable for multifunctional devices [5,6]. The starting point of the route is the preparation of a glass by a melting procedure. In order to obtain glass formation, besides the constituents of the ferroelectric phase, also glass forming oxides have to be added. Lithium niobate ($LiNbO_3$) is a very important and interesting ferroelectric material for applications in optics and electronics, such as electro-optical, acusto-optical, piezoelectric and nonlinear optical devices [7–9]. It has a very high Curie temperature (T_c = 1140–1210 °C), good ferroelectric properties and it is still ferroelectric at room temperature [10]. $LiNbO_3$ has poor glass forming ability and hence in order to obtain a glassy material, it is usually required to add a glass former. In previous works, SiO_2 concentrations ≥35 mol% were added to $LiNbO_3$ composition in order to promote the glass formation [4,11]. In the present study, SiO_2 was chosen and the respective SiO_2 concentrations were in the range of 20 to 35 mol% and hence smaller than in previous reports. Furthermore, other intermediate oxide such as Al_2O_3 was not added. The smaller concentrations of SiO_2 should lead to a larger quantity of the ferroelectric phase and hence to larger dielectric constants. In order to obtain transparent glass-ceramics, the crystallites of the ferroelectric phase should be much smaller than the wavelength of the visible light (<200 nm) and the crystal size distribution should be narrow.

2. Experimental procedure

Glasses with the composition (100-x)$LiNbO_3$-xSiO_2 where $20 \leq x \leq 35$ were melted from reagent grade $LiNbO_3$ and SiO_2 in a batch quantity of 30 g at temperatures in the range from 1300–1350 °C in a platinum crucible using an electric furnace. The melts were quenched by pouring onto a brass mould and immediately pressed with another brass plate to obtain 1.5–2.0 mm thick glass sheets. Subsequently the glass samples were placed into a furnace preheated to 550 °C kept for 1 h and then slowly cooled down using a rate of 1 $K \cdot min^{-1}$. In the following, these samples are denoted as "quenched". The quenched samples were annealed at different temperatures ranging from 580 to 975 °C (kept for 1 h) using heating and cooling rates of 10 $K \cdot min^{-1}$. The ground powders of the quenched and annealed samples were investigated by X-ray powder diffraction, using CuKα radiation (XRD; Siemens D5000, Germany). The crystallite size was estimated using the Scherrer Eq. (1) [12,13],

$$L = \frac{k\lambda}{\beta \cos\theta} \quad (1)$$

where L is the mean diameter of a crystal, k is a geometry factor (0.94), λ is the wavelength used (1.5406 Å), β is a full width at half maximum (FWHM) and θ is the Bragg angle. The quenched and annealed samples were characterized using scanning electron microscopy (SEM; Zeiss DSM 940 A, Germany). The capacitances of the quenched and annealed samples (1–2 mm thick and 10 mm in diameter) were measured using impedance spectroscopy (IM5d Zahner Elektrik, Kronach, Germany) at temperatures in the range

* Corresponding author. Tel.: +49 3641 948501; fax: +49 3641 948502.
E-mail address: ccr@rz.uni-jena.de (C. Rüssel).

0167-577X/$ – see front matter © 2009 Published by Elsevier B.V.
doi:10.1016/j.matlet.2009.01.082

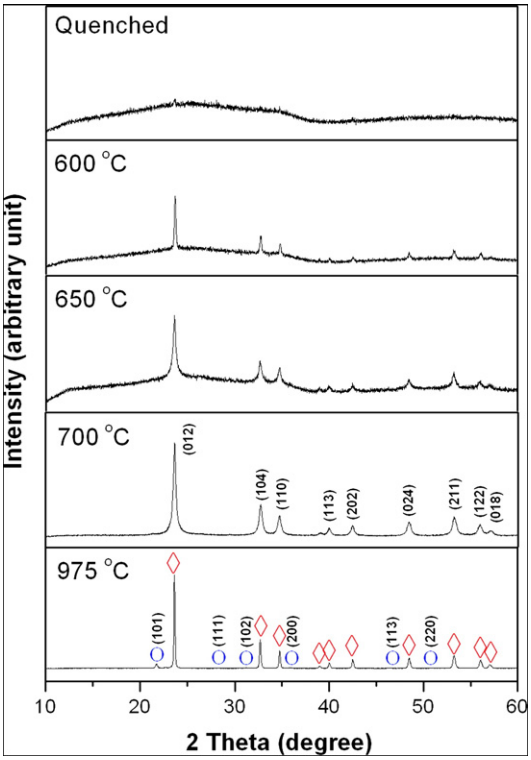

Fig. 1. XRD patterns of the quenched and annealed samples at 600, 650, 700 and 975 °C for 1 h with 30 mol % SiO_2, ◊ $LiNbO_3$, **O** SiO_2 (cristobalite).

from 30 to 150 °C. The amplitude used was 50 mV. The relative dielectric constant (ε_r) was then calculated from the geometry of the sample and the capacitance [14].

3. Results and discussion

The quenched samples were transparent without any visible inclusions. The XRD patterns of all quenched samples (not shown) confirm their amorphous nature. XRD patterns of a sample with the composition $x=30$ are shown in Fig. 1 for various annealing temperatures. The XRD lines observed could be attributed to crystalline lithium niobate and indexed to $LiNbO_3$ (JCPDS file No. 20-0631) which lattice parameters are $a=b=5.1494$ Å, $c=13.862$ Å. After annealing at 975 °C, additional small intensity lines due to cristobalite (SiO_2; JCPDS file No. 82-0512) were observed. The width of the XRD-lines decreased with increasing annealing temperature (not shown). The corresponding crystallite size calculated using Scherrer Equation is shown in Table 1. After annealing at a temperature of 975 °C, the line broadening is too small to enable the calculation of mean crystallite sizes with acceptable errors. In this case the crystals are larger than 50 nm.

Fig. 2 shows SEM-micrographs of a sample with $x=30$ after annealing at temperatures of 600, 700 and 975 °C for 1 h. The $LiNbO_3$ crystals show bright appearance because they possess a larger mean

Table 1
Mean crystallite sizes (calculated by Eq. (1)) of samples annealed at 600, 650, 700 and 975 °C for 1 h with 20, 25, 30 and 35 mol% SiO_2

SiO_2 concentration in mol%	Mean crystallite sizes (in nm) of annealed samples			
	600 °C	650 °C	700 °C	975 °C
20	15	20	35	42
25	14	23	37	43
30	17	26	42	>50
35	25	47	48	>50

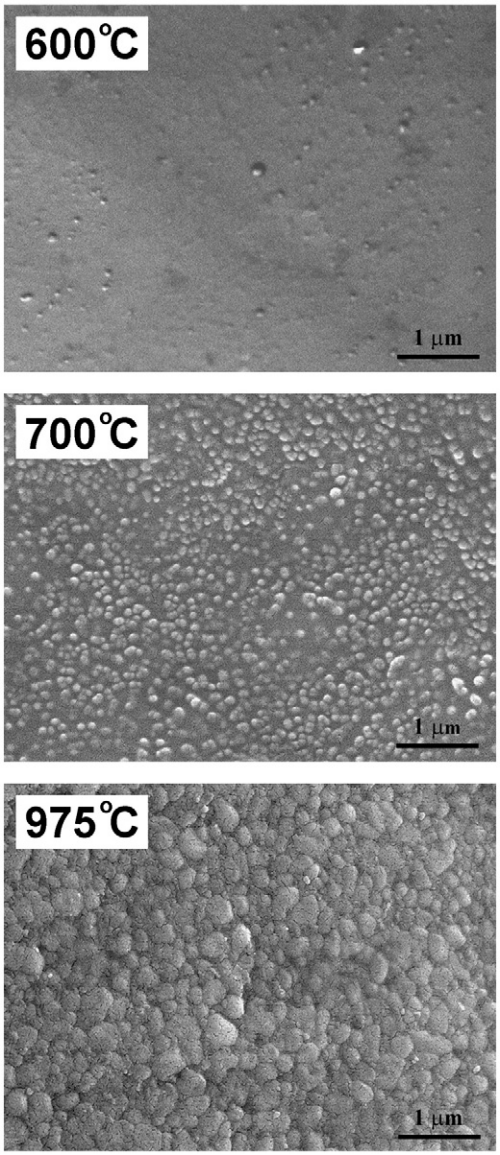

Fig. 2. SEM micrographs of annealed samples at 600, 700 and 975 °C for 1 h with 30 mol % SiO_2.

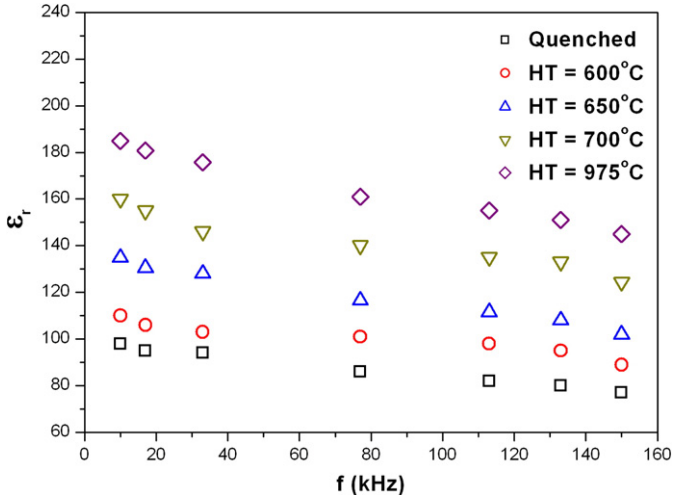

Fig. 3. Variation of the relative dielectric constant (ε_r) as a function of frequency with 30 mol% SiO_2.

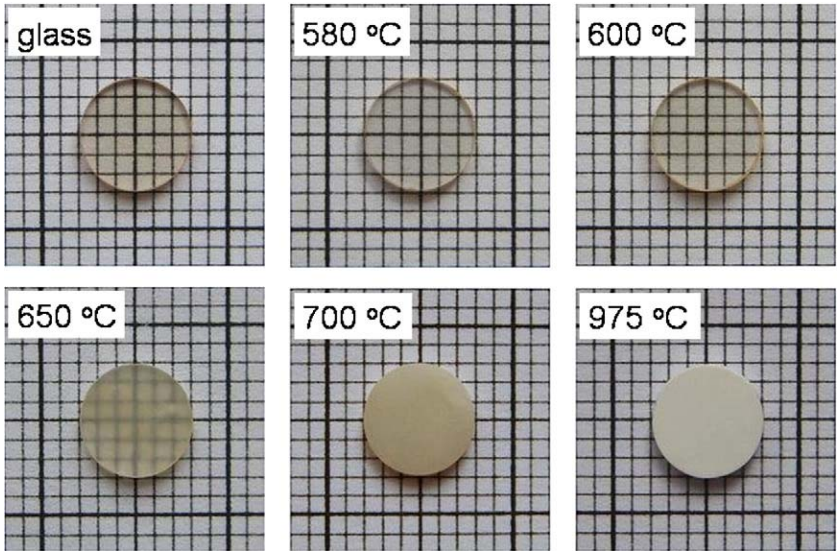

Fig. 4. The images of the quenched and annealed samples at 580, 600, 650, 700 and 975 °C for 1 h with 30 mol% SiO_2.

atomic weight than the SiO_2-rich phase. Fig. 2 shows a micrograph of a sample annealed at 600 °C. A minor quantity of small crystals with sizes of approximately 30 nm is seen. After annealing at a temperature of 700 °C, a number of much larger crystals with the average size of 50 nm are observed. Annealing of the sample at 975 °C leads to the growth of crystals with sizes in the range of 200 to 300 nm. The crystal sizes are in agreement with those calculated from XRD-line broadening.

The variation of the relative dielectric constant (ε_r) as a function of frequency (f) for the samples with $x=30$ is depicted in Fig. 3 for various temperatures. The ε_r values of the samples annealed at 600, 650, 700 and 975 °C for 1 h were larger than those of the quenched samples. The relative dielectric constants increased with increasing annealing temperature and with increasing frequency, the ε_r values decreased. For the sample with $x=30$, the values of the tanδ (δ = loss angle) at 100 kHz were 0.12 and 0.063 after annealing at 600 and 700 °C, respectively.

Fig. 4 shows images of the quenched sample and of annealed samples with $x=30$. The quenched sample and samples annealed at 580 and 600 °C are transparent. Samples annealed at 700 °C and 975 °C are opaque due to the occurrence of larger crystals. For visible light (400 to 800 nm in wavelength), samples possessing crystals larger than 200 nm should show light scattering and hence the respective samples should be opaque [15,16]. Transparent samples showed crystals $\ll$200 nm. The effect of temperature on the mean size of the crystals was surprisingly small: for example in the sample with 20 mol% SiO_2: the size are 15 and 42 nm after annealing at 600 and 975 °C, respectively, giving rise to all transparent glass ceramics in this composition. During crystallization of $LiNbO_3$, the residual glassy phase is enriched in SiO_2, therefore their viscosities should increase during the course of the crystallization. In analogy to previous reports on the crystallization of CaF_2 [17] from silicate glasses, this should lead to a diffusion barrier around the crystals which hinders crystal growth as well as Ostwald ripening.

4. Conclusions

Annealing of glasses in the (100-x)$LiNbO_3$-xSiO_2 system (with $20 \leq x \leq 35$) at temperatures up to 600 °C led to transparent samples containing ferroelectric $LiNbO_3$ crystals. Annealing at 650 °C resulted in samples showing slightly light scattering while samples annealed at $\geq$700 °C are opaque. The mean sizes of the $LiNbO_3$ crystals are in the range of 13 to 50 nm and increased with annealing temperature and SiO_2 concentration of the sample. The relative dielectric constants were in the range of 75 to 190. They increased with increasing annealing temperature and decreasing frequency. For the first time, transparent $LiNbO_3$ glass-ceramics with SiO_2-concentrations as small as 20 mol% were prepared.

Acknowledgements

The authors would like to thank the Thailand Research Fund, Faculty of Science, Graduate School, Chiang Mai University, the Commission on Higher Education, Thailand.

References

[1] Zeng HC, Tanaka K, Hirao K, Soga N. J Non-Cryst Solids 1997;209:112–21.
[2] Shankar MV, Varma KBR. J Non-Cryst Solids 1998;226:145–54.
[3] Nara CS, Ronan L, Maria CCC, Hernandes AC. J Non-Cryst Solids 2000;273:94–9.
[4] Todorovic M, Radonjic L. Ceram Int 1997;23:55–60.
[5] Hu Y, Huang CL. J Non-Cryst Solids 2000;278:170–7.
[6] Prasad NS, Varma KBR. J Non-Cryst Solids 2005;351:1455–65.
[7] Prasad NS, Varma KBR, Takahashi Y, Benino Y, Fujiwara T, Komatsu T. J Solid State Chem 2003;173:209–15.
[8] Xue D, Kitamura K. J Cryst Growth 2003;249:507–13.
[9] Kim JE, Kim SJ, Ohshima K, Hwang ZH, Yang ZS. Mater Sci Eng A 2004;375–377:1255–8.
[10] Radonjic L, Todorovic M, Miladinovic J. Mater Sci Eng B 2005;121:64–70.
[11] Shankar MV, Varma KBR. J Non-Cryst Solids 1999;243:192–203.
[12] Patterson AL. Phys Rev 1939;56:978–82.
[13] Chattopadhyay C, Ayyuby P, Palkar VR, Gurjar AV, Wankar RM, Multani M. J Phys Condens Matter 1997;9:8135–45.
[14] Gerth K, Rüssel C. J Non-Cryst Solids 1999;243:52–60.
[15] Hayashi H, Tanabe S, Hanada T. J Appl Phys 2001;89:1041–5.
[16] Shioya K, Komatsu TK, Kim HG, Sato R, Masusita K. J Non-Cryst Solids 1995;189:16–24.
[17] Rüssel C. Chem Mater 2005;17:5843–7.

Materials Chemistry and Physics 113 (2009) 913–918

Contents lists available at ScienceDirect

Materials Chemistry and Physics

journal homepage: www.elsevier.com/locate/matchemphys

Phase separation and crystallization in $LiNbO_3/SiO_2$ glasses

Pattamaporn Prapitpongwanich[a,b], Kamonpan Pengpat[a], Christian Rüssel[b,*]

[a] Department of Physics, Faculty of Science, Chiang Mai University, Chiang Mai 50200, Thailand
[b] Otto-Schott-Institut, Jena University, Fraunhoferstr. 6, Jena 07743, Germany

ARTICLE INFO

Article history:
Received 23 May 2008
Received in revised form 6 August 2008
Accepted 12 August 2008

Keywords:
Phase separation
Crystallization
Nano-crystals
Ferroelectrics
Lithium niobate
Glass–ceramics

ABSTRACT

Various samples with the compositions $(100-x)LiNbO_3{\cdot}xSiO_2$ (with $x = 10$, 20, 25, 30, 35, 40, 50 and 60) were prepared by conventional melting technique. Samples with $20 \leq x \leq 35$ were transparent, while products with $x = 10$ or $x \geq 40$ were at least partly opaque under the conditions supplied. TEM-micrographs of replicas gave evidence on phase separation in these glasses. At SiO_2-concentrations >30 mol%, the formed structures consist of SiO_2-rich droplets in a $LiNbO_3$-rich matrix phase. The size of the structures increases with increasing SiO_2-concentration. At an SiO_2-concentration of 50 mol%, the droplets are as large as 450 nm. During thermal treatment, the $LiNbO_3$-rich matrix phase crystallizes and forms lithium niobate.

1. Introduction

Lithium niobate is a very interesting ferroelectric material for applications in optics and electronics. Among these applications, electro-optical, acusto-optical and non-linear optical as well as ferroelectric, especially piezoelectric properties are to be mentioned [1–4]. Lithium niobate has a very high Curie temperature ($T_c = 1140\,^\circ C$) and hence can also be applied as ferroelectrics at elevated temperatures [5,6].

Lithium niobate ceramics can be produced by conventional sintering techniques, however, also single crystals can be prepared by the Czochralski method [7]. Besides, in the past few years, the crystallization of lithium niobate glass–ceramics from $Li_2O/Nb_2O_5/SiO_2$, $Li_2O/Nb_2O_5/SiO_2/Al_2O_3$, $Li_2O/Nb_2O_5/TeO_2$ and $Li_2O/Nb_2O_5/B_2O_3$ glasses has been reported in the literature [8–12]. Niobium oxide is a conditional glass former and hence, pure $LiNbO_3$ glasses can only be produced by rapid quenching of a melt, e.g. by using twin roller techniques [4,13]. In order to obtain glasses using cooling rates convenient in glass technology, it is necessary to add network-forming oxides, such as B_2O_3 or SiO_2 [8]. In order to obtain durable materials, the crystallization from borate glasses is less advantageous, because the residual glassy matrix has a poor corrosion resistance. In the literature, the glass formation after addition of ≥ 50 mol% SiO_2 has for example been reported in Ref. [9]. Usually, the procedure is as follows: First a homogeneous glass is melted and in a second preparation step it is thermally treated which results in the crystallization of the ferroelectric phase. By analogy, also the crystallization of other ferroelectric phases such as langasite ($La_3Ga_5SiO_{14}$) or $BaTiO_3$ has been reported in the literature especially for cheap multifunctional devices [14,15]. If using smaller SiO_2 additions, the cooled samples were no longer transparent. Lithium niobate-based glasses with SiO_2-concentrations ≥ 50 mol% have been studied with respect to their glass formation and crystallization behaviour. Here also the preparation of oriented glass–ceramics by surface crystallization [16] or electrochemically induced nucleation has been reported [17]. Using this technique, an orientation along the crystallographic *c*-axis, i.e. the polar axis can be achieved.

This paper reports on a fundamental study on glass formation, phase separation and crystallization in glasses with the compositions $(100-x)LiNbO_3{\cdot}xSiO_2$ where x is in the range from 10 to 60.

2. Experimental procedure

Glasses in the system $(100-x)LiNbO_3{\cdot}xSiO_2$ with $x = 10$, 20, 25, 30, 35, 40, 50 and 60 were prepared from reagent grade $LiNbO_3$ and SiO_2 by conventional melting technique. First, $LiNbO_3$ was prepared by thermal treatment of equimolar quantities of Li_2CO_3 and Nb_2O_5 within a solid state reaction at 800 °C for 2 h in air. Then, the glasses were melted in a platinum crucible in batches of 30 g at 1300–1400 °C kept for 1 h. The melts were quenched by pouring them onto a brass mould and pressing another brass plate onto the melt for avoiding crystallization. The samples obtained were 1–2 mm thick. Subsequently all the samples were given to a furnace preheated to 550 °C kept for 1 h to reduce thermal stresses and then slowly cooled to room temperature using a rate of $1\,K\,min^{-1}$. These samples in the following are denoted as "quenched". Subsequently, the quenched

* Corresponding author. Tel.: +49 3641 948500; fax: +49 3641 948502.
E-mail address: ccr@rz.uni-jena.de (C. Rüssel).

0254-0584/$ – see front matter © 2008 Elsevier B.V. All rights reserved.
doi:10.1016/j.matchemphys.2008.08.070

samples were annealed at 700 °C for 1 h using a heating and cooling rate of 10 K min^{-1}.

The melted samples were characterized by differential thermal analysis (DTA-50; Shimadzu, Germany) using a heating rate of 10 K min^{-1}. The density was measured by Archimedean principle with distilled water as immersion liquid. The quenched samples as well as thermally treated samples were characterized by X-ray diffraction using Cu Kα radiation (XRD; Siemens D 5000, Germany). The microstructures of the annealed samples were characterized by scanning electron microscopy (SEM; Zeiss DSM 940 A, Germany); the respective samples were ground and polished and subsequently coated with gold. The micrographs were obtained using a backscatter electron detector (BSE). The quenched samples were further investigated by transmission electron microscopy (TEM; Hitachi H 8100, Japan) using an acceleration voltage of 200 kV. The following replica technique was used: the samples were fractured in vacuum and coated with a thin Pt–Ir–C layer. After treatment with acid, the film was removed from the surface and studied by TEM (for a detailed description see [18]). The replica film shows only the topography of the fractured surface and is not affected by the etching procedure.

3. Results

The products obtained after quenching the melt as described in the Section 2 were opaque in the case of an SiO_2-concentration of 10 mol%. Samples with 20–35 mol% SiO_2 were transparent and yellowish colored, the sample with 40 mol% SiO_2 exhibited some transparent and some opaque regions, while glasses with larger SiO_2-concentrations were opaque again. A transparent sample with an SiO_2-concentration of 30 mol% is shown in Fig. 1.

Fig. 2 shows XRD-patterns of quenched samples of all compositions studied. The sample with 10 mol% SiO_2 shows distinct XRD-lines all attributable to crystalline $LiNbO_3$ (JCPDS nr. 20-0631). Samples with 20 and 25 mol% SiO_2 showed lines of marginal intensities also due to $LiNbO_3$; while the sample with 60 mol% SiO_2 shows low intensity lines (see $2\theta = 22^\circ$) caused by cristobalite. The XRD-patterns of all other samples did not show distinct lines of larger intensity and exhibited an appearance typing for glasses.

Fig. 3 shows DTA-profiles of quenched samples with 20, 25, 30, 35, 40, 50 and 60 mol% SiO_2. Whereas T_g is 557 °C for the sample with the smallest SiO_2-concentration (20 mol%), it is larger at higher SiO_2-concentrations. In the range from 654 to 699 °C, a first exothermic peak is observed (T_{Cr}) and at temperatures of around 1150 °C an endothermic reaction is seen.

Fig. 4 shows T_g and the temperature of the first exothermic peak; T_{Cr} both plotted against the SiO_2-concentration. The crystallization temperature increases from 654 to 699 °C for the samples with 20 and 35 mol% SiO_2, respectively. At higher SiO_2-concentrations, T_{Cr} is around 680 °C and, within the limits of error, does not depend on the SiO_2-concentration.

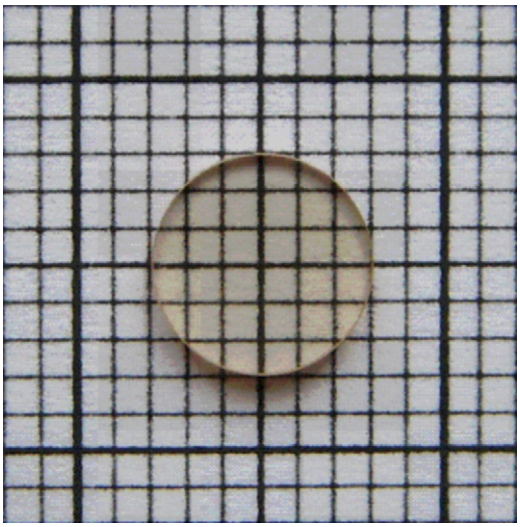

Fig. 1. Image (minor scale = 1 mm) of a glassy sample with an SiO_2-concentration of 30 mol%.

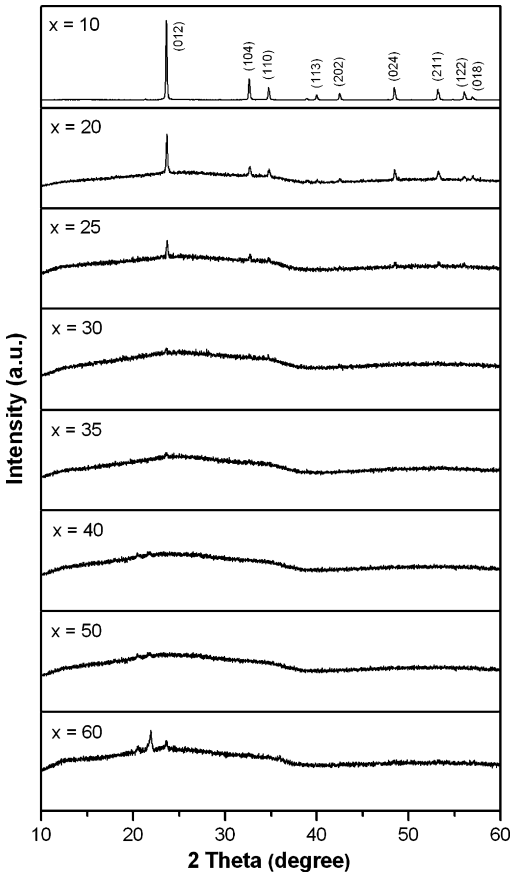

Fig. 2. XRD-patterns of quenched samples with SiO_2-concentrations of 20, 25, 30, 35, 40, 50 and 60 mol%.

Fig. 5 shows XRD-patterns of samples annealed at 700 °C for 1 h. All the samples exhibit distinct lines due to crystalline lithium niobate (JCPDS nr. 20-0631). Hence at the temperature supplied all glasses crystallized and no other phase than lithium niobate was formed. In comparison to Fig. 1, graph $x = 10$, the XRD-lines are notably broadened.

Table 1 shows the densities of quenched samples from 10 to 60 mol% SiO_2 and thermally treated samples from 20 to 35 mol% SiO_2 with the compositions $(100-x)LiNbO_3{\cdot}xSiO_2$. The densities decrease with increasing SiO_2-concentrations.

Fig. 6 shows TEM-micrographs of samples with 20, 25, 30, 35, 40 and 50 mol% SiO_2. All micrographs possess the same magnifications. The sample with 20 mol% SiO_2 shows some heterogeneity with sizes in the range of 30–50 nm. The sample with 25 mol%

Table 1
The densities of quenched and annealed samples with the compositions $(100-x)LiNbO_3{\cdot}xSiO_2$

SiO_2-concentration (x)	Density (g cm^{-3})	
	Quenched samples	Annealed samples at 700 °C for 1 h
10	4.263 ± 0.007	–
20	3.977 ± 0.002	4.233 ± 0.007
25	3.899 ± 0.007	4.102 ± 0.003
30	3.834 ± 0.001	3.949 ± 0.004
35	3.750 ± 0.009	3.862 ± 0.007
40	3.664 ± 0.008	
50	3.451 ± 0.002	
60	3.224 ± 0.004	

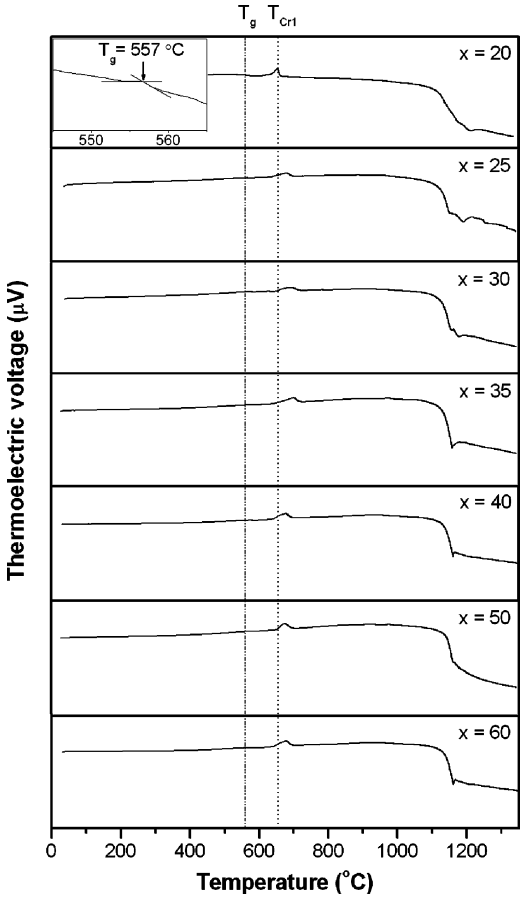

Fig. 3. DTA-profiles of quenched samples with SiO_2-concentrations of 20, 25, 30, 35, 40, 50 and 60 mol%.

SiO_2 is notably more homogeneous. The size of the heterogeneities is below 30 nm. In the sample with 30 mol% SiO_2, the heterogeneities are larger again (approximately 150 nm). In the sample with 35 mol%, the structures observed exhibit a size of around 250 nm and appears as elongated droplets, while in the sample with 40 mol% SiO_2, they are as large as 350 nm. In the sample with 50 mol% SiO_2, the sizes of the heterogeneous structures are around

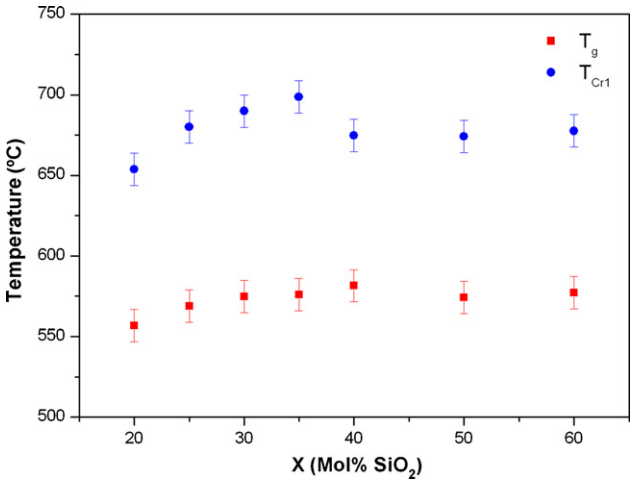

Fig. 4. The glass transition temperature, T_g and the temperature of the first crystallization peak as a function of the SiO_2-concentration (error in the temperatures ±10 K).

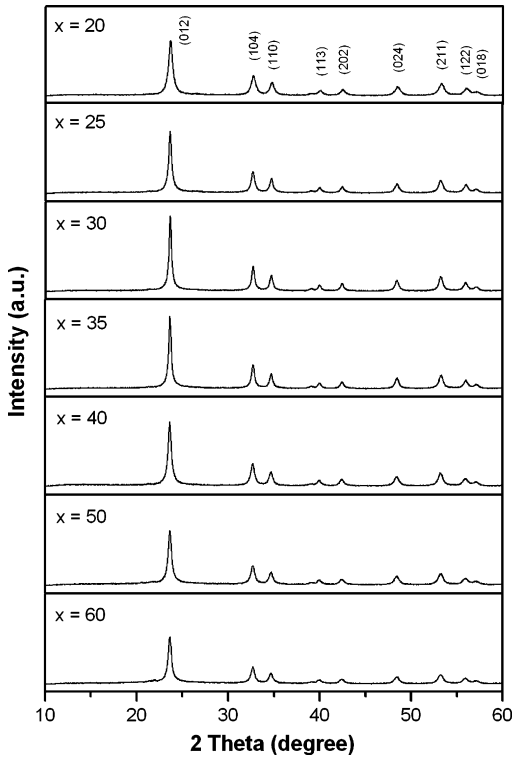

Fig. 5. XRD-patterns of samples with SiO_2-concentrations of 20, 25, 30, 35, 40, 50 and 60 mol% annealed at 700 °C for 1 h.

450 nm. In the case of samples with 40 and 50 mol% SiO_2, the heterogeneities possess a droplet shape.

Fig. 7 shows SEM-micrographs of samples with 40, 45, 50 and 60 mol% SiO_2 all annealed at 700 °C for 1 h. Here, a phase of dark appearance which exhibit an almost spherical shape and a matrix phase of light appearance are seen. In the case of the samples with 45 and 60 mol% SiO_2, the size of the spherical crystals is in the range from 400 to 1000 nm, while it is 1–3 μm for the sample with 50 mol% SiO_2.

4. Discussion

The system $LiNbO_3$–SiO_2 exhibits a fairly broad glass forming range [9]. An SiO_2-concentration of 20 mol% is large enough to obtain transparent light yellowish and nearly amorphous samples. It is interesting to note that the color observed is similar to $LiNbO_3$ single crystals prepared by Czochralski method [19]. At an SiO_2-concentration of only 10 mol%, and the cooling rates supplied, spontaneous crystallization of $LiNbO_3$ occurred. An SiO_2-concentration of 20 mol%, under the cooling conditions applied, however, was large enough to provide transparent and mainly amorphous samples, which, however, exhibit a heterogeneous microstructure as shown by TEM (see Fig. 6). The heterogeneities were 30–50 nm large. The sample with 25 mol% SiO_2 showed the smallest heterogeneities with sizes below 30 nm. Then, with increasing SiO_2-concentration, the size of the structures observed in the TEM-micrographs increased again. Todorovic and Radonjic [9] already reported on phase separation in the Li_2O–Nb_2O_5–SiO_2–Al_2O_3 glass system. In a glass with an SiO_2-concentration of 37.2 and an Al_2O_3-concentration of 5.4 mol%, droplets with diameters in the range from 20 to 50 nm were formed during annealing at 610 °C for 10 min. Also these samples were reported to be transparent.

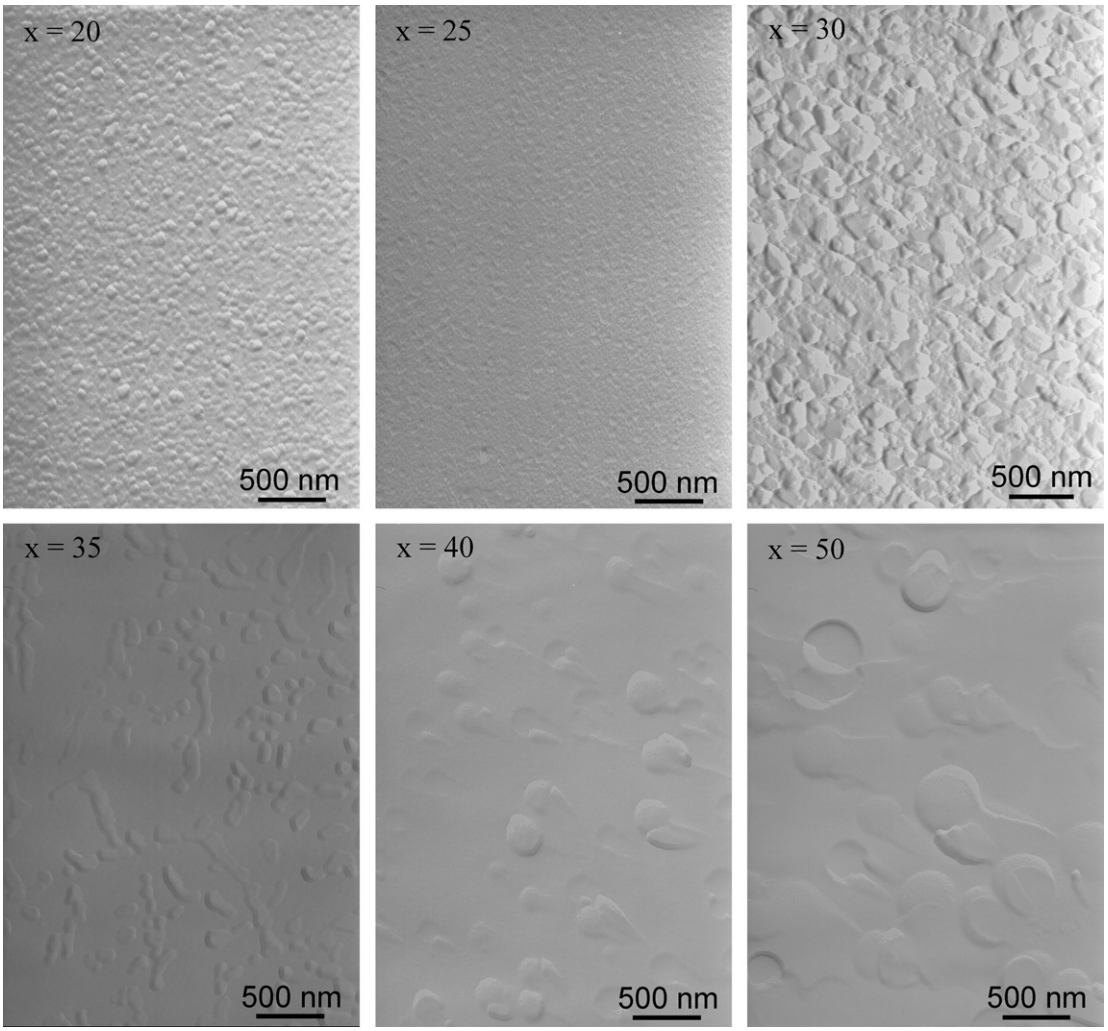

Fig. 6. TEM-micrographs of replicas; samples with 20, 25, 30, 35, 40 and 50 mol% SiO_2.

Samples with an SiO_2-concentration of 40 mol% show light scattering and are opaque. Since the XRD-patterns of the quenched samples do not show lines of large intensities, the light scattering is caused by phase separation. As shown in the TEM-micrographs (see Fig. 6), droplets with a size of 350 nm are observed. In principle, all glassy samples which exhibit phase separation with structures larger than 100 nm, are usually opaque (see also Ref. [20]). In the case of the samples with 40 and 50 mol% SiO_2, the droplet shape of the heterogeneities also gives evidence for phase separation. During the course of the phase separation process, supposedly $LiNbO_3$- and SiO_2-rich phases are formed.

The effect of the SiO_2-concentration on the glass transition temperature is fairly small; within the range from 20 to 35 mol% SiO_2. The glass transition temperature, T_g increases less than 20 K. It should be noted that the increase in the crystallization temperature is more pronounced, it increases from 654 to 690 °C, while increasing the SiO_2-concentration from 20 to 30 mol%. A further increase leads to more pronounced phase separation and the crystallization temperature remains approximately constant (690 °C ± 10 K).

At a first glance, it is surprising that the glass transition temperature does not notably depend on the SiO_2-concentration. However, in the phase-separated structure, two phases, a $LiNbO_3$-rich matrix phase and an SiO_2-rich droplet phase are formed. The compositions of these two phases should not depend so much on the SiO_2-concentration. With increasing SiO_2-concentration, mainly the quantity of the SiO_2-rich phase should increase. Without the occurrence of phase separation, the glass transition temperature should steadily increase with the SiO_2-concentration. By contrast in the TeO_2/$LiNbO_3$-system, Shankar and Varma [12] reported that T_g increases with decreasing TeO_2-concentration. These glasses are not phase-separated and the melting point of TeO_2 is 730 °C, i.e. much lower than that of SiO_2 (1723 °C).

During annealing of the samples, crystallization of lithium niobate occurs. Other phases, such as $LiNb_3O_8$ were not observed (see e.g. Refs. [11,21]). Kim et al. [4] studied glasses in the $LiNbO_3$/SiO_2-system; however, they quenched the melts by using a twin roller technique. They reported the occurrence of two exothermic peaks in the DTA-profiles which are attributed to crystallization of $LiNbO_3$ and $Li_6Si_2O_7$, respectively.

In the SEM-micrographs of annealed samples (see Fig. 7); spherical structures of dark appearance as well as a matrix phase of light appearance are observed. The size of the spherical structures is approximately the same as that of the droplet phase as shown in Fig. 6. The phase of dark appearance is the SiO_2-rich phase because this phase possesses the smaller mean atomic weight in comparison to the $LiNbO_3$-rich phase. Then, the droplet phase shown in Fig. 6 should also be the SiO_2-rich phase. During thermal treatment at 700 °C, the matrix phase crystallizes and forms lithium niobate.

In principle, phase separation in glass forming melts is a well-known phenomenon. It might occur above the liquidus tem-

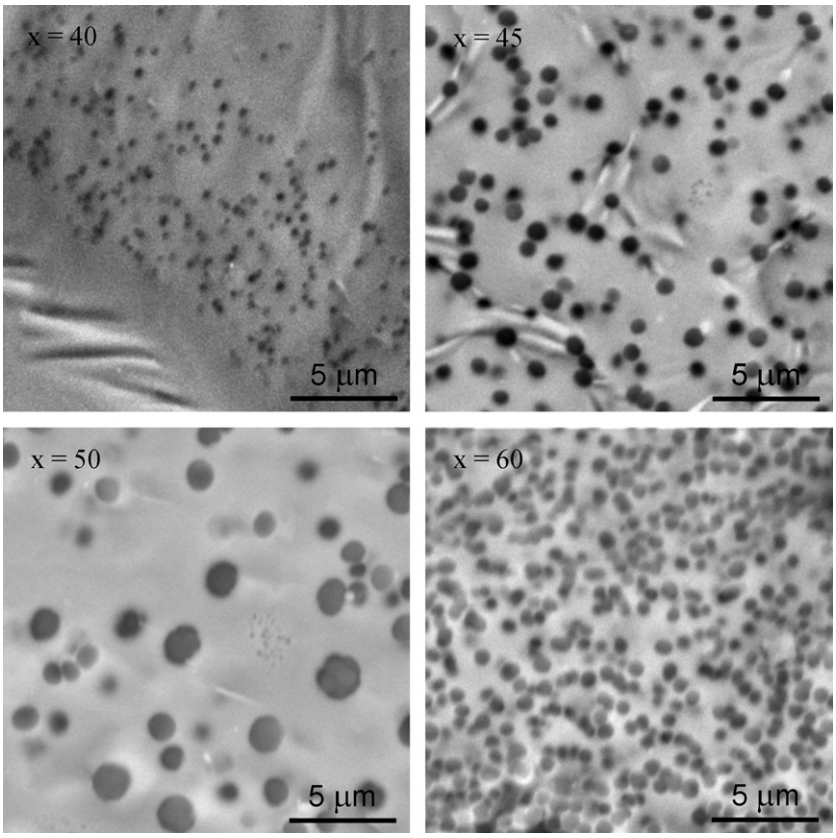

Fig. 7. SEM-micrographs (BSE detector) of polished samples annealed at 700 °C for 1 h with 40, 45, 50 and 60 mol% SiO_2.

perature, for example in the MgO–SiO_2, CaO–SiO_2 and PbO–SiO_2 [22] systems. A liquid of a composition within such a miscibility gap, during cooling usually shows phase separation and subsequently sedimentation and finally two glassy layers with different compositions are observed. Systems exhibiting metastable liquid–liquid phase separation (below the liquidus temperature), such as the systems BaO–SiO_2 [23] or Na_2O–B_2O_3–SiO_2 [24] widely enable to tailor the microstructure, for example the sizes of droplets or interpenetrating structures by annealing. Here, the phase separation process is much slower, because of the higher viscosities of the respective liquids. These effects have intensively been studied since the pioneer investigations of Porai-Koshits [25] and Vogel [26]. A phase-separated droplet structure is a good prerequisite for a subsequent crystallization process. In many cases, the crystal formed from the droplet phase has a size comparable to that of the droplet.

This facilitates to tailor the final size of the crystallites. For example in the case of apatite glass–ceramics [27], droplets enriched in CaO and P_2O_5 are formed which during annealing are transferred to crystalline apatite. In the present case, however, the droplet phase, which is enriched in silica does not crystallize during annealing. However, the matrix phase is crystallizing and forms lithium niobate. This leads to a microstructure which is composed by a continuous ferroelectric phase with embedded SiO_2 droplets and is supposed to possess favourable dielectric properties. Usually, a droplet structure is considered as a binodal structure, while an interpenetrating microstructure is supposed as spinodal. It should, however, be mentioned that the structure may change during the course of the cooling process and hence, the attribution of a certain structure to binodal or spinodal is never completely clear. In our case, the structures in the case of an SiO_2-concentration $\geq$40% is that of droplets and hence supposedly binodal, while for an SiO_2-concentration of 35%, the structure might be interpenetrating and hence probably spinodal. The miscibility gap hence seems to process a maximum near 35% SiO_2. At smaller SiO_2-concentration again a droplet structure is formed.

It should be noted that in all previous studies on the $LiNbO_3$/SiO_2 system, the SiO_2-concentrations were much larger than in the present study.

5. Conclusions

Glasses with the compositions $(100-x)LiNbO_3{\cdot}xSiO_2$ (with x = 10, 20, 25, 30, 35, 40, 50 and 60) were transparent for $20 \leq x \leq 35$ while glasses with x = 10 or $x \geq 40$ were at least partly opaque under the conditions supplied. As shown by TEM-micrographs from replicas phase separation occurred and SiO_2-rich droplets in a $LiNbO_3$-rich matrix phase were formed. The size of the droplets increased with increasing SiO_2-concentration. During thermal treatment at 700 °C, the $LiNbO_3$-rich matrix phase crystallized and formed rhombohedral lithium niobate.

Acknowledgments

This work was supported by the Thailand Research Fund, Faculty of Science, Graduate School, Chiang Mai University and the Commission on Higher Education, Thailand.

References

[1] J.-J. Shyu, J.-R. Wang, J. Am. Ceram. Soc. 83 (2000) 3135.
[2] N.S. Prasad, K.B.R. Varma, Y. Takahashi, Y. Benino, T. Fujiwara, T. Komatsu, J. Solid State Chem. 173 (2003) 209.
[3] D. Xue, K. Kitamura, J. Cryst. Growth 249 (2003) 507.
[4] J.E. Kim, S.J. Kim, K. Ohshima, Y.H. Hwang, Y.S. Yang, Mater. Sci. Eng. A 375–377 (2004) 1255.

[5] X. Zhang, D. Xue, J. Phys. Chem. B 111 (2007) 2587.
[6] M.N. Palatnikov, N.V. Sidorov, V.I. Skiba, D.V. Makarov, I.V. Biryukova, Y.A. Serebryakov, O.E. Kravchenko, Y.I. Balabanov, V.T. Kalinnikov, Inorg. Mater. 36 (2000) 489.
[7] M.P.E. Graca, M.A. Valente, M.G. Ferreira da Silva, J. Non-Cryst. Solids 325 (2003) 267.
[8] H.C. Zeng, K. Tanaka, K. Hirao, N. Soga, J. Non-Cryst. Solids 209 (1997) 112.
[9] M. Todorovic, L. Radonjic, Ceram. Int. 23 (1997) 55.
[10] Y. Hu, C.-L. Huang, Mater. Res. Bull. 35 (2000) 1999.
[11] H.G. Kim, T. Komatsu, R. Sato, K. Matusita, J. Mater. Sci. 31 (1996) 2159.
[12] M.V. Shankar, K.B.R. Varma, J. Non-Cryst. Solids 243 (1999) 192.
[13] H. Engelmann, W. Gatzweiler, I. Dezsi, U. Gonser, Phys. Stat. Sol. 105 (1988) 219.
[14] J. Stade, L. Bohaty, M. Hengst, R.B. Heimann, Cryst. Res. Technol. 37 (2002) 1113.
[15] K.-L. Ying, T.-E. Hsieh, Mater. Sci. Eng. B 138 (2007) 241.
[16] Y. Ding, Y. Miura, S. Nakaoka, T. Nanba, J. Non-Cryst. Solids 259 (1999) 132.
[17] K. Gerth, C. Rüssel, J. Non-Cryst. Solids 243 (1999) 52.
[18] W. Vogel, L. Horn, H. Reiß, G. Völksch, J. Non-Cryst. Solids 49 (1982) 221.
[19] H.J. Lee, J.W. Shur, T.I. Shin, H.D. Yoon, Opt. Mater. 30 (2007) 85.
[20] S. Morimoto, J. Non-Cryst. Solids 352 (2006) 756.
[21] N.S. Prasad, K.B.R. Varma, J. Non-Cryst. Solids 351 (2005) 1455.
[22] H. Scholze, Glas, Natur, Struktur und Eigenschaften, Springer, Berlin, Heidelberg, New York, 1988.
[23] E.D. Zanotto, P.F. James, A.F. Craievich, J. Mater. Sci. 21 (1986) 3050.
[24] W. Vogel, J. Non-Cryst. Solids 25 (1977) 172.
[25] E.A. Porai-Koshits, V.I. Averjanov, J. Non-Cryst. Solids 1 (1968) 29.
[26] W. Vogel, K. Gerth, Glastechn. Ber 31 (1958) 15.
[27] C. Moisescu, C. Jana, C. Rüssel, J. Non-Cryst. Solids 248 (1999) 169.

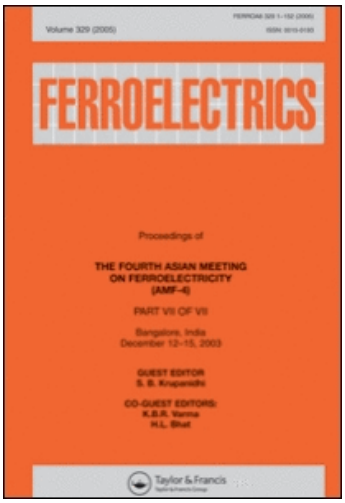

Ferroelectrics
Publication details, including instructions for authors and subscription information:
http://www.informaworld.com/smpp/title~content=t713617887

Ferroelectric and Pyroelectric Properties of $0.8PbZr_{0.52}Ti_{0.48}O_3$-$0.2BaFe_{0.5}Nb_{0.5}O_3$ Ceramics

S. Eitssayeam [a]; U. Intatha [b]; K. Pengpat [a]; G. Rujijanagul [a]; P. Thavornyutikarn [c]; T. Tunkasiri [a]
[a] Department of Physics, Faculty of Science, Chiang Mai University, Chiang Mai, Thailand [b] School of Science, Mae Fah Luang University, Chiang Rai, Thailand [c] Department of Chemistry, of Science, Chiang Mai University, Chiang Mai, Thailand

Online Publication Date: 01 January 2008

To cite this Article Eitssayeam, S., Intatha, U., Pengpat, K., Rujijanagul, G., Thavornyutikarn, P. and Tunkasiri, T.(2008)'Ferroelectric and Pyroelectric Properties of $0.8PbZr_{0.52}Ti_{0.48}O_3$-$0.2BaFe_{0.5}Nb_{0.5}O_3$ Ceramics',Ferroelectrics,376:1,116 — 121
To link to this Article: DOI: 10.1080/00150190802440922
URL: http://dx.doi.org/10.1080/00150190802440922

Ferroelectrics, 376:116–121, 2008

ISSN: 0015-0193 print / 1563-5112 online
DOI: 10.1080/00150190802440922

Taylor & Francis
Taylor & Francis Group

Ferroelectric and Pyroelectric Properties of $0.8PbZr_{0.52}Ti_{0.48}O_3$–$0.2BaFe_{0.5}Nb_{0.5}O_3$ Ceramics

S. EITSSAYEAM,[1] U. INTATHA,[2] K. PENGPAT,[1]
G. RUJIJANAGUL,[1] P. THAVORNYUTIKARN,[3]
AND T. TUNKASIRI[1,*]

[1]Department of Physics, Faculty of Science, Chiang Mai University, Chiang Mai, 50202, Thailand
[2]School of Science, Mae Fah Luang University, Chiang Rai, 57100, Thailand
[3]Department of Chemistry, of Science, Chiang Mai University, Chiang Mai, 50202, Thailand

The solid solution $0.8PbZr_{0.52}Ti_{0.48}O_3$–$0.2BaFe_{0.5}Nb_{0.5}O_3$ (P8B2) ceramic was prepared by the mixed oxide method. The aim of this work is to focus on the ferroelectric and pyroelectric properties of the ceramic. The phase formation behavior was studied using X-ray diffraction (XRD) methods. The ferroelectric properties were measured by a Sawyer-Tower circuit. Particularly, we measured the dielectric and pyroelectric properties by an automatic corrected data with Hewlett-Packard LCZ meter in the environmental chamber. The optimum conditions for fabrication of 0.8PZT–0.2BFN ceramics were found at 1100°C for calcination and 1200°C for sintering temperature. From the hysteresis loop measurement, the remanent polarization (P_r) and coercive field were 21 $\mu C/cm^2$ and 6.4 kV/cm, respectively. The phase transition temperatures (T_c) obtained by pyroelectric measurements are in good agreement with the values obtained from the dielectric study.

Keywords Ferroelectric properties; Pyroelectric properties; PZT

PACS numbers: 77.65.-j; 77.70.+a; 77.84.Dy

1. Introduction

Piezoelectricity is the ability of certain crystalline materials to develop an electric charge proportional to a mechanical stress. It was discovered by J. and P. Curie in 1880 [1, 2]. It was realized that materials showing this phenomenon must also show the converse effect, a geometric strain (deformation) proportional to an applied voltage. Among all of these materials, lead zirconate titanate (PZT) has been most extensively used in piezoelectric applications. These ceramics have high values for the piezoelectric charge coefficient (d_{33}), electromechanical coupling coefficient (k_p) and dielectric constant (ε_r) [3]. They also have low dielectric loss. Modifications of the PZT ceramics, the effects of dopants and preparation method had been studied to find out the optimum condition for PZT ceramics applications.

Received March 11, 2008; in final form July 3, 2008.
*Corresponding author. E-mail: tawee@chiangmai.ac.th

Due to the rapid development of functional ceramics, many kinds of piezoelectric materials have been employed for ceramic actuators to find out the advantages of fast response, high generating force, and low power consumption. $BaFe_{0.5}Nb_{0.5}O_3$ is also another interesting perovskite compound which possesses a considerably high dielectric constant. This work then aimed at developing the dielectric and piezoelectric properties of PZT by adding BFN. For this purpose, we first prepared the PZT-BFN ceramics by the conventional mixed oxide method to find out the suitable condition for actuator applications. In earlier work [4], (1-x)$PbZr_{0.52}Ti_{0.48}O_3$ – x$BaFe_{0.5}Nb_{0.5}O_3$ (x = 0.1, 0.2, 0.3, 0.4 and 0.5) ceramic system was investigated. It was reported that the (1-x)PZT-xBFN ceramic of x = 0.2 has interesting dielectric and piezoelectric properties. Therefore, in this study we have emphasized the composition of x = 0.2 on (1-x)PZT-xBFN ceramic system. The phase evolution of the samples was investigated by an x-ray diffractometer. The pyroelectric, ferroelectric and dielectric properties of PZT-BFN ceramics were determined.

2. Experimental

The 0.8PZT–0.2BFN ceramics used in this study are prepared from powders using the conventional mixed-oxide method. The 0.8$PbZr_{0.52}Ti_{0.48}O_3$–0.2$BaFe_{0.5}Nb_{0.5}O_3$ powders were first prepared by mixing the starting materials of PbO, ZrO_2, TiO_2, $BaCO_3$, Fe_2O_3 and Nb_2O_5 powders in the desired ratio. These powders were ball-milled for 24 h in polyethylene container with zirconia balls. Ethanol was used as a milling medium. After drying, the mixed powders were then calcined at 800–1100°C for 2 h with heating and cooling rate of 5°C/min. Subsequently, the most appropriate calcined samples were pressed into disc shape and sintered at various temperatures ranging from 1150 to 1300°C. The samples were heated for 2 h with constant heating and cooling rates of 5°C/min. The densities of the sintered ceramics were measured by the Archimedes method. The phase formations of the calcined powders were studied by an X-ray diffractometer (Philips Model PW 1729). The diffractometer was operated at the voltage and current of 30 kV and 40 mA respectively. Monochromatic Cok_α radiation of wavelength 1.78901 Å was used throughout the measurement. The dielectric measurements were carried out on the automated systems. The system consists of a precision impedance analyzer (Agilent 4294A), an environmental chamber (Delta 9023), and a desktop computer. This system was capable of making dielectric measurements in the frequency range from 1 kHz to 1 MHz and temperature range from room temperature to 300°C. Prior to measurement, the surfaces of the samples were polished with 1 μm Al_2O_3 powders and electroded by silver paste. The P-E hysteresis loops were measured using a Sawyer-Tower circuit at temperature between room temperature and 155°C. The temperature dependence of pyroelectric coefficient was determined by direct measurement method.

3. Result and Discussion

Powder XRD patterns of the calcined powders are given in Fig. 1. The XRD results of calcined 0.8PZT–0.2BFN powders show that the perovskite structure of PZT started to form at 800°C and more pronounced at higher calcining temperature. The pyrochlore phase was not observed by this method. The XRD phase analysis was based on the JCPDS file No 33-784 [5] for PZT and ICSD No.43622 [6] for BFN. The powder calcined at 1100°C was employed to prepare ceramic samples. The density results show that the density depends on the sintering temperatures, varying from 5.95, 6.94, 7.50 and 7.33 g/cm^3 for the samples sintered at 1150, 1200, 1250 and 1300°C, respectively.

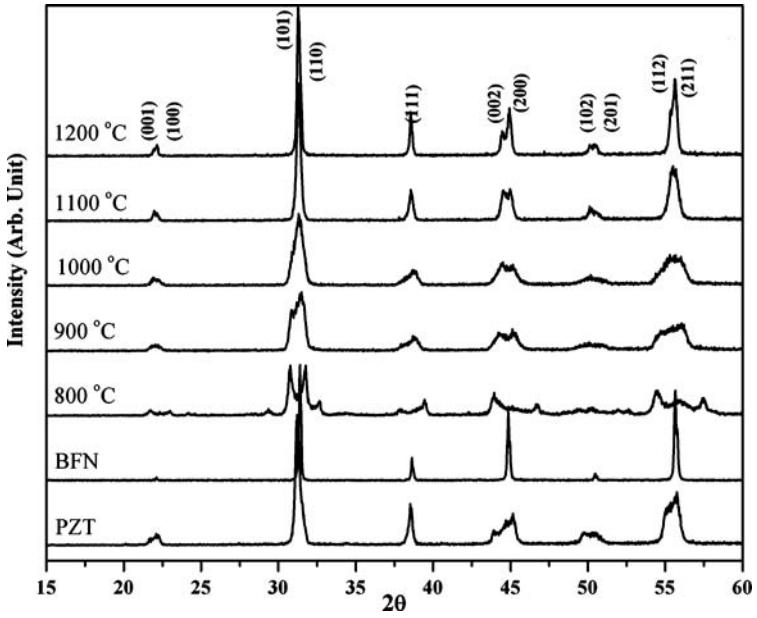

Figure 1. XRD patterns of 0.8PZT-0.2BFN powder at various calcination temperatures.

The temperature dependence of dielectric constant at various frequencies is illustrated in Fig. 2. It was clearly shown that the dielectric constant depends on temperature, but no significant change on the dielectric loss was observed in the temperature range 50–220°C. The Curie temperature of the ceramic is 200°C lower than that of pure PZT (390°C). The dielecric constant at room temperature measured at 1 KHz was 3270 and increased up to 7620 at the curie point. The maximum value of dielectric constant and dielectric loss slightly decreased with increasing frequency. The sample displays a normal ferroelectric behavior, based on the Curie–Weiss law. Thus, the characteristics of the phase transition of

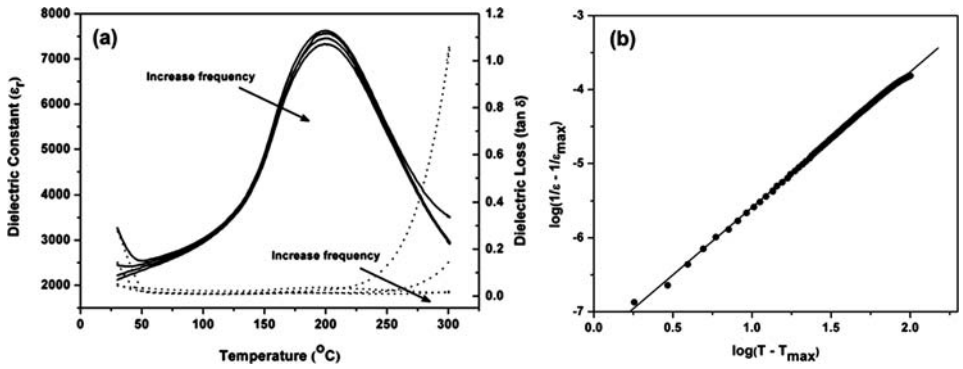

Figure 2. (a) Temperature and frequency dependence of dielectric constant and dielectric loss of 0.8PZT-0.2BFN ceramics and (b) plots of $\log((1/\varepsilon) - (1/\varepsilon_m))$ vs. $\log(T - T_m)$ for 0.8PZT-0.2BFN ceramics.

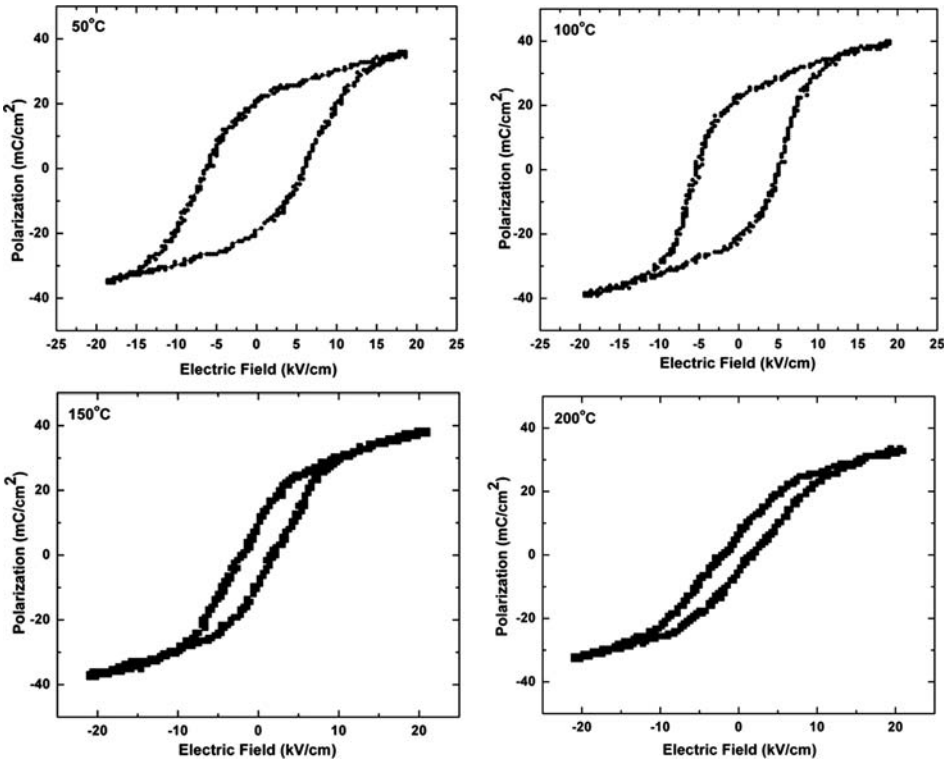

Figure 3. P-E hysteresis loops of 0.8PZT-0.2BFN ceramics at various temperatures.

this ceramic can be explained in term of a generalized empirical equation of the type:

$$\frac{1}{\varepsilon} = \frac{1}{\varepsilon_m}\left[1 + \left(\frac{T - T_m}{\Delta}\right)^{\gamma}\right] \tag{1}$$

where ε_m is maximum permittivity, γ and Δ are the index showing the roundness and a parameter indicating the temperature width of the peak of the dielectric constant, respectively. For 0.8PZT–0.2BFN composition, γ can be estimated from the slope of the dielectric data and Δ can be calculated from the intercept of the dielectric data as shown in Fig. 2(b). The γ and Δ values are 1.734 and 91, respectively. The γ value is normally equal to 2 for relaxor, but the γ value in this work was less than 2 [7].

The ferroelectric behaviour was also investigated by the hyteresis loop measurement. Fig. 3 shows the polarization vs. electric field ($P - E$) hysteresis loops of various temperatures. It can be seen that the higher temperature the thinner of hysteresis loop was obtained. P_r were found to be 21, 22, 12 and 7 μC/cm^2 with coercive fields were 6.4, 5.6, 2.3 and 2.2 kV/cm for measurement at 50, 100, 150 and 200°C, respectively. The value of P_r at room temperature of 0.8PZT-0.2BFN is slightly higher than that reported in the previous work [8].

Figure 4 shows the variation of pyroelectric coefficient, p_i, with temperature for 0.8PZT-0.2BFN samples. The value of p_i was found to be 0.72 nC/cm^2 K at 60°C. This curve shows continuous increase in p_i with the increase in temperature up to the transition temperature with a maximum value of 3.2 nC/cm^2 K at 200°C. It is clearly seen from

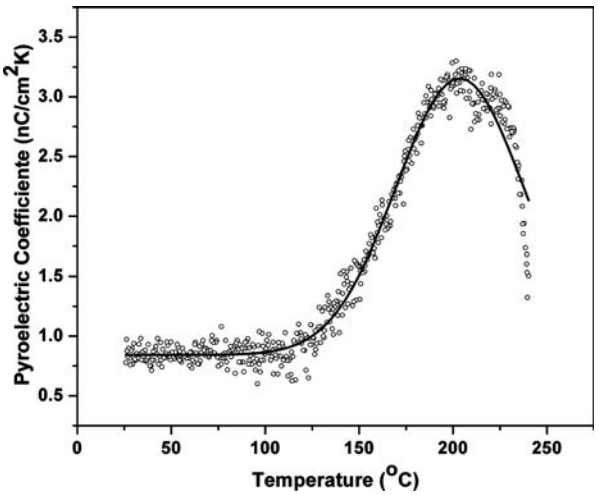

Figure 4. Variation of pyroelectric coefficient (p_i) with temperatures of 0.8PZT-0.2BFN ceramics.

Fig. 2(a) and Fig. 4 that the phase transition temperatures (T_c) obtained by pyroelectric measurement is in good agreement with the values obtained from the dielectric study.

4. Conclusion

In this work the solid solution $0.8PbZr_{0.52}Ti_{0.48}O_3$–$0.2BaFe_{0.5}Nb_{0.5}O_3$ ceramic was prepared by the mixed oxide method. The 0.8PZT–0.2BFN ceramics of optimum properties were fabricated by using 1100°C and 1200°C for calcination and sintering temperatures respectively. The XRD patterns present single phase of perovskite structure without pyrochlore phase. The dielectric properties of the ceramics depend on temperature and frequency to a certain extent. However, the dielectric constants were found to slightly decrease with the temperature and frequency. The phase transition temperature (T_c) decreased to 200°C, lower than that of pure PZT (390°C) and this value is in good agreement with that obtained from pyroelectric measurement. The typical ferroelectric behavior of the sample was confirmed by its hyteresis loop and based on the Curie–Weiss law.

Acknowledgments

The authors would like to express their sincere thanks to the Thailand Research Fund (TRF), the Commission on Higher Education, Graduate school and Faculty of Science, Chiang Mai University, THAILAND for financial supports.

References

1. B. Jaffe, W. R. Cook, and H. Jeffe: Piezoelectric Ceramics. USA: Academic Press Limited; 1971.
2. W. G. Cady, Piezoelectricity. USA: McGraw-Hill Book Company, Inc.; 1946.
3. S. L. Swartz, Topics in Electronic Ceramics. IEEE T. Dielect. El. In. **48**, 151 (2000).
4. S. Eitssayeam, U. Intatha, G. Rujijanagul, K. Pengpat, and T. Tunkasiri, Structural and electrical properties characterization of (1-x) $PbZr_{0.52}Ti_{0.48}O_3$ –x$BaFe_{0.5}Nb_{0.5}O_3$ system. *Appl. Phys. A.* **83**, 295–299 (2006).

5. Powder diffraction file. Joint committee on Powder Diffraction Standards. No. 33–784.
6. The Inorganic Crystal Structure database (ICSD) No. 43622.
7. N. Vittayakorn, G. Rujijanagul, X. Tan, M. A. Marquardt, and D. P. Cann, The morphotropic phase boundary and dielectric properties of the xPb($Zr_{1/2}Ti_{1/2}$)O_3- (1–x)Pb($Ni_{1/3}Nb_{2/3}$)O_3 perovskite solid solution. *J. Appl. Phys.* **96**(9), 5103–5109 (2004).
8. A. Wu, P. M. Vilarinho, I. M. M. Salvado, and J. L. Baptista, Sol–gel preparation of lead zirconate titanate powders and ceramics: Effect of alkoxide stabilizers and lead precursors *J. Am. Ceram. Soc.* **83**(6), 1379–1385 (2000).

Available online at www.sciencedirect.com
ScienceDirect
Current Applied Physics 8 (2008) 253–257
Current Applied Physics
An official journal of the KPS
www.elsevier.com/locate/cap
www.kps.or.kr

Development of electrical properties in lead-free bismuth sodium lanthanum titanate–barium titanate ceramic near the morphotropic phase boundary

P. Jarupoom, K. Pengpat *, N. Pisitpipathsin, S. Eitssayeam, U. Intatha, G. Rujijanagul, T. Tunkasiri

Department of Physics, Faculty of Science, Chiang Mai University, Chiang Mai 50200, Thailand

Available online 25 October 2007

Abstract

The near morphotropic phase boundary (MPB) of lead-free piezoelectric ceramics based on bismuth sodium lanthanum titanate ($Bi_{0.487}Na_{0.487}La_{0.017}TiO_3$:BNLT) and barium titanate ($BaTiO_3$:BT) was carefully investigated by a modified two step mixed-oxide method. In this case the BNLT and BT powders were produced separately using calcination temperatures of 900 °C and 1200 °C, respectively. After that they were mixed with the desired compositions of $(1-x)$BNLT–xBT, where $x = 0.00$, 0.02, 0.04, 0.06, 0.08, and 0.10. Then the powders were pressed and subsequently sintered at various temperatures to obtain the maximum density under each condition. It was found that the BT addition has a significant effect on grain growth inhibition of the BNLT–BT ceramics and this in turn gave rise to an enhancement in dielectric constant (ε_r) of the corresponding ceramics. The piezoelectric coefficient (d_{33}) was also improved greatly to about 130 pC/N in the 0.96BNLT–0.04BT ceramic sample sintered at 1125 °C. This offered an opportunity to obtain a good candidate for replacing the lead-based piezoelectrics.

PACS: 77.65.Bn; 71.45.Gm; 61.05.cp; 68.37.Hk

Keywords: BNLT; BT; Lead-free piezoelectric ceramic; Two step mixed-oxide method

1. Introduction

In the past few decades, extensive studies have been carried out in order to find replacements for lead-based piezoelectric materials, such as (Pb, Zr)TiO_3 (PZT), $PbTiO_3$ (PT) and $Pb(Mg_{1/3}Nb_{2/3})O_3$ (PMN), because of environmental concern. One of the most studied compounds is ferroelectric bismuth sodium titanate ($Bi_{0.5}Na_{0.5})TiO_3$ (BNT), discovered by Smolenskii et al. [1]. It has interesting electrical properties (good dielectric constant (ε_r) and acceptable piezoelectric coefficient (d_{33})). Its crystal structure is rhombohedral with strongly ferroelectric behavior. The Curie temperature T_c is about 320 °C, remanent polarization $P_r = 38\ \mu C/cm^2$ and coercive field $E_c = 73$ kV/cm. Another phase transition occurs at about 200 °C (T_p) which is believed to be the transition from ferroelectric rhombohedral to antiferroelectric tetragonal, which is further changed to the paraelectric cubic phase at T_c [2,3]. It is normally found that the ε_r–T curve at the T_c of this material has a high degree of broadness, indicating relaxor-type ferroelectric behavior.

However, the Bi ion is highly volatile at high temperature above 1130 °C during sintering, making this material difficult to pole due to its high conductivity [4]. The solution to this problem has been found by many researchers who were able to modify the BNT crystal by the substitution of other A- and B-site cations, such as in $(Bi_{0.5}Na_{0.5})_{(1-1.5x)}La_xTiO_3$: BNLT [5], BNT–$BaTiO_3$ [6], BNT–$KNbO_3$ (KN) [7], and BNT–Ba(Ti, Zr)O_3 [8]

* Corresponding author.
E-mail address: kpengpat@gmail.com (K. Pengpat).

1567-1739/$ - see front matter © 2007 Elsevier B.V. All rights reserved.
doi:10.1016/j.cap.2007.10.010

solid-solution ceramic systems. The piezoelectric properties of these ceramics were significantly improved. Recently, another interesting system was reported by Pengpat et al. [9] who combined two ideas, (1) the rare earth additive of La^{3+} suggested by Herabut and Safari [5], and (2) a solid solution of BNT–BT suggested by Takenaka et al. [6], in order to produce a new system of $(1-y)(Bi_{0.5}Na_{0.5})_{(1-1.5x)}La_xTiO_3$ (BNLT)–$yBaTiO_3$ (BT), where $x = 0.017$ and $y = 0$, 0.06, 0.1, 0.15, 0.2. They found that a maximum d_{33} of about 112 pC/N could be achieved with the composition of $y = 0.15$ which is not the morphotropic phase boundary (MPB) composition ($y = 0.1$) reported in this work. Moreover, this MPB composition is different from that of the $(1-x)$BNT–xBT system of Takenaka et al. whose MPB was observed at about $x = 0.06$. This may be due to different homogeneity of the samples prepared using different preparation methods. Moreover, the series of compositions of varying BT content (y) from $(1-y)$BNLT–yBT is not complete enough to determine the exact MPB of this system, making it difficult to compare the results to those of the previous works.

In this work, the $(1-x)$BNLT–xBT system has been further investigated by conventional methods, where the range of x values was chosen near the MPB of BNT–BT system (about 6 mol% BT) and 1.7 mol% La^{3+} doped BNT which is the optimum composition of the BNLT system. The physical, dielectric and piezoelectric properties of the BNLT–BT ceramics were investigated. The microstructures of the ceramics in this system were also examined. The results were compared to those of the previous works.

2. Experimental procedure

High purity (purity > 99.0%) powders of bismuth oxide (Bi_2O_3), sodium carbonate (Na_2CO_3), lanthanum oxide (La_2O_3), titanium oxide (TiO_2) and barium carbonate ($BaCO_3$) were used as starting materials for producing $(1-x)(Bi_{0.487}Na_{0.487}La_{0.017}TiO_3)$–$x(BaTiO_3)$, where $x =$ 0.0, 0.02, 0.04, 0.06, 0.08 and 1.0. The batch compositions of BNLT and BT were weighed and mixed by ball-milling for 24 h. Then both mixtures of BNLT and BT compositions were dried and calcined at 900 °C and 1200 °C, respectively, which are the optimum calcination temperatures for producing highly pure powders of both phases. Both powders were then mixed corresponding to the above formula by ball-milling for 24 h with acetone as the dispersion media. After drying and sieving the mixtures, the obtained powder was made into pellets of 15 mm in diameter by uniaxial pressing in a stainless steel die. The pellets were sintered between 1050 °C and 1150 °C in an electric furnace in an air atmosphere under controlled heating and cooling rates of 5 °C/min with 2 h dwell time. The phase identification and density of the sintered ceramic samples was investigated using X-ray diffraction (XRD: Siemen D-500) and Archimedes' method, respectively. Scanning electron microscopy (SEM: JSM-6335F) was used to observe the microstructures of the ceramics. The grain sizes of each sample were measured by the mean linear intercept. The two parallel surfaces of the sintered ceramics were polished and coated with silver paste as electrodes for electrical contact. To measure the relevant electrical properties, the prepared ceramic samples were poled in a silicone oil bath at 50 °C at 3.0 KV/mm for 15 min. The samples were then left at room temperature for 24 h after poling, and the piezoelectric measurements were measured using a piezoelectric-d_{33}-meter (Model 8000, Pennebaker). The dielectric constant (ε_r) of all ceramic samples was measured at various frequencies from 1 kHz, 10 kHz and 100 kHz and their temperature vs ε_r curves were also measured using an LCZ-meter (Model 4276A, Hewlett Packard).

3. Results and discussion

The XRD patterns of the dense ceramics from BNLT–BT system are shown in Fig. 1. It can be seen that all the peaks in the XRD pattern of the BNLBT0 ceramic correspond to the BNT phase of the JCPDS file No. 34-0360 with rhombohedral structure. The addition of BT phase of $x \geqslant 0.04$ resulted in a splitting of the 200 peak into two peaks of (002) and (200) reflections. This splitting is obvious at $x = 0.06$ and can be clearly seen in the extended XRD patterns of the corresponding ceramics at 2θ between 44° and 48° (Fig. 2). This indicates the change in crystal structure from rhombohedral to tetragonal symmetry of these ceramics and the MPB of this system is found to lie between $x = 0.04$ and $x = 0.06$, where the rhombohedral and tetragonal symmetries coexist, with more BT added, more of the tetragonal phase could be detected in the XRD patterns of the BNLBT ceramics. From the previous work, it was reported that the MPB of the $(1-x)$BNT–xBT system was at $x = 0.06$ [6]. In this work, La^{3+} doping of the BNT–BT has, however, shown no significant effect on the MPB as we found our MPB in the similar region of x between 0.4 and 0.6. This may be attributed to the difference between the ionic radius of La^{3+} ion (130 pm) and

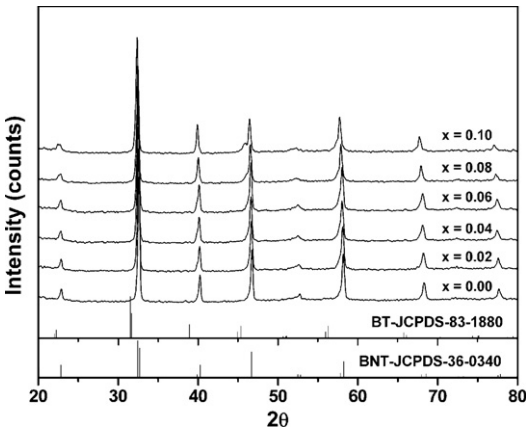

Fig. 1. X-ray diffraction patterns of $(1-x)$BNLT–xBT ceramics, where $x = 0.0$–0.10.

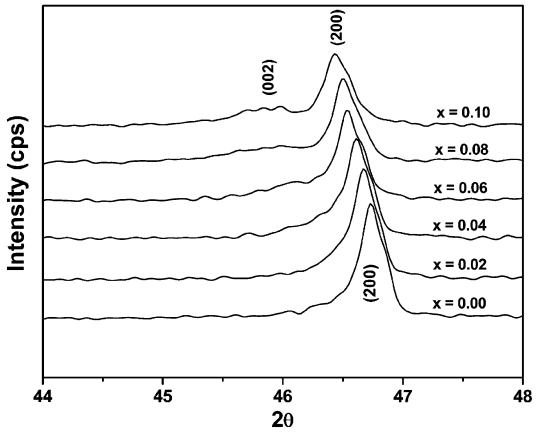

Fig. 2. X-ray diffraction patterns of $(1-x)$BNLT–xBT ceramics at 2θ between 44° and 48°.

Bi^{3+} ion (131 pm) being so small (about 0.8%) and both ions also having the same valency.

The microstructural analysis of all ceramics has been carried out and the SEM micrographs of the as-formed surfaces are illustrated in Fig. 3. All have a dense structure with low porosity. The small addition of BT, however, inhibited grain growth dramatically, as can be seen from the average grain size (Table 1) which was reduced from 4.10 ± 0.46 μm for pure BNLT (Fig. 3(a)) to about 1.86 ± 0.19 μm for the 2 mol% BT added sample (Fig. 3b). This may be attributed to the large difference between ionic radius of Ba^{2+} (156 pm) and Bi^{3+} (131 pm) and the possibility that Ba^{2+} aggregates and forms secondary phases on a very small scale at the grain boundaries. This may prevent grain boundary movement during the sintering process [10]. However, increasing the amount of BT from 0.04 to 0.10 had no significant effect on the grain size and shape of the ceramics as can be seen in Fig. 3c–f.

The experimental on dielectric measurements at room temperature for various BT contents are graphically presented in Fig. 4. It can be clearly seen that ε_r increases with

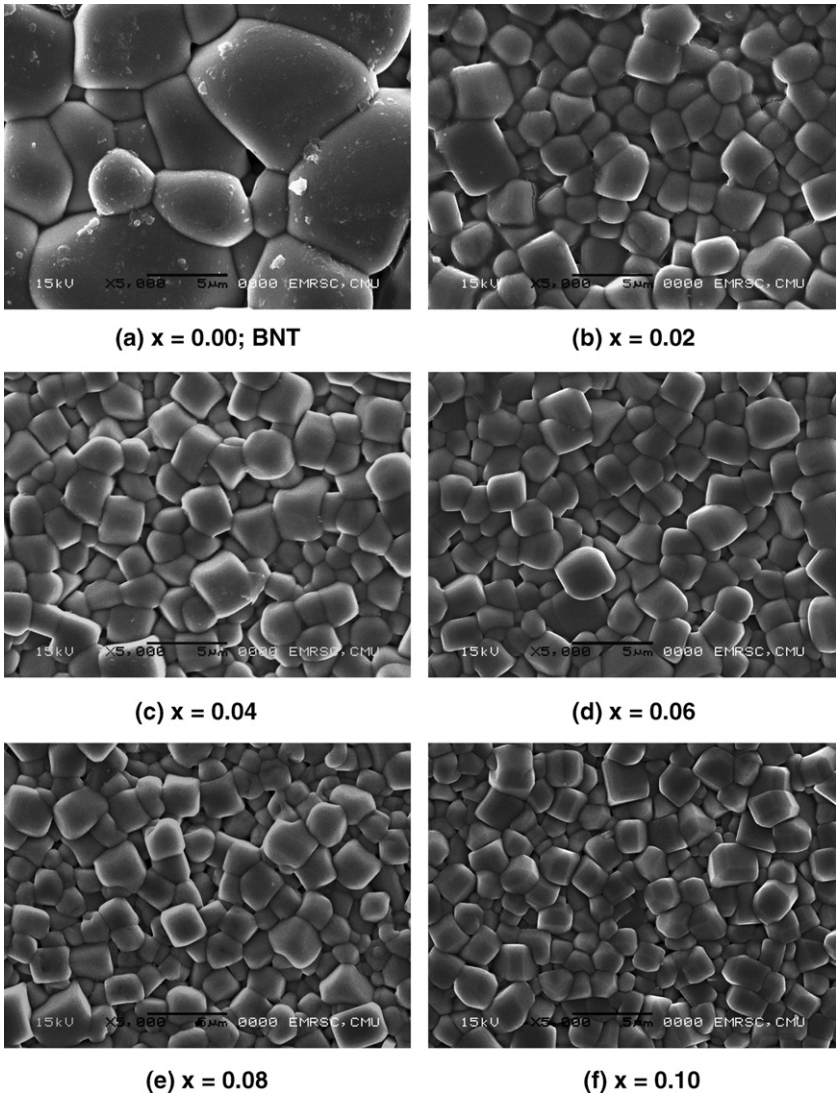

Fig. 3. SEM micrographs of (a) BNT and $(1-x)$BNLT–xBT ceramics, where (b) $x = 0.02$ to (f) $x = 0.10$.

Table 1
The values of density, grain size, dielectric constant (ε_r) and piezoelectric coefficient (d_{33}) at room temperature of $(1-x)$BNLT–xBT samples

Samples	Density (g/cm^3)	Grain size (μm)	ε_r ($T_{room/1\,kHz}$)	d_{33} (pC/N)
BNLT	5.85 ± 0.02	4.10 ± 0.46	780	72
0.98BNLT–0.02BT	5.86 ± 0.03	1.86 ± 0.19	863	118
0.96BNLT–0.04BT	5.86 ± 0.01	1.69 ± 0.16	1060	125
0.94BNLT–0.06BT	5.85 ± 0.01	1.57 ± 0.19	1547	52
0.92BNLT–0.08BT	5.84 ± 0.01	1.55 ± 0.23	1598	24
0.90BNLT–0.10BT	5.84 ± 0.01	1.47 ± 0.15	1615	25

increasing BT (x) and reaches a maximum at $x = 0.06$. Further addition of BT gradually increases ε_r up to $x = 0.10$. Initially, the considerable increase in ε_r values from $x = 0.02$ (rhombohedral structure) to $x = 0.06$ (rhombohedral + tetragonal structures) may be mainly due to the presence of tetragonal phase coexisting in the MPB compositions, but above this point the grain size and density may play a more important role in controlling the ε_r values of these ceramics, since the density values and grain size of the BNLT–BT samples changes slightly with increasing BT as shown in Table 1. This trend was observed at all frequencies. The dielectric loss ($\tan\delta$) was found to increase slightly up to $x = 0.04$, above which it increases monotonically with increasing BT content. This can be related to the density, which was found to decrease, indicating greater porosity, when the BT content is greater than $x = 0.04$.

The temperature dependence of the dielectric constant for all the BNLT–BT ceramics is shown in Fig. 5. A reduction of T_c was observed for the BT-containing samples, which is expected because the BT ceramic has a lower value of T_c (~130 °C compared with that of BNLT, ~340 °C). This result is consistent with the previous work [6]. The $\tan\delta$ value of all BT-containing samples is found to be lower than that of the pure BNLT sample, leading to the lower conductivity of these BNLT–BT ceramics at higher temperature (>90 °C). The important mechanism of ionic

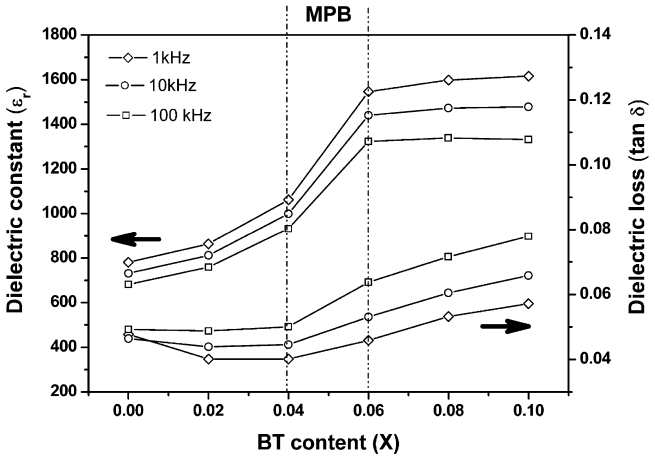

Fig. 4. The dielectric constant (ε_r) and loss tangent ($\tan\delta$) at room temperature vs BT content (x) in the $(1-x)$BNLT–xBT system.

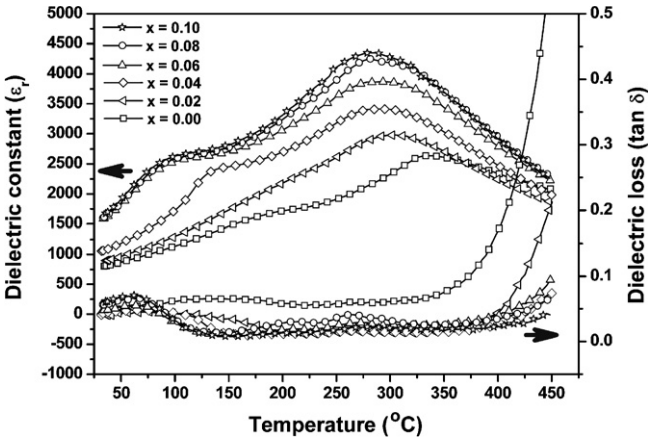

Fig. 5. Variation of dielectric constant (ε_r) and loss tangent ($\tan\delta$) with temperature for $(1-x)$BNLT–xBT ceramics at 1 kHz.

conductivity in these ceramics is the movement of ions which are the current carriers. It has been long known that the alkali ion is a good current carrier in ceramics; therefore, this ion plays an important role in the conductivity of the BNLT ceramics, since the Na^+ ions in BNLT move easily upon heating, resulting in the increase in conductivity with increasing temperature. In BT doping ceramics, the large Ba^{2+} (156 pm) ions are substituted into the A-sites of the BNLT, which possibly blocks the passage of the Na^+ current carriers, causing a reduction of conductivity in the BNLT–BT ceramics which gradually increases upon heating. When the temperature is further increased above T_c, the conductivity or ($\tan\delta$) is found to increase dramatically, as a result of the structural change from tetragonal to cubic at the Curie temperature.

The piezoelectric coefficient (d_{33}) values were measured by a d_{33} meter. Table 2 shows that BT content reaches a limit in enhancing the d_{33} value at $x = 0.04$ at which the maximum d_{33} value is about 130 pC/N. After that, the increase in tetragonal phase lowers the d_{33} value of the ceramics, reducing it to as low as 32 pC/N in the $x = 0.10$ sample. This may be attributed to the decrease in density of the high BT content samples.

Table 2 shows the important properties of the BNLT, and BNLT–BT samples prepared in this work, compared to previous results. It is clearly seen that the BT phase has a significant effect in enhancing the d_{33} of BNLT ceramics. In this work, the maximum d_{33} value was about

Table 2
The values of dielectric constant (ε_r), loss tangent ($\tan\delta$) and piezoelectric coefficient (d_{33}) at room temperature of selected samples compared to the literature values

Samples	ε_r (T_{room})	$\tan\delta$ (T_{room})	d_{33} (pC/N)
BNLT (this work)	730 (1 kHz)	0.05 (1 kHz)	72
0.96BNLT–0.04BT (this work)	1000 (10 kHz)	0.04 (10 kHz)	130
BNLT [5]	550 (1 kHz)	0.04 (1 kHz)	91
0.94BNT–0.06BT [3]	950 (10 kHz)	0.01 (10 kHz)	125

130 pC/N at the MPB composition of $x = 0.04$ (0.96BNLT–0.04BT), which is slightly higher than for the BNT–BT system (about 125 pC/N) [3].

4. Conclusions

The dielectric and piezoelectric properties of $(1 - x)$BNLT–xBT ceramics were determined. The piezoelectric coefficient (d_{33}) can be improved to a value of about 130 pC/N in the 0.96BNLT–0.04BT ceramic sample. The dielectric constant (ε_r) of the BNLT–BT ceramics was enhanced by the addition of BT content, while at the same time, their T_c was lowered. Moreover, BT doping helped to reduce the dielectric loss ($\tan\delta$) of the ceramics at high temperature.

Acknowledgements

The authors would like to thank the Thailand Research Fund and Faculty of Science, Chiang Mai University for financial support. The sincere thanks also go to the Research Laboratory for Excellent Electronic Materials, Department of Physics, and Graduate School, Chiang Mai University.

References

[1] G.A. Smolenskii, V.A. Isupov, A.I. Agranovskaya, N.N. Kraink, Sov. Phys. Solid State 2 (1961) 2651.
[2] K. Sakata, Y. Masuda, Ferroelectrics 5 (1994) 347.
[3] T. Takenaka, K. Maruyama, K. Sakata, Jpn. J. Appl. Phys. 30 (9B) (1991) 2246.
[4] T. Takenaka, H. Nagata, J. Eur. Ceram. Soc. 25 (2005) 2693.
[5] A. Herabut, A. Safari, J. Am. Ceram. Soc. 80 (11) (1997) 2954.
[6] T. Takenaka, K. Sakata, K. Toda, Jpn. J. Appl. Phys. 28 (1989) 59.
[7] H. Ishii, H. Nagata, T. Takenaka, Jpn. J. Appl. Phys. 40 (9B) (2001) 5660.
[8] C. Peng, J.F. Li, W. Gong, Mater. Lett. 59 (2005) 1576.
[9] K. Pengpat, S. Hanphimol, S. Eitssayeam, U. Intatha, G. Rujijanagul, T. Tunkasiri, J. Electroceram. 16 (2006) 301.
[10] S.H. Lee, C.B. Yoon, S.B. Seo, H.E. Kim, J. Mater. Res. 18 (2003) 1765.

Ferroelectrics Letters Section
Publication details, including instructions for authors and subscription information:
http://www.informaworld.com/smpp/title~content=t713871498

Structures and Properties of Lead-Free NKN Piezoelectric Ceramics

P. JARUPOOM[a]; K. PENGPAT[a]; S. EITSSAYEAM[a]; U. INTATHA[a]; G. RUJIJANAGUL[a]; T. TUNKASIRI[a]
[a] Department of Physics, Faculty of Science, Chiang Mai University, Chiang Mai, Thailand

To cite this Article JARUPOOM, P. , PENGPAT, K. , EITSSAYEAM, S. , INTATHA, U. , RUJIJANAGUL, G. and TUNKASIRI, T.(2008) 'Structures and Properties of Lead-Free NKN Piezoelectric Ceramics', Ferroelectrics Letters Section, 35: 5, 119 — 127
To link to this Article: DOI: 10.1080/07315170802520110
URL: http://dx.doi.org/10.1080/07315170802520110

Ferroelectric Letters, 35:119–127, 2008

ISSN: 0731-5171 print / 1563-5228 online
DOI: 10.1080/07315170802520110

Taylor & Francis
Taylor & Francis Group

Structures and Properties of Lead-Free NKN Piezoelectric Ceramics

P. JARUPOOM, K. PENGPAT, S. EITSSAYEAM, U. INTATHA, G. RUJIJANAGUL, and T. TUNKASIRI*

Department of Physics, Faculty of Science, Chiang Mai University, Chiang Mai 50200, Thailand

Communicated by Professor Yoshihiro Ishibashi

(Received June 22, 2008)

In this work, the preparation of sodium potassium niobate $(Na_{0.5}K_{0.5})NbO_3$ (NKN) ceramics were carried out by the conventional method. The effect of calcination temperatures, dwell time and heating rate on phase formation was investigated. Earlier work reported that to achieve the density of NKN ceramic over 95% of its theoretical density is rather difficult. In this work, firing conditions and heating and cooling rates were carefully varied to fabricate the NKN ceramics. X-ray diffraction (XRD) techniques were used to investigate the phase evolution of the calcined powders and sintered bodies. Microstructures of sintered pellets were studied by the scanning electron microscopic (SEM) techniques. Dielectric and ferroelectric properties were also investigated and reported.

Keywords: dielectric properties; piezoelectric properties; perovskite; lead-free materials

INTRODUCTION

Lead free sodium potassium niobate $(Na_{0.5}K_{0.5})NbO_3$ (NKN) ceramics show interesting properties such as high electromechanical coupling coefficient, high piezoelectric properties with perovskite structure and considerably high dielectric constant. It has a high Curie temperature ($T_c \sim 420^\circ$C), where the transformation of the ferroelectric phase to paraelectric phase occurs [1–6]. This composition has been reported as the morphotropic phase boundary,

*Corresponding author. E-mail: k.pengpat@yahoo.com

where the crystal structure of NKN possesses the orthorhombic symmetry at room temperature [11–13].

Earlier work revealed that high density ceramic was rather difficult to obtain via the conventional mixed-oxide route. An alternative solution is the hot pressing and spark plasma sintering (SPS) methods. Although these methods yield high densities and better properties compared of that obtained via the conventional mixed-oxide method, however, they were found unappropriate for using in mass production [7].

In the present study, fabrication of NKN ceramics via the conventional mixed-oxide method was carried out. Firing conditions were carefully controlled in order to obtain high density. The phase evolution of the calcined powder and sintered samples were investigated by an X-ray diffractometer and a simultaneous thermal analysis (STA). The microstructure of the NKN ceramics was examined by the scanning electron microscopic (SEM) technique. Measurement of the dielectric properties, electromechanical coupling coefficient (k_p) and piezoelectric coefficient (d_{33}) were carried out in the frequency range from 1 kHz – 10 MHz at room temperature.

EXPERIMENTAL PROCEDURE

Sodium potassium niobate $(Na_{0.5}K_{0.5})NbO_3$ (NKN) ceramics were prepared from the powders by using the conventional mixed-oxide method. The NKN powder was first prepared by mixing the starting materials, reagent grade $NaCO_3$ (Riedel-de Haën, extra pure), K_2CO_3 (Sigma-Aldrich, puriss >99%) and Nb_2O_5 (Sigma-Aldrich, puriss >99.9%), in the desired mole ratio. The starting materials were dried at 100°C for 24 h to remove absorbed moisture. The stoichiometric amounts of starting powders were weighed and transferred to 250 ml plastic jar, which was previously filled with 7 mm diameter zirconia grinding balls. They were ball milled at 385 rpm for 24 h using acetone as a milling medium. After milling, the slurry was dried and kept in an oven at 100°C.

Calcination profile was programmed based on results of the simultaneous thermal analyzer (STA 449C, Neztsch), using a heating rate of 1.7°C/min from 30 up to 1300°C. The mixtures were calcined at two calcination conditions in an alumina crucible. The firing temperatures were 700°C and 800°C denoted as NKN-700 and NKN-800 respectively, kept at that temperature for 2 h with heating rate of 100°C/h and cooling rate of 300°C/h in air atmosphere, to choose the optimum calcination temperature. The phase observation of calcined powders were studied by an X-ray diffractometer

(JDX-3530, JEOL) to identify the phase formation and optimum calcination conditions for preparation of NKN powder. The pellets with 20 mm in diameter were uniaxially pressed at 1 ton and sintered at temperature ranging from 1000 to 1200°C for 1 and 2 h with a heating rate of 100°C/h and cooling rate of 300°C/h in the air atmosphere. Densities were measured by Archimede's technique. The grain size of each sample was determined by the mean linear intercept. Differential scanning calorimetry (DSC 822^e, Mettler Toledo) was employed to study the phase transformation of ceramic powder at a heating rate of 10°C/min. The pellets were polished and electroded with the silver paste. The dielectric constant (ε_r), dissipation factor (tanδ) and electromechanical coupling coefficient (k_p) at the room temperature were measured at the frequency of 1, 10, 100 kHz and 1, 10 MHz using 4194A Impedance Grain/Phase analyzer (Hewlett Packard). The P-E hysteresis loops were investigated using a ferroelectric testing unit (RT66A, Radiant Technologies Inc.). The piezoelectric coefficients (d_{33}) were also measured using piezometer system.

RESULTS AND DISCUSSION

The STA analysis of a mixed oxide powder in stoichometric proportion of $(Na_{0.5}K_{0.5})NbO_3$ is given in Fig. 1. The TGA curve showing overall weight

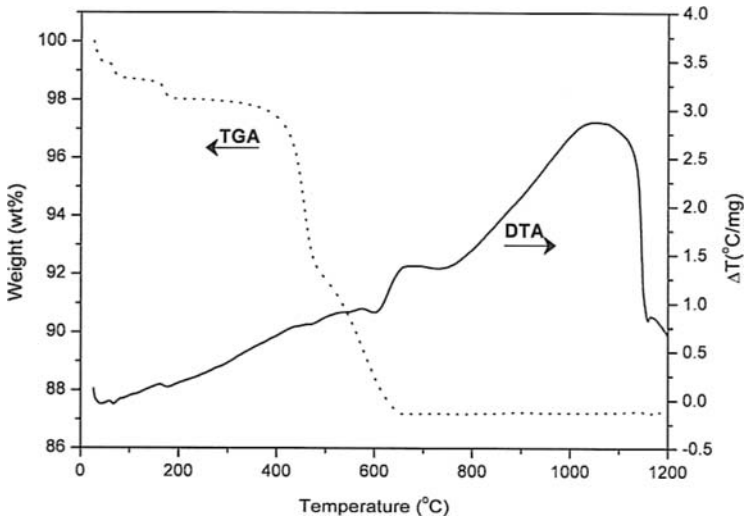

Figure 1. STA curves for $(Na_{0.5}K_{0.5})NbO_3$ mixed oxide powder.

loss was equal to 12.8% from room temperature to 1150°C. It shows a 1.98% weight loss between 30 to 220°C. In the same temperature range, the DTA curve shows two endothermic peaks positioned at around 80 and 175°C, which are associated to the decomposition of water during the thermal decomposition of the precursor. According to TGA curve, the highest weight loss is around 10%, occurring between 220 to 650°C. These losses were correlated with the endothermic peak at 620°C, in accordance with DTA curve, which can be related to the elimination of CO and CO_2 molecules originated from the decomposition of an oxalate group. The crystallization of sodium potassium niobate was observed for the temperature above 650°C in the TGA curve, indicating that no decomposition above this temperature occurs. These STA data were used to define the range of calcination and sintering temperatures. The XRD patterns of calcined powders are shown in Fig. 2. After calcination at 700°C (NKN-700), the major Bragg peaks corresponding to the single perovskite phase of orthorhombic structure without second phase was detected by this method. The increase of calcination temperature leads to the increase of the intensity of the diffraction peak. Splitting of some peaks becomes more pronounced at 800°C, indicating the increase of its crystallinity.

The pellets of NKN ceramic produced from the powder calcined at 700 and 800°C, were sintered at 1150°C for 1 h, which based on results of

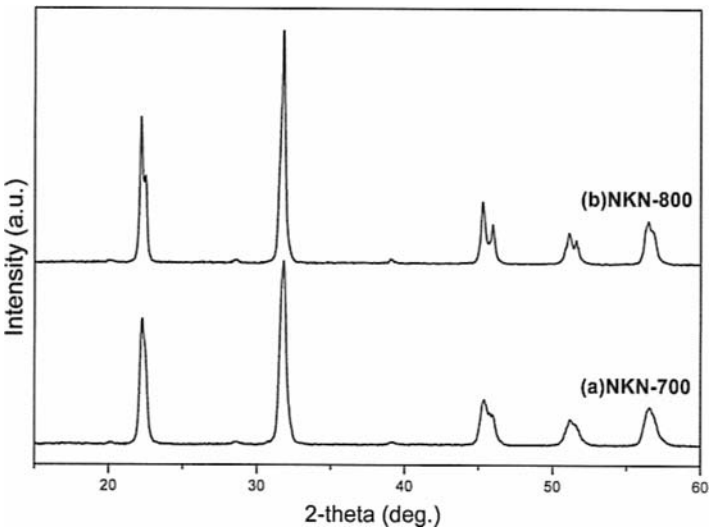

Figure 2. XRD patterns of NKN calcined powder (a) Calcined 700°C (b) Calcined 800°C.

TABLE I Dielectric properties of NKN ceramics

	1 kHz		10 kHz		100 kHz		1 MHz		10 MHz	
	ε_r	$\tan_\delta$	ε_r	$\tan_\delta$	ε_r	$\tan_\delta$	ε_r	$\tan_\delta$	ε_r	$\tan_\delta$
NKN-700	446	0.0610	296	0.0265	241	0.0179	133	0.0217	81	0.0688
NKN-800	489	0.0521	327	0.0236	281	0.0934	264	0.0984	211	0.0539

STA. The density of the NKN ceramic is increased with increasing calcine temperature. The optimum density of NKN is about 97.17% of the theoretical density (4.17 g/cm^3) for NKN-800. The microstructures of NKN ceramic surface are shown in Fig. 3. The average grain size of rectangular grain of NKN-800 is about 8.5 μm which larger than NKN-700 is about 10.8 μm (Fig. 3a) as generally expected. DSC analysis was performed and shown in Fig. 4. The DSC curve of all NKN ceramics reveals two peaks, which correspond to the respective phase transitions. The NKN ceramic is orthorhombic at room temperature and it transition to tetragonal phase at around 190°C and from tetragonal to cubic phase at around 410°C which is the Curie temperature. This is close to the work obtained from Jaeger and Egerton [8] which form that T_c of NKN was about 420°C.

The dielectric properties of NKN in the frequency range from 1 kHz – 10 MHz at room temperature are shown in Table I. The ε_r, tanδ, k_p and d_{33} values obtained at 1 kHz are in the same order with that of the air sintered and hot pressed of NKN [8], PZT [14] and BNT [15] as tabulated in Table II. In order to characterize the ferroelectricity, P-E hysteresis loops of NKN ceramics are plotted in Fig. 5, at room temperature. The remanent polarization P_r is 11.20 μC/cm^2 and the coercive electric field E_c is 6.94 kV/cm can also be obtained from NKN-800 ceramics.

TABLE II Comparison of dielectric constant and piezoelectric properties of NKN, NKN-700, NKN-800, BNT and PZT ceramics

Property	Air-sintered NKN-700	Air-sintered NKN-800	Air-sintered NKN [8]	Hot-pressed NKN [8]	Air-sintered BNT [15]	PZT-4 [14]
%TD	96.89	97.17	94.24	98.89	—	—
ε_r (1kHz)	446	489	290	420	310	1400
tanδ (1kHz)	0.061	0.052	—	—	0.013	0.053
d_{33} (pC/N)	96	98	80	160	66	225
k_p	0.40	0.42	0.36	0.45	—	0.054

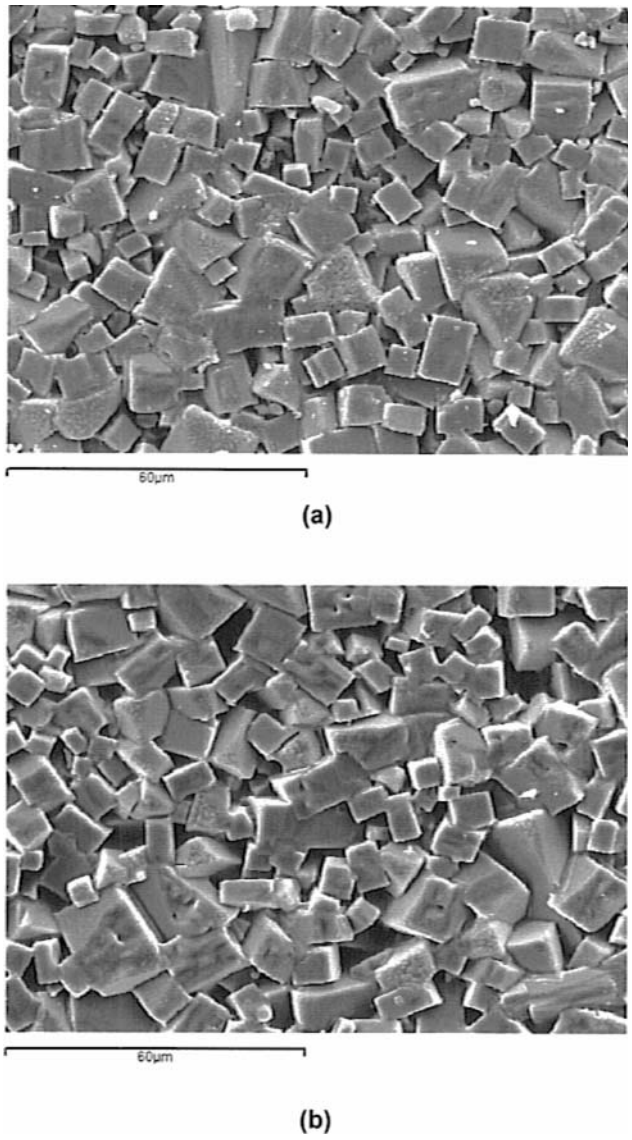

Figure 3. SEM micrographs of NKN ceramics (a) NKN-700 (b) NKN-800.